University of Cyprus
Department of Biological Sciences

FACULTY OF PURE AND APPLIED SCIENCES
DEPARTMENT OF BIOLOGICAL SCIENCES
LABORATORY OF BIOTECHNOLOGY AND MOLECULAR VIROLOGY
PROFESSOR LEONDIOS G. KOSTRIKIS

Detection of SARS-CoV-2 in Clinical Samples Using Mismatch-Tolerant Molecular Beacons and Real-Time RT-PCR

Georgia Stathi

A Research-Based Master's Thesis
for the
Degree of Magister Scientiae in Biomedical Sciences

December 14, 2021

THE LABORATORY OF BIOTECHNOLOGY & MOLECULAR VIROLOGY

ABSTRACT

Infectious diseases that arise from pathogens are considered as a major threat towards global public health. Most recently, the novel coronavirus disease 2019 (COVID-19) caused by the severe acute respiratory syndrome coronavirus 2 (SARS-CoV-2) was denoted as the first pandemic of the 21st century, by the World Health Organization (WHO). Since its emergence in December 2019 in Wuhan, China, it has infected more than 255 million people resulting in more than 5 million deaths worldwide. Due to its severe consequences on humanity and its rapid spread, it is imperative to develop efficient and accurate diagnostic assays for early detection of infection by SARS-CoV-2. However, it is crucial to validate these diagnostic assays using clinical samples to ensure their sensitivity and specificity. This validation process is essential to evaluate the reliability of the assay's performance and results. This study presents the design and validation of a mismatch-tolerant molecular beacon-based real-time reverse transcription (rt RT-PCR) assay, developed by the laboratory of Biotechnology and Molecular Virology, of the University of Cyprus (BMV, UCY), for the detection of SARS-CoV-2. The aforementioned assay was designed to detect the four genes S, E, M and N of SARS-CoV-2 and was initially tested by External Quality Assessments (EQAs). The assay was then validated through public diagnostic surveillance testing at the University of Cyprus (September 2020-January 2021), using clinical samples. Importantly, during this period, the pooling method was used, and 534 pools (~ 5 samples per pool) were collected from students and employees of the University, amounting to 2231 study subjects. Consequently, through this study, there were 16 individual clinical samples that were identified to be infected with SARS-CoV-2. Overall, this study provides the methodology necessary for the development of a detection assay for SARS-CoV-2 and highlights the importance of validation using clinical samples. Thus, through this study a powerful asset for the detection of SARS-CoV-2 is presented, that is designed to identify the virus despite possible mutations that may arise and can be easily modified for other emerging pathogens.

DEDICATION

This thesis is dedicated to the memory of my beloved sister Anastasia. Everything I do, I do it for you. I love you.

ACKNOWLEDGEMENTS

Profusely I would like to thank the University of Cyprus for their support and for providing the opportunity for the successful accomplishment of this research. Also, a heartfelt thanks goes to all the medical personnel for their valuable help during the sampling process of the research. Without their kind assistance, this research would not have been possible.

I would like to acknowledge and express my deep sense of thanks and gratitude to my mentor and supervisor Professor Leondios G. Kostrikis for this special opportunity of being a member of his laboratory and work on this interesting project. His dedication and guidance have been mainly responsible for completing my work.

A debt of appreciation is also owed to Andreas C. Chrysostomou, a doctoral student of the laboratory, for his advice and help during my time at the laboratory. Also, I would like to thank Johana Hezka Rodosthenous, the laboratory manager, for her continues guidance, and helpful suggestions. I am also thankful to Cicek Topcu, a doctoral student of the laboratory, Antonia Aristokleous and Vasilis Georgiou, two master students of the laboratory, for their continuous encouragement and support.

I am deeply indebted to my cousin Maria Koletsiou, for her significant support and trust in me. Her keen encouragement and positivity were an invaluable help throughout the course of my research work.

Last but not least, I would like to thank my parents for everything. Thank you for always being there for me no matter what and supporting me in every decision I make. I would have not made it this far without you by my side. I owe you the world.

COMPOSITION OF THE EXAMINATION COMMITTEE

Thesis Supervisor (Examination Committee coordinator): Professor Leondios G. Kostrikis, Department of Biological Sciences, University of Cyprus

Committee Member: Assistant Professor Chrysoula Pitsouli, Department of Biological Sciences, University of Cyprus

Committee Member: Assistant Professor Katerina Strati, Department of Biological Sciences, University of Cyprus

SEMINAR ANNOUNCEMENT

University of Cyprus
Department of Biological Sciences

Master Research Dissertation in Biomedical Sciences (BIO 830/600)

Student Presentation

Tuesday, 14 December 2021 at 11:00

This seminar is open to the public via Zoom at the following link:

https://ucy.zoom.us/j/94197001790?pwd=ZnI5blhFUDJuSEFldm1lVTZxbkUrZz09

Georgia Stathi

Thesis Supervisor: Prof. Leondios Kostrikis

"Detection of SARS-CoV-2 in Clinical Samples Using Mismatch-Tolerant Molecular Beacons and Real-Time RT-PCR"

Infectious diseases that arise from pathogens are considered as a major threat towards global public health. Most recently, the novel coronavirus disease 2019 (COVID-19) caused by the severe acute respiratory syndrome coronavirus 2 (SARS-CoV-2) was denoted as the first pandemic of the 21st century, by the World Health Organization (WHO). Since its emergence in December 2019 in Wuhan, China, it has infected more than 255 million people resulting in more than 5 million deaths worldwide. Due to its severe consequences on humanity and its rapid spread, it is imperative to develop efficient and accurate diagnostic assays for early detection of infection by SARS-CoV-2. However, it is crucial to validate these diagnostic assays using clinical samples to ensure their sensitivity and specificity. This validation process is essential to evaluate the reliability of the assay's performance and results. This study presents the design and validation of a mismatch-tolerant molecular beacon-based real-time reverse transcription (rt RT-PCR) assay, developed by the laboratory of Biotechnology and Molecular Virology, of the University of Cyprus (BMV, UCY), for the detection of SARS-CoV-2. The aforementioned assay was designed to detect the four genes S, E, M and N of SARS-CoV-2 and was initially tested by External

TABLE OF CONTENTS

LIST OF FIGURES

LIST OF TABLES

1. INTRODUCTION

1.1 Emergence of Infectious Diseases and Viruses

The emergence of infectious diseases from pathogens has a severe effect on public health globally (Devaux, 2012). Most human pathogens of infectious diseases show patterns of evolution beginning by their emergence, which may lead to epidemics or pandemics, then their adaptation to human populations with a potential of an outbreak again in the future (Fauci and Morens, 2012). Emerging or re-emerging pathogens either from bacteria or viruses are considered as the second leading cause of death worldwide, among which are Mycobacterium tuberculosis, human immunodeficiency virus (HIV), influenza as well as severe acute respiratory syndrome (SARS) (Fauci, 2001). These pathogens usually originate from animal infections and later spread through interspecies transmission to humans (Dhama et al., 2020). As they enter a new host, they begin to spread rapidly, which in the absence of therapy may lead to the host's death (Fauci and Morens, 2012). In this study we will be focusing on a viral pathogen, the Severe Acute Respiratory Syndrome Coronavirus 2 (SARS-CoV-2), the causative agent of the Coronavirus disease 2019 (COVID-19) that was first identified in December 2019 (Hedman et al., 2021). Since then, humanity has been facing a global pandemic caused by this coronavirus. Global efforts have been underway to study SARS-CoV-2, face the new scientific challenges that were raised, and ultimately protect public health. These global efforts entailed the development of methods to screen for and identify SARS-COV-2, therapeutics, and vaccines, as well as ways to be prepared for the future emergence or re-emergence of this coronavirus or any other pathogen that may threaten public health (Hadjinicolaou et al., 2011, Wu et al., 2020).

1.2 Past Coronavirus Outbreaks and Emergence of SARS-CoV-2

Over the past two decades, coronaviruses (CoVs) have been related with critical infection outbreaks in East Asia and the Middle East (Dhama et al., 2020). There are seven CoVs in total that have been identified in humans, these are the HCoV-OC53, HCoV-229E, HCoV-NL63, HCoV-HKU1, MERS-CoV, SARS-CoV, and SARS-CoV-2 (Hedman et al., 2021). The first four

emerged CoVs (HCoV-OC53, HCoV-229E, HCoV-NL63, HCoV-HKU), were known to cause common cold in humans (Vellas et al., 2020). Nonetheless, the emergence of two new CoVs known as SARS-CoV in 2002 (Peiris et al., 2003) and MERS-CoV in 2013 (Zaki et al., 2012) had crucial effects on humanity because of their high infectivity caused by their increased adaptability to the host (Vellas et al., 2020).

The knowledge gained from studying previous coronavirus outbreaks provided a substantial foundation to study the novel Coronavirus, SARS-CoV-2, which is considered to be the seventh CoV affecting humans (Shang et al., 2020). As stated above, SARS-CoV-2 had emerged in December 2019, specifically, after a cluster of pneumonia incidents was reported at the Huanan South seafood market (HSSM) in Wuhan, Hubei Province, China (Vellas et al., 2020, Wang et al. 2020). The association between the pneumonia cases in the HSSM and the SARS-CoV-2 pandemic was confirmed by the World Health Organization (WHO), however, phylodynamic analysis results revealed that SARS-CoV-2 probably emerged in October 2019 and the HSSM was just the hotspot of spreading (do Vale et al. 2021, Hedman et al., 2021). Following the initial outbreak, SARS-CoV-2 rapidly spread around the world, and in just a few months, by March 2020, it was declared as the COVID-19 pandemic by WHO threatening the whole world (WHO, 2021). As of November 2021, more than ~255 million cases were reported, which resulted in more than ~5 million deaths (Petrosillo et al., 2020, Shang et al., 2020) (https://coronavirus.jhu.edu/map.html).

1.3 Evolutionary Origins and Classification of SARS-CoV-2

The study of the evolutionary origins of SARS-CoV-2 was based on the association of the initial outbreak of pneumonia cases, with the HSSM, since a wide variety of wildlife was sold there such as, poultry, badgers, hedgehogs, snakes, bats, and pangolins, as well as animal-food products (Hedman et al., 2021). Furthermore, it was not the first time an outbreak of pneumonia cases was reported to be associated with this seafood market, supporting the likely initial location of the emergence of SARS-CoV-2 (Hedman et al., 2021). Thus, it was highly probable that the virus was transmitted by an animal sold in the market, and based

on phylogenetic studies, it is strongly supported that SARS-CoV-2 was transmitted to humans through bats (Hedman et al., 2021). This is because of the high genetic similarity of SARS-CoV-2 with the bat coronavirus RaTG13 (96%) (Friend and Stebbing, 2021). Additionally, there are theories supporting that bats transmit viruses through intermediate hosts that are in close contact with humans (Han et al. 2015). Yet, regardless of the assumptions, nothing was confirmed about the exact route of transmission of the virus to humans (do Vale et al. 2021).

Despite of the obscurity behind the intermediate host of SARS-CoV-2, genetic analyses classify this RNA virus into the *Nidovirales* order (Zhou et al., 2021). It is further classified to the family *Coronaviridae* and specifically the subfamily *Coronavirina*e. The subfamily of *Coronavirinae* is subsequently divided into four different genera which are the *Alphacoronavirus, Betacoronavirus, Gammacoronavirus* and *Deltacoronavirus*. SARS-CoV-2 belongs to the *Betacoronavirus* genera along with SARS-CoV and MERS-CoV (Khalil and Khalil, 2020) (Figure 1).

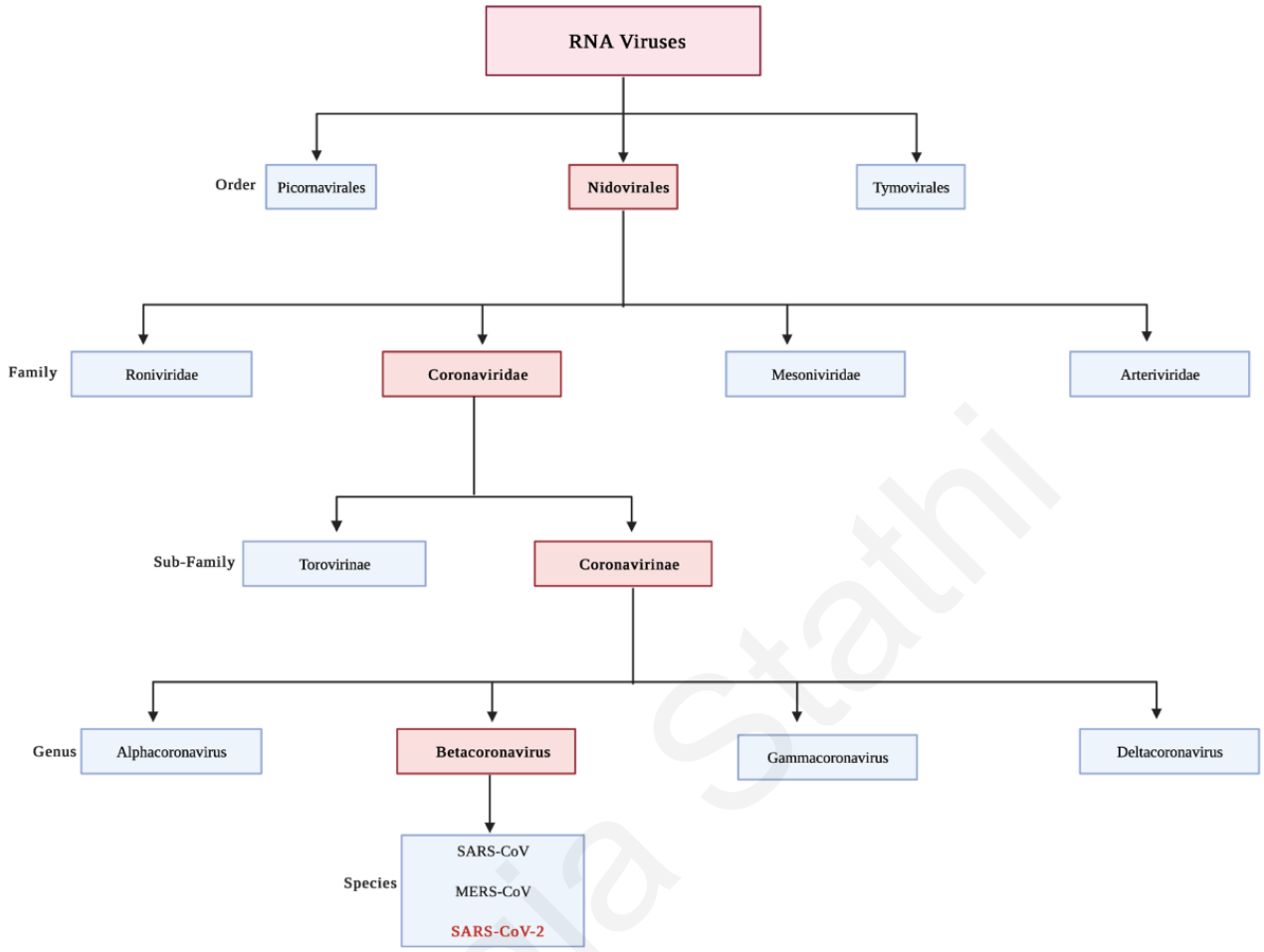

Figure 1. Schematic representation of the classification of SARS-CoV-2. The red boxes indicate the specific order, family, sub-family, and genera that SARS-CoV-2 belongs as an RNA virus. (Khalil and Khalil, 2020) . The figure was created with the use of BioRender.com web application.

1.4 Genomic Characterization of SARS-CoV-2

Coronaviruses are enveloped with a non-segmented, positive sense, single-stranded RNA which is considered to have the largest known genome in size among RNA viruses (Yang et al., 2020). Specifically, SARS-CoV-2 has a linear genome of approximately 29,903 nucleotides (Shi et al., 2020). The genome consists of a 5' cap domain together with a 3' poly (A) tail which gives the viral RNA the ability to act as an mRNA molecule for translation by the host without the need of additional modification (Fehr and Perlman, 2015, Fernandez and Melamed, 2020). The virion

of SARS-CoV-2 is spherical with a diameter of approximately 60-140 nm. Also, it presents distinct spikes of 9-12 nm, giving the characteristic appearance of a solar corona inspiring the name coronavirus (Dhama et al., 2020) (Figure 2).

The genome of the virus consists of multiple open reading frames (ORFs) of which the first ORF1 is located near the 5' terminus and encodes 16 non-structural proteins (nsp1-16) that are important for the replication machinery of the virus (Fernandez and Melamed, 2020, Yang et al., 2020). The 3' domain contains other ORFs which encode the four major structural proteins of the virus, the surface (S), envelope (E), membrane (M) and nucleocapsid (N) as well as eight accessory proteins (3a, 3b, p6, 7a, 7b, 8b, 9b, and ORF14). These four structural proteins are essential for the formation of the viral particles, viral entry, fusion, and survival of the virus in the cells of the host (Naqvi et al., 2020, Yang et al., 2020). However, the eight accessory proteins do not participate in the viral replication but are important for virus pathogenesis and virus-host interactions (Redondo et al., 2021) (Figure 3).

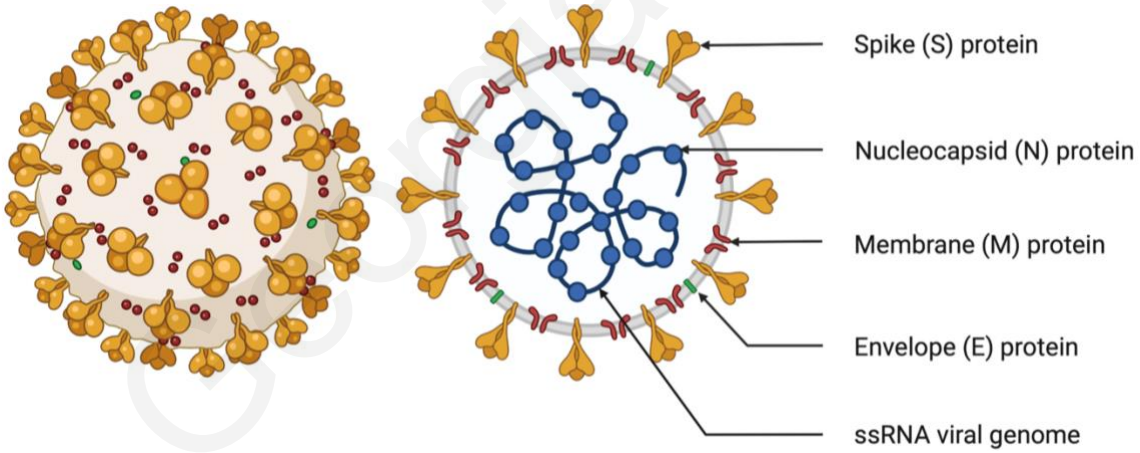

Figure 2. Schematic representation of the SARS-CoV-2 virion. The picture on the left shows the exterior view of the virion. The picture on the right shows the interior view of the virion. (Giacobbo et al., 2021). The figure was created with the use of BioRender.com web application.

Figure 3. Schematic representation of the SARS-CoV-2 genome order. The figure designates the major structural proteins of the SARS-CoV-2 as well as the two untranslated regions (UTR) at each end of the genome. (Naqvi et al., 2020). The figure was created with the use of BioRender.com web application.

1.5 Spike (S) Protein

The coronavirus Spike (S) glycoprotein is a major protein that is encoded by the S gene and its size varies from 180-200 kDa (Huang et al., 2020, Janik et al., 2021). It lies in a trimer on the surface of the virion which creates the illusion of a crown shaped appearance, that was the inspiration for the name Coronavirus {corona-a crown (Latin)} (Dhama et al., 2020, Satarker and Nampoothiri, 2020). These spike proteins on the envelope of a corona virion are responsible for recognizing the receptor on the host's cell surface, binding on it, and fusing with the host's membrane initiating the infection (Naqvi et al., 2020, Satarker and Nampoothiri, 2020). The S protein has a crucial role in pathogenesis (Naqvi et al., 2020). The S1 subunit initiates infection by allowing interaction of its receptor-binding domain (RBD) with the host cell receptor Angiotensin-converting enzyme 2 (ACE2) which causes the attachment of virions with the host cell membrane (Satarker and Nampoothiri, 2020). The S2 subunit acts as a fusion protein that allows the fusion of the virion with the membrane of the mammalian cells (Satarker and Nampoothiri, 2020). S protein normally exists in a metastable, prefusion conformation but when the ACE2 engages with the RBD and the viral infection takes place, it causes it to undergo extensive structural alternations (Chan et al. 2020, Huang et al., 2020). The S protein is cleaved by host cell furin-like proteases in the two distinct subunits S1 and S2 (Santos- Sánchez and Salas-Coronado 2020). S2 is also cleaved by other proteases from the host Type II transmembrane Serine Protease (TMPRSS2) to initiate the process of cellular entry (Chan et al. 2020). The critical role of the S protein in enabling the interaction with the host's cell membrane designates that it is potential target for therapies and vaccine developments (Huang et al., 2020, Pillay 2020).

1.6 Envelope (E) Protein

Envelope (E) protein is the smallest of the major structural proteins of the virus with 76-109 aa, ranging from 8.4-12 kDa in size (Malik, 2020, Schoeman and Fielding, 2019). It is an integral membrane protein which consists of three domains, an amino (N)-terminal domain (NTD), a transmembrane domain (TMD) and a carboxy (C)-terminal domain (CTD) (Satarker and Nampoothiri, 2020). When the replication cycle happens, the E protein is expressed in large quantities inside the host's cells, however only a small amount of it is incorporated into the envelope of the virion (Schoeman and Fielding, 2019). Its function is to participate in the production and maturation of the virus itself, but it is also important for pathogenesis (Janik et al., 2021, Sofi et al., 2020). E protein is known to act as viroporins that connect to form the host membrane protein-lipid pores which are involved in ion transport (Naqvi et al., 2020). Consequently, the inactivation or deficiency of E protein can cause changes in virulence of coronaviruses because of the alternations in tropism and morphology (Dhama et al., 2020).

1.7 Membrane (M) Protein

The Membrane (M) protein is the most abundant protein of all proteins in coronaviruses composed of 222 aa, varying in size from 25-30 kDa (Malik, 2020, Naqvi et al., 2020, Satarker and Nampoothiri, 2020). It is a small protein with three transmembrane domains which are attached to a short length N-terminal domain (NTD) outside the virion and a longer carboxyl-terminal domain (CTD) inside the virion (Dhama et al., 2020, Fehr and Perlman, 2015). M protein is responsible for most of the protein-protein interactions required for the assembly of coronaviruses (Malik, 2020). Nonetheless, the M protein alone is not sufficient to form the virion envelope. Binding of the M protein to the Nucleocapsid (N) protein leads to stabilisation of the nucleocapsid and the internal core of the virions which subsequently encourages accomplishment of the assembly of the virus (Schoeman and Fielding, 2019). To make up the viral envelope, M protein must be expressed together with E protein and form the virus-like particles (VLPs) which are then released through exocytosis (Malik, 2020).

1.8 Nucleocapsid (N) Protein

The Nucleocapsid (N) protein is a viral protein that is expressed in host's cells during the initial stages of infection, and it is around 40-50 kDa long (Masters, 2019, Satarker and Nampoothiri, 2020). It is also the only protein that is located in the nucleocapsid (Fehr and Perlman, 2015). It is composed of two distinct domains, the N-terminal domain (NTD) and the C-terminal domain (CTD) which both are capable of optimal RNA binding (Sofi et al., 2020). This protein has the ability to bind to the viral RNA, forming a core of a ribonucleoprotein that enables host cell entry and interaction with cellular processes that take place after the fusion of the virus (Satarker and Nampoothiri, 2020). The N protein is also involved in viral assembly and budding (Malik, 2020). When the N protein binds to the M protein, the nucleocapsid and the internal core of the virions are stabilised and so the completion of the viral assembly takes place (Schoeman and Fielding, 2019).

1.9 Symptoms of COVID-19 and High-Risk Groups

Having established the evolutionary and genomic characteristics of the virus, it is important to review the effects of its infection. Patients with COVID-19 vary from asymptomatic, mild/moderate or in some cases severe illness which may even lead to death (Larsen et al., 2020). Infected individuals can present milder symptoms such as fever, cough, shortness of breath, loss of taste and/or smell, headache, sore throat, runny nose, irritated eyes, myalgia, nausea, vomiting, diarrhoea, and rash on skin (Esakandari et al., 2020). However, patients with severe illness may show symptoms such as difficulty in breathing, chest pain, confusion, and loss of speech (WHO, World Health Organization). COVID-19 not only affects the respiratory system, but also the gastrointestinal system and the central nervous system (CNS) (Villapol 2020). Due to such evidence, people with underlying diseases such as asthma, diabetes, cardiovascular diseases, and cancer along with elderly people are considered to have higher risk developing serious illness from COVID-19 (Shi et al., 2020). Some of the aforementioned symptoms may be persistent even after the patient has recovered from COVID-19 (Carfì at al., 2020). It is important to know that asymptomatic patients are also dangerous, since they can

continue to infect other individuals without being aware that they are transmitting the virus (Syangtan et al., 2021).

1.10 Diagnostic Methods of SARS-CoV-2

Infected individuals with SARS-CoV-2 are able to transmit the virus through air droplets, sneezing and aerosols. The incubation period of the disease lasts from 3-14 days and the infection rate from each patient is 2.2 individuals (Oliveira et al., 2020). Due to such rapid spread and high number of COVID-19 cases, the development of fast and accurate detection methods is considered vital (Tahamtan, Ardebili 2020). Because the virus triggers a lower respiratory tract disease, the specimens for testing are mostly captured from the nose (Nasopharyngeal) or the mouth (oropharyngeal) with a swab (Ravi et al., 2020). Currently, there are several diagnostic approaches for the detection of active positive cases and past infections (Deeks et al. 2020).

1.10.1 Real-Time RT-PCR test

Real-time reverse transcription polymerase chain reaction (real-time RT-PCR) in respiratory samples is currently considered the "gold standard" for virus detection and more specifically SARS-CoV-2 acute infection (Chau et al. 2020, Scohy et al. 2020) (Figure 4). This method is characterised by its speed of detection and high levels of sensitivity and specificity (Shen et al. 2020). WHO and the Centres of Disease Control and Prevention (US CDC) have approved this laboratory-based technique for the diagnosis of COVID-19 (Abduljalil, 2020). The samples used in real-time RT-PCR are captured from the upper or lower respiratory tract of patients and the RNA is then extracted with the use of viral isolation kits (D'Cruz et al., 2020). The extracted genetic material is then amplified with the reverse transcription of the PCR technique (Kubina and Dziedzic, 2020). The majority of the available real-time RT-PCR tests use specific oligonucleotide primers and probes that fluoresce and identify specific parts of the viral genome (Ravi et al., 2020). Generally, PCR methods amplify a certain gene after separating the double stranded DNA which contains the gene segment. However, coronaviruses have single-stranded RNA for genome and by

reverse transcription it is transferred into cDNA (Shen et al. 2020). The fluorescent reporter probes included in the reaction will identify and hybridize to sections of the amplification products indicating the presence of the virus (Oliveira et al., 2020). Moreover, from the cycle threshold value (Ct) of a clinical sample it is indicated if it is a positive or a negative outcome and the viral load of it. The Ct value signifies the amplification cycle at which the sample crosses the threshold line (Sule and Oluwayelu, 2020). Nonetheless, like every method of viral detection, real-time RT-PCR also has drawbacks. A limitation of this method is considered to be the appearance of false positive results, which could be due to inactivated virus or viral fragments recognition or due to contamination of reagents in the laboratory (Ravi et al., 2020). Also, real-time RT-PCR requires specialised instrument and expertise (Kubina and Dziedzic, 2020, Scohy et al. 2020).

1.10.2 Antigen Rapid test

Rapid antigen tests are used as direct detectors of the viral proteins of SARS-CoV-2 (Deeks et al. 2020) (Figure 4). These kits are characterised by suboptimal specificity and sensitivity with the advantage of obtaining results in just a few minutes outside of laboratory conditions (Abduljalil, 2020, Gremmels et al., 2021). Antigenic tests have been proved more valid during the peak of infection when the viral load in the nasopharynx is higher (Candel et al., 2020). A common antigen test begins with the collection of samples with a nasopharyngeal or oropharyngeal swab. Then the sample is mixed with a solution that causes the breakage of the virus and release of specific viral proteins, in a tube. After that, a few drops of the mix are added to a paper strip with specific antibodies that bind to the viral proteins if present (Guglielmi, 2020). In order for an antigen test to be considered positive, two lines must be present on the paper strip. The first line indicates the test control which must always appear, and the second line represents the antigens. If only one line is present this denotes a negative result, and if no line appears it indicates an invalid result (Oliveira et al., 2020). Nonetheless, false-negative results are possible in antigen rapid tests due to decreased sensitivity (Guglielmi, 2020). If the patient has a low viral load, the test is possible to come out as negative (Guglielmi, 2020).

1.10.3 Serological Antibody test

Serological antibody tests are blood-based tests for the detection of SARS-CoV-2 that measure antibodies or antigens present in the blood when the organism of the patient is responding the infection (Younes et al., 2020) (Figure 4). Generally, antibody tests are used in later stages of the infection because the aim is to detect existing antibodies produced by the humoral immune system of the patient as a reaction to virus exposure (Chau et al. 2020). IgG and IgM are considered to be the specific antibodies developed in response to SARS-CoV-2 infection (Rai et al., 2021). The existence of IgG antibodies in the sample of a patient indicates previous infection with SARS-CoV-2, while presence of IgM antibodies shows recent exposure to the virus (Rai et al., 2021). Unlike the other diagnostic tests, serological antibody tests are conducted by collection of a blood sample. Then, the plasma is isolated and examined for the presence of the aforementioned antibodies (Younes et al., 2020). These tests are more accurate after the second week of infection, because that is when the viral RNA decreases in the organism of a patient, and therefore only the antibodies are present (Galipeau et al., 2020). Nonetheless, evidence supports that asymptomatic patients may not present antibodies in their blood at all after the infection (Chau et al. 2020). Serological tests are important for validating results of real-time RT-PCR or antigen rapid tests and for determining the herd immunity of an individual that was previously infected with SARS-CoV-2 (Kontou et al. 2020).

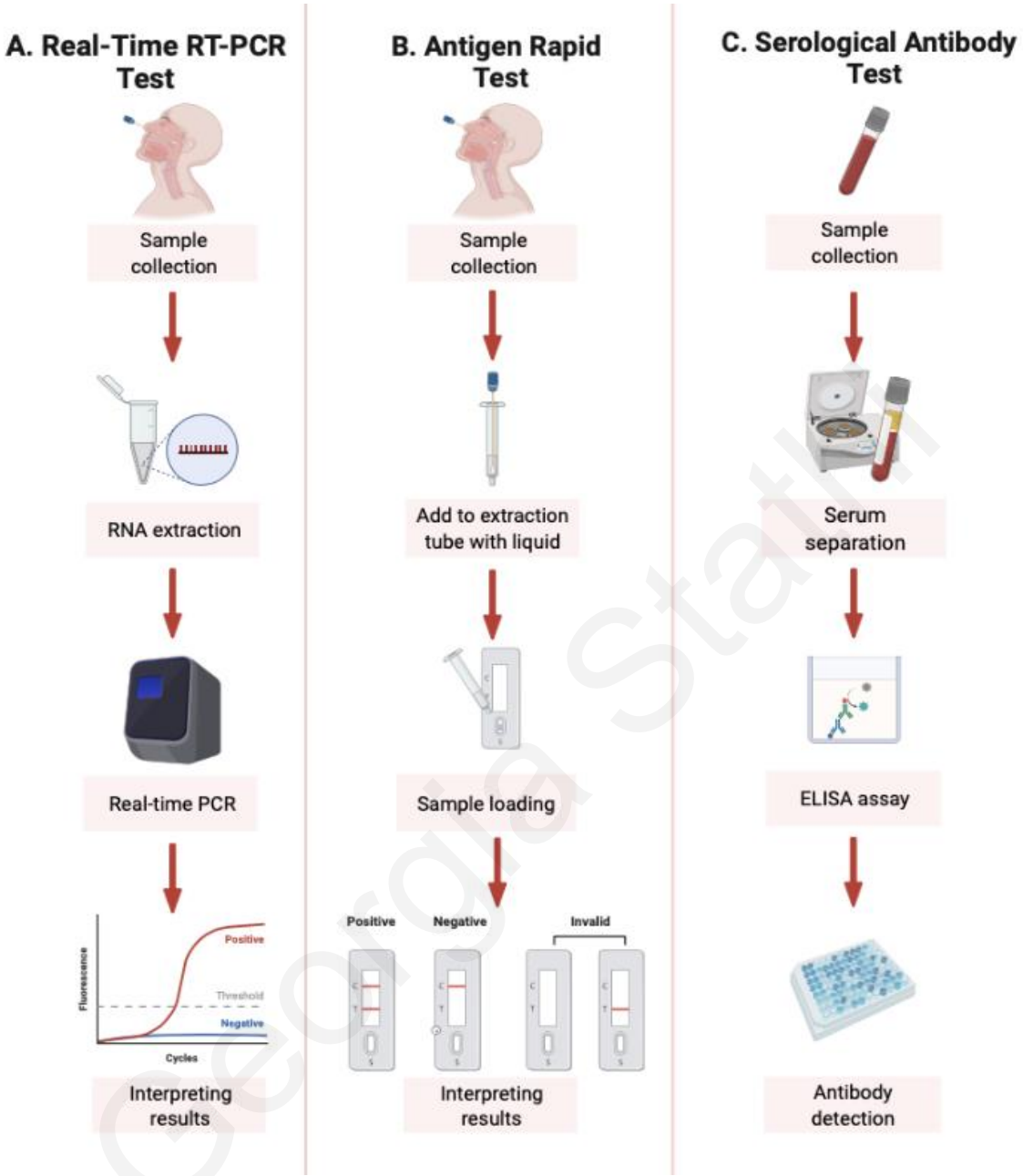

Figure 4. Graphical illustration of three diagnostic methods of SARS-CoV-2. **A.** The procedure followed during a real-time RT-PCR test for detection of viral RNA. **B.** The procedure followed during an Antigen Rapid test for detection of viral RNA. **C.** The procedure followed during a Serological Antibody test for detection of viral RNA. The figure was created with the use of BioRender.com web application.

1.11 Molecular Beacon Probes

Having explained the methods of detection, the real-time RT-PCR method was used for SARS-CoV-2 detection in this study. This method requires incorporation of molecular probes, which in this study specifically were the molecular beacon probes. Molecular beacons (MBs) are single-stranded DNA probes, that form a stem-and-loop structure and become fluorescent in the presence of the target (Marras et al., 2005, Han et al., 2013). The hybridization of the MB with the target happens during the annealing stage of the PCR cycle, nonetheless, in absence of target, MB must remain closed and not fluoresce (Vet and Marras, 2005). The unique hairpin structure of MBs must follow certain criteria, explained below (and in detail in the Material and Methods section 2.1), to ensure the best possible results. In general, MBs are composed of three distinct but equally important, parts. The first part is the loop, which is usually between 15-30 nucleotides long and it is the region that hybridizes with the complementary target sequence (Kostrikis et al., 1998). The second part is the stem, that is comprised by 5 to 8 base pairs and is rich in GC (Guanine and Cytosine) content. The stem dissociates during the formation of the beacon-target hybrid (Li et al., 2008). The third is the fluorophore attached to the 5' end and a quencher to the 3' end (Monroy-Contreras and Vaca, 2011). In the absence of the correct target, MB remains in a closed state. Because the 5' fluorophore is located next to the 3' quencher during the closed state of the MB, no fluorescence is observed (Bonnet et al., 1999, Monroy-Contreras and Vaca, 2011). However, in the presence of the target, the hairpin structure of the MB opens and creates a hybrid with the complementary target sequence. This reorganization of the MB causes the separation of the fluorophore from the quencher, and because of this, the molecule exhibits fluorescence (Bonnet et al., 1999). Due to their high levels of sensitivity and selectivity, they are used for the diagnosis of different diseases (Han et al., 2013). In this study four distinct mismatch-tolerant MBs were developed for a real-time RT-PCR assay, each one targeting a different SARS-CoV-2 gene, S, E, M and N.

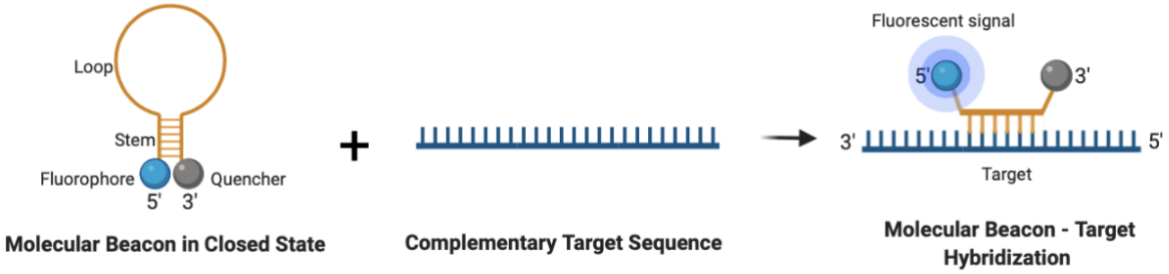

Figure 5. Graphical representation of a molecular beacon probe. The picture on the left shows the molecular beacon in a closed state in the absence of target. Fluorophore is shown in blue, and quencher is shown in grey. The picture in the middle shows the complementary target sequence. The picture on the right represents the hybrid created with the molecular beacon and the target. (Marras et al., 2005). The figure was created with the use of BioRender.com web application.

1.12 Aim of the Study

Due to the continuous evolution and fast spread of SARS-CoV-2, it is imperative to create rapid and accurate detection methods to monitor and prevent the transmission of this virus (Ravi et al., 2020). These detection methods must be validated for their performance on clinical samples before recognised as suitable diagnostic tools for the detection of infection (Garrido, N., 2020). Thus, the aim of this study was based on the design and development of a real-time RT-PCR assay (by the Biotechnology and Molecular Virology laboratory of the University of Cyprus (BMV, UCY)), that employs molecular beacons, to target four different genes of the SARS-CoV-2 virus, the S, E, M and N. Specifically, the validation of the accuracy, sensitivity, and specificity of the assay by two external quality assessments (EQAs), WHO and the Quality Control for Molecular Diagnostics (QCMD), but most importantly the validation of the assay using clinical samples collected from the public diagnostic surveillance performed at the UCY, for the detection of SARS-CoV-2.

2. MATERIALS AND METHODS

2.1 Overview

The design and development of the assay including the MBs and primer design, thermal denaturation profiles, uniplex real-time RT-PCR reactions, external quality assessments (EQAs) and RNA transcripts were completed from personnel of the BMV laboratory (Chrysostomou et al., 2021a); however, it is essential for them to be described in order for the clinical validation methodology of this thesis to be comprehensively explained. Thus, the methodology described here was an important procedure for the assay's later application on clinical samples.

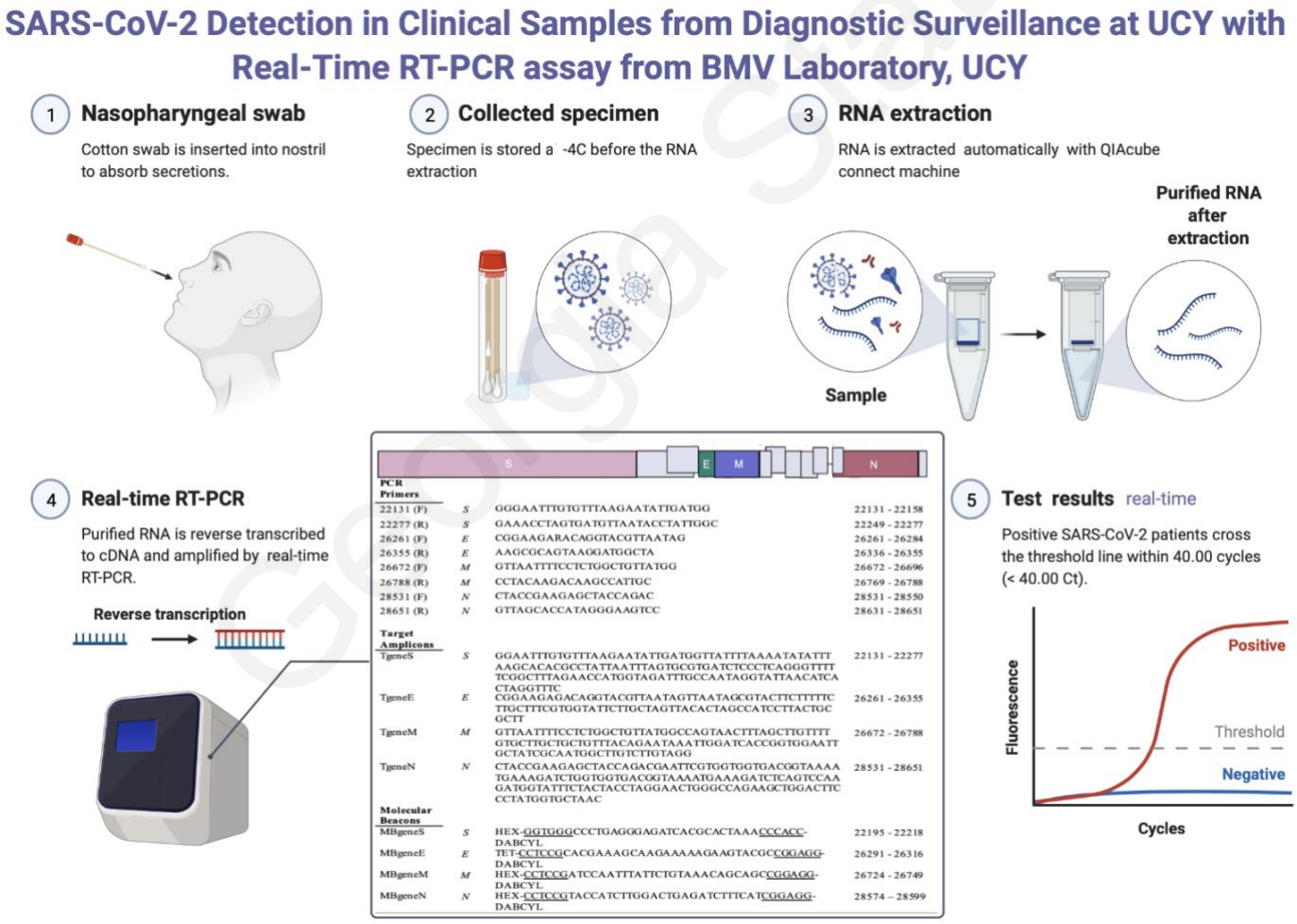

Figure 6. Graphical representation outlining the required methodology conducted during the diagnostic surveillance testing for SARS-CoV-2 at the UCY for its students and personnel.

2.2 Molecular Beacon and Primer Design

All the MB and primer sequences as well as all target amplicons were designed de novo for this study (Table 1). Small sections (~95-147 nucleotides long) of the four major SARS-CoV-2 genes, the S, E, M and N, were targeted for detection by the designed assay (Figure 6). With the use of Geneious® and ClustalW bioinformatics software for sequence data analysis, multiple sequence alignment of both SARS-CoV and SARS-CoV-2 sequences was performed in order to identify appropriate regions of the coronaviruses for detection and to design the oligonucleotides of the assay. The MBs and primers that were designed specifically for the S, M and N genes of SARS-CoV-2 were used as discrimination tools and this was achieved by identifying genomic regions that display the maximum genetic divergence between the two coronaviruses used in the alignment. However, the MB and primers designed for the E gene of the virus were used to identify both SARS-CoV and SARS-CoV-2 sequences because of the conserved character of the E gene among the two coronaviruses.

MBs which are fluorescent-labelled oligonucleotides range in length between 25 to 35 nucleotides depending on their purpose and are composed of a loop, a stem, a 5' fluorophore and a 3' quencher. The loop of the MBs of this assay was designed to contain 24-26 nucleotides. The reason of this, is because the MBs for this assay aimed to be mismatch tolerant. By means, be able to recognize the target amplicon despite the emergence of future mutations in the specific region of the design, however, without losing its specificity towards the target. Consequently, this is achievable with longer loops that form stronger hybrids with the targets. The loop section of the beacons was also designed to be rich in Guanine-Cytosine (GC) content. The stronger hydrogen bonds between these two bases (compared with bonds formed between Adenine and Thymine) enhance the durability and stability of the hybrids. High GC content was also considered during the design of the stem part of MBs. Stems or "arms" of MBs are usually between 5-7 nucleotides long and are created by intramolecular hybridization. In this specific assay, the stems were designed to be six nucleotides long in all MBs with a GC content of approximately ~85%. The MBs were designed intentionally with high GC content to ensure that in the absence of the target, they will remain close and non-fluorescent. For the 5' fluorophore a combination of fluorescent dyes was used. For the MBs detecting the S, M and N gene, the N-HEX-6-aminohexanol (HEX) fluorophore was selected. For the E gene the N-TET-6-aminohexanol (TET) fluorescent dye was

used. For the 3' quencher which is a nonfluorescent dye attached the 3' end of the MBs, N-[4-(4-dimethylamino) phenylazo] benzoic acid (DABCYL) was used for the S, E, M, N genes. Each MB was named accordingly to the gene they were designed and targeted for in the assay (e.g., MBgeneS) (Table 1). The structure, folding and thermodynamic characteristics of all the designed MBs were inspected through the Mfold DNA folding web server (http://www.unafold.org/mfold/applications/dna-folding-form.php). The melting temperature (Tm) of each gene target was calculated with the help of the OligoAnalyzer tool of Integrated DNA Technologies (IDT) (https://www.idtdna.com/calc/analyzer).

The primers were designed to be 20-29 nucleotides long and rich in GC content. The reason for designing primers with high GC content is the same as described before for the MBs design. Despite, MBs purpose to be mismatch tolerant, primers were designed to precisely detect SARS-CoV-2 (MN908947). All the primers were named based on their 5' end binding position on the SARS-CoV-2 pathogenic strain (MN908947.3) used in the multiple sequence alignment. The Tm for the primers were also estimated with the use of the Oligo Analyzer tool of IDT (https://www.idtdna.com/calc/analyzer).

MBs and primers were inspected for possible homodimer (primer-primer and beacon-beacon) and heterodimer (forward primer – reverse primer and beacon-primer) formation through the OligoAnalyzer tool of the IDT. The MBs for this assay were manufactured by LGC Biosearch Technologies (Risskov, Denmark) while, primers together with the target amplicons were synthesised by LGC Biosearch Technologies (Risskov, Denmark) and Macrogen Europe (Amsterdam, The Netherlands). Each MB and primer arrived in a lyophilised form as ssDNA and then they were reconstituted by adding an appropriate volume of nuclease-free water as suggested by the manufacturer to prepare a stock solution of concentration 100 picomole/µl. Subsequently, the beacons and primers were further diluted to working solutions.

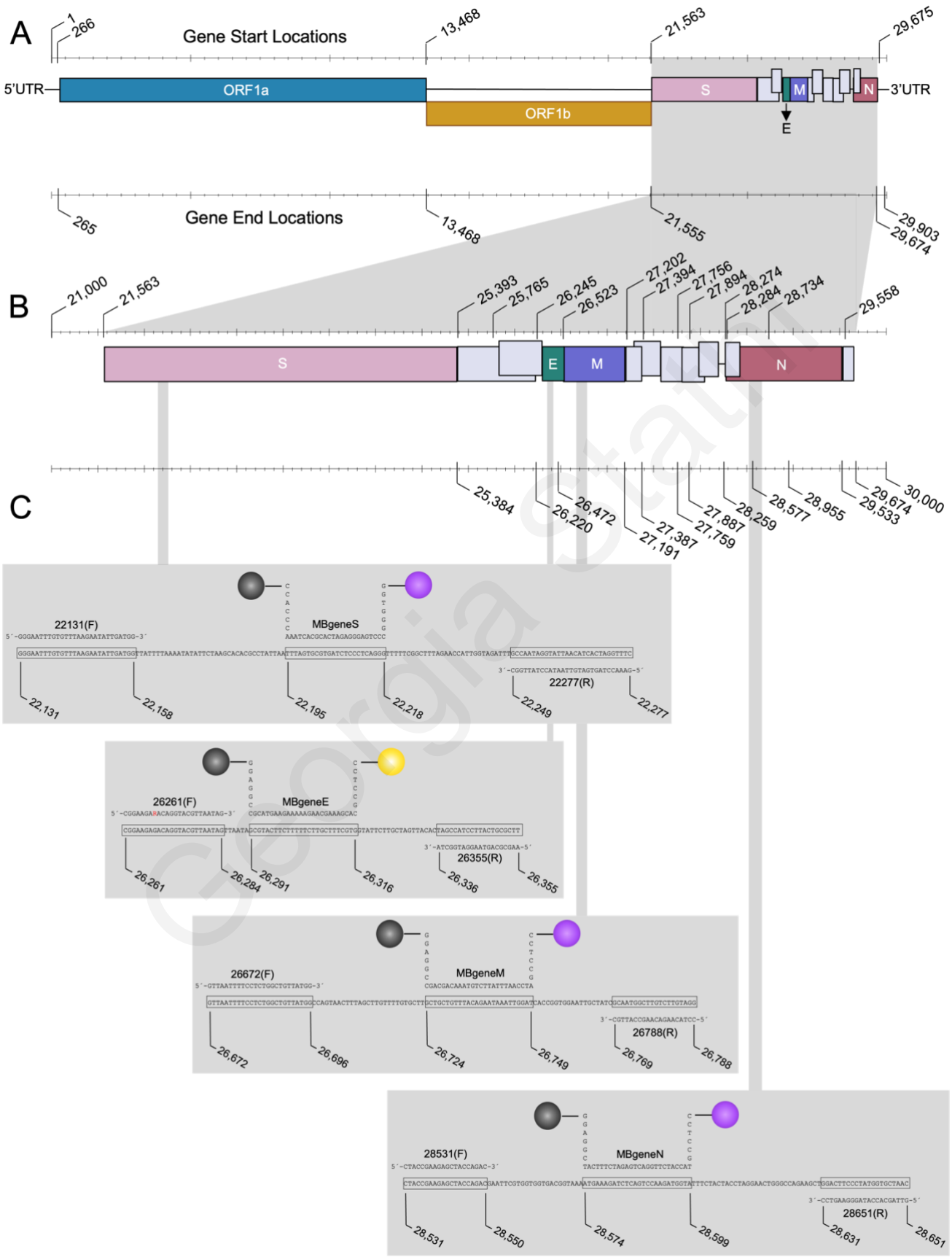

Figure 7. Graphical representation of the SARS-CoV-2 RNA genome used for the design of the assay. **A.** The genome order of SARS-CoV-2 with designated the major structural proteins of the virus. The genomic sequence was obtained from GenBank with accession number MN908947.3. The numbers above and below of the coloured bars indicate the start and end of the depicted areas. The grey shaded area represents the region that the designed assay was based on. **B.** The four structural proteins of SARS-CoV-2, S, E, M and N in a magnified view. **C.** In grey boxes are viewed more magnified specific target sequences of the four gene S, E, M and N of SARS-CoV-2 integrated in the developed assay. All the designed sequences of molecular beacons and forward primers are depicted in the figure above the amplicon sequence, while the sequences related to the reverse primers are positioned below the amplicon sequence. The target sequences of the primers and molecular beacons are presented in the frames. The purple sphere represents the fluorophore N-HEX-6-aminohexanol (HEX) which is attached to the 5' end of the molecular beacons for S, M and N. The yellow sphere signifies the N-TET-6-aminohexanol (TET) fluorophore that was attached to the 5' end of the molecular beacon of E gene. The black spheres indicate the quencher N-[4-(4-dimethylamino) phenylazo] benzoic acid (DABCYL) attached on the 3' end of each molecular beacon. The figure was adapted from the Chrysostomou et al., 2021a.

Table 1. Oligonucleotides designed for PCR. The table depicts the oligonucleotide sequences including PCR primers, target amplicons and molecular beacons that were used in real-time PCR assay. Moreover, the position of the oligonucleotide on the sequence used as a template for the designed and amplicon length in nucleotides are present. The parenthesis in the designation of the PCR primers indicate the orientation of the primer (F: forward, R: reverse). The underlined regions in the sequence of MBs designate the stems while the HEX and TET denote the different fluorescent dyes used in the design of the MBs. The table was adapted from the Chrysostomou et al., 2021a.

Designation	Target Gene	Sequence	Position	Amplicon Length (nts)
PCR Primers				
22131 (F)	*S*	GGGAATTTGTGTTTAAGAATATTGATGG	22131 - 22158	
22277 (R)	*S*	GAAACCTAGTGATGTTAATACCTATTGGC	22249 - 22277	
26261 (F)	*E*	CGGAAGARACAGGTACGTTAATAG	26261 - 26284	
26355 (R)	*E*	AAGCGCAGTAAGGATGGCTA	26336 - 26355	
26672 (F)	*M*	GTTAATTTTCCTCTGGCTGTTATGG	26672 - 26696	
26788 (R)	*M*	CCTACAAGACAAGCCATTGC	26769 - 26788	
28531 (F)	*N*	CTACCGAAGAGCTACCAGAC	28531 - 28550	
28651 (R)	*N*	GTTAGCACCATAGGGAAGTCC	28631 - 28651	
Target Amplicons				
TgeneS	*S*	GGAATTTGTGTTTAAGAATATTGATGGTTATTTTAAAATATATTT AAGCACACGCCTATTAATTTAGTGCGTGATCTCCCTCAGGGTTTT TCGGCTTTAGAACCATGGTAGATTTGCCAATAGGTATTAACATCA CTAGGTTTC	22131 - 22277	147
TgeneE	*E*	CGGAAGAGACAGGTACGTTAATAGTTAATAGCGTACTTCTTTTTC TTGCTTTCGTGGTATTCTTGCTAGTTACACTAGCCATCCTTACTGC GCTT	26261 - 26355	95
TgeneM	*M*	GTTAATTTTCCTCTGGCTGTTATGGCCAGTAACTTTAGCTTGTTTT GTGCTTGCTGCTGTTTACAGAATAAATTGGATCACCGGTGGAATT GCTATCGCAATGGCTTGTCTTGTAGG	26672 - 26788	117
TgeneN	*N*	CTACCGAAGAGCTACCAGACGAATTCGTGGTGGTGACGGTAAAA TGAAAGATCTGGTGGTGACGGTAAAATGAAAGATCTCAGTCCAA GATGGTATTTCTACTACCTAGGAACTGGGCCAGAAGCTGGACTTC CCTATGGTGCTAAC	28531 - 28651	121
Molecular Beacons				
MBgeneS	*S*	HEX-GGTGGGCCCTGAGGGAGATCACGCACTAAACCCACC-DABCYL	22195 - 22218	
MBgeneE	*E*	TET-CCTCCGCACGAAAGCAAGAAAAAGAAGTACGCCGGAGG-DABCYL	26291 - 26316	
MBgeneM	*M*	HEX-CCTCCGATCCAATTTATTCTGTAAACAGCAGCCGGAGG-DABCYL	26724 - 26749	
MBgeneN	*N*	HEX-CCTCCGTACCATCTTGGACTGAGATCTTTCATCGGAGG-DABCYL	28574 – 28599	

2.3 Thermal Denaturation Profiles of Molecular Beacons

The thermal denaturation profiles of the MBs of the in-house molecular beacon-based real-time RT-PCR assay were done by the BMV laboratory of UCY. The basic methodology is presented here because it contributed to the later application of the assay for detection of SARS-CoV-2 in clinical samples obtained from the diagnostic surveillance at UCY. The thermodynamic characteristics of all the molecular beacons used in the study were tested by melting curve analysis which was performed on a 7900HT Fast Real-Time PCR System (Applied Biosystems, Foster City, USA). A range of molecular beacon concentrations were used to determine the optimal fluorescence which must be neither saturating nor too low. Each target was received in lyophilized form as a ssDNA and the specific volume of nuclease free water was added, as recommended by the manufacturer, to prepare a stock solution of concentration 100 picomole/μl. The volume of each melting curve reaction was 25 μl. Two distinct master mixes were prepared for each beacon, one with no target and one with the correct target. The master mix with no target consisted of 1.5 μl of $MgCl_2$ (50 mM), 2 μl of molecular beacon and 21.5 μl of dH_2O (Table 2). The reaction with the correct target consisted of 1.5 μl of $MgCl_2$ (50 mM), 2 μl of molecular beacon, 1 μl of a single-stranded oligonucleotide complementary to the target sequence (100 pmol/μl), and 20.5 μl of dH_2O (Table 3). A variety of beacon concentrations were used beginning from 5, then 7.5 and eventually 10 picomole/μl for a total of 10, 15 and 20 picomole per reaction. The PCR cycling parameters comprised of 1 cycle for 2 minutes at 95 °C, then 50 cycles divided in two steps. During the first step, the temperature was set at 80 °C for 30 seconds and in each cycle, there was a decrease by 1 °C, until the temperature of the reaction was 30 °C. Throughout the first step the data collection was conducted. The second step begun again at 80 °C for 10 seconds and decreasing by 1 °C per cycle until the final temperature of 30 °C (Table 4). The fluorescence was recorded after every cycle and was measured at 521 nm for TET, and 535 nm for HEX. After the run was completed, the fluorescence signal data from both reactions were normalized and plotted.

Table 2. Volume of reagents for Melting Curve reaction with no target and total volume of master mix. The table portrays the reagents and the volume of all necessary reagents used in the preparation of the Melting Curve reaction with no target as well as the total volume of the reaction.

Reagents	Volume / Reaction (µl)
$MgCl_2$ (50 mM)	1.5
MBgene (5 pmol/µl)	2.0
dH_2O	21.5
Total Volume	**25.0**

Table 3. Volume of reagents for Melting Curve reaction and total volume of reaction with correct target. The table portrays the reagents and the volume of all necessary reagents used in the preparation of the Melting Curve reaction with correct target as well as the total volume of the reaction.

Reagents	Volume / Reaction (µl)
$MgCl_2$ (50 mM)	1.5
MBgene (5 pmol/µl)	2.0
dH_2O	20.5
Tgene (100 pmol/µl)	1.0
Total Volume	**25.0**

Table 4. Thermocycling conditions for Melting Curve Analysis. The table shows the steps of the Melting Curve Analysis which was performed on a 7900HT Fast Real-Time PCR System (Applied Biosystems, Foster City, USA), the temperatures, the duration of each step and the number of cycle repeats for each step.

Step	Temperature (°C)	Time (min)	Cycle Number
Step 1	95	2:00	1X
Step 2	80 (-1/cycle)	0:30	50X
	80 (-1/cycle)	0:10	

2.4 Real-Time RT-PCR: Uniplex Reaction for S, E, M and N genes

The uniplex reaction for each gene was performed by personnel of the BMV laboratory to check the validity of the developed assay which was later used for the detection of SARS-CoV-2 in clinical samples. Purified SARS-CoV-2 RNA from Coronavirus strain grown in cell culture (BetaCoV/Germany/BavPat1/2020 p.1" grown in cell culture (Charité, Berlin, European Virus Archive goes Global, EVAg)) was used in uniplex reactions as a positive control. The sample arrived in stabilised RNA form, consequently the RNA extraction was not required. The initial concentration of the sample was 10^4 copies/µl and was further diluted to a working concentration of 10^3 copies/µl for the purposes of the reaction. The analysis of the sample was conducted through real-time RT-PCR which was executed on a 7900HT Fast Real-Time PCR System (Applied Biosystems, Foster City, CA, USA) with the use of TaqPath™ 1-Step Multiplex Master Mix (No ROX) (Life Technologies, Frederick, MD, USA). The master mix of the reaction was of total volume of 30 µl and was prepared with 10 µl of RNA, 7.5 µl of 4X TaqPath™ 1-Step Multiplex Master Mix, 1.5 µl of 20 picomole/µl of FW primer, 1.5 µl of 20 picomole/µl of RV primer, 3 µl of 5 picomole/µl molecular beacon and 6.5 µl of dH_2O (Table 5). All the sequences of primers and MBs for all the targeted genes are shown in Table 1. The thermal cycling condition for the reverse transcription included: 1 cycle for 2 minutes at 25 °C for the Uracil-N-glycosylase (UNG) incubation, followed by 1 cycle for 10 minutes at 53 °C for the reverse transcription. Then, 1 cycle for 2 minutes at 95 °C for the reverse transcriptase (RT) inactivation, denaturation of the DNA and activation of polymerase. After that, 5 cycles for 3 seconds at 95 °C, and 30 seconds at 53 °C, at which the annealing step happen. Lastly, another 35 cycles followed at 95 °C for 3 seconds, and 53 °C for 30 seconds, the fluorescence data were collected during the annealing step (Table 6). As mentioned before, for these runs, the positive control used was the purified EVAg strain of SARS-CoV-2. For negative control no-template control (NTCs) was used and replaced the 10 µl of RNA with 10 µl of distilled water (dH_2O). These controls were analysed in duplicate for each reaction and after the end of the run, the fluorescence signal data were normalised and plotted.

Table 5. Volume of reagents for real-time RT-PCR Uniplex reaction for the S, E, M and N genes and total volume of reaction. The table portrays the reagents and the volume of all necessary reagents used in the preparation of the real-time RT-PCR Uniplex reaction for the genes S, E, M and N as well as the total volume of the reaction.

Reagents	Volume / Reaction (µl)
RNA (10^3)	10.0
4X TaqPath™ 1-Step Multiplex Master Mix	7.5
MBgene (5 pmol/µl)	3.0
FW primer (20 pmol/µl)	1.5
RV primer (20 pmol/µl)	1.5
dH_2O	6.5
Total Volume	**30.0**

Table 6. Thermocycling conditions for real-time RT-PCR Uniplex reaction for the S, E, M and N genes. The table shows the steps which were performed on a 7900HT Fast Real-Time PCR System (Applied Biosystems, Foster City, USA), the temperatures, the duration of each step and the number of cycle repeats for each step.

Step	Temperature (°C)	Time (min)	Cycle Number
UNG Incubation	25	2:00	1X
Reverse Transcription	53	10:00	1X
RT Inactivation, Initial Denaturation and DNA Polymerase Activation	95	2:00	1X
Annealing	95 53	0:03 0:30	5X
Annealing/ Data Collection	95 **53** **(data collection)**	0:03 **0:30**	35X

2.5 External Quality Assessment for Validation of the Assay

For the validation of the developed assay, samples were sent from different organisations to be analysed and to evaluate the assay's ability to detect SARS-CoV-2 with the use of molecular beacon method. The BMV laboratory has registered in two EQAs organized by the QCMD and WHO. The EQAs were completed by the BMV laboratory as a validation step before the assay was applied on clinical samples.

The EQA from WHO (WHO EQAP for the Detection of SARS-CoV-2 by RT-PCR (2020)) provided a panel of five blinded samples including SARS-CoV-2 RNA in different concentrations and other currently circulating human coronaviruses. Additionally, the testing panel also included a positive control of SARS-CoV-2. The lyophilised samples were stored in -80 °C until further use as per the instruction of WHO. The samples were reconstituted prior to their use by adding 50 µl of dH_2O in order to be used in real-time RT-PCR for detection of SARS-CoV-2. The samples were treated as clinical material and tested according to the in-house developed method. The reagents and volume of reagents used in real-time RT-PCR was the same as the uniplex reaction described before. The thermocycling conditions for real-time RT-PCR reaction performed on the samples were also kept the same as the uniplex reaction aforementioned.

The EQA program from QCMD (QCMD 2020 Coronavirus Outbreak Preparedness EQA Pilot Study) provided a panel of total eight vials containing frozen transport medium samples with various concentrations of Coronavirus or samples negative for Coronavirus. The samples arrived in a transport medium and were stored in the laboratory at -20 °C until used as per the instruction of QCMD. All of the samples were treated as clinical material and analysed with the use to the in-house developed assay. RNA extraction for the isolation of the viral RNA was completed for the samples, with the use of the QIAmp Viral RNA Mini Kit (Qiagen, Hilden, Germany) and an automated QIAcube Connect machine (Qiagen, Hilden, Germany). However, the steps for this method are described later in the clinical samples section (2.6). The reagents and volume of reagents used in real-time RT-PCR was the same as the uniplex reaction described before (Table 5). The thermocycling conditions for real-time RT-PCR reaction performed on the samples were also kept the same as the uniplex reaction aforementioned (Table 6).

Furthermore, for the EQA testing panels a positive control, the purified SARS-CoV-2 RNA from Coronavirus strain grown in cell culture (BetaCoV/Germany/BavPat1/2020 p.1" grown in cell culture (Charité, Berlin, European Virus Archive goes Global, EVAg)) was used for each reaction.

2.6 RNA Transcripts

The generation of RNA transcripts as a validation method for the accuracy and sensitivity of the developed assay was originally produced from an undergraduate student of the laboratory, Ms. Christina Papa, during her experimental thesis "Synthetic RNA transcripts for the test and evaluation of a molecular-beacon-based multi allelic real-time RT-PCR assay for the detection of SARS-CoV-2" presented in June 2021. Nonetheless, the methodology is briefly described here because of their later use as positive controls in the analysis of the clinical samples with the in-house developed assay.

For each gene targeted by the assay, synthetic RNA transcripts were generated by in vitro transcription with the use of the MEGAscript T7 transcription kit following the instructions of the manufacturer (Ambion, Houston, TX, USA). A template for the RNA transcription is required to have a double stranded DNA with incorporated T7– promoter recognition site to be transcribed. dsDNA templates were produced using PCR with FW primers (Table 1). The 5' end of the FW primers included the bacteriophage T7 RNA polymerase/promoter system (TAATACGACTCACTATAGG) that is responsible for generating RNA transcripts for each gene target. Because purified SARS-CoV-2 RNA from Coronavirus strain grown in cell culture (BetaCoV/Germany/BavPat1/2020 p.1" grown in cell culture (Charité, Berlin, European Virus Archive goes Global, EVAg)), was used to produce the RNA transcripts for the S, E, M and N genes, RT-PCR was performed.

The total volume of each RT-PCR reaction was 50 μl. The master mix consisted of 25.0 μl of 2X platinum SuperFi RT-PCR Master Mix from the SuperScript IV One-Step RT-PCR System (Thermo Fisher Scientific, Waltham, MA, USA), 12.5 μl of nuclease-free water, 1 μl of 20 picomole/μl of FW primer, 1 μl of 20 picomole/μl of RV primer, 0.5 μl of SuperScript IV RT Mix

(Thermo Fisher Scientific, Waltham, MA, USA) and 10 µl of 10^3 copies per µl of SARS-CoV-2 RNA (Table 7). As the first step of the RT-PCR, RNA was incubated to break its secondary structures (Table 8). The incubation was carried out at 70 °C for 20 seconds and after its completion, the RNA was placed on ice for 1 minute to stabilise. The cycling parameters of the RT-PCR included 1 cycle for 10 minutes at 50 °C for the reverse transcription step. Then, 1 cycle for 2 minutes at 98 °C for the deactivation of reverse transcription and initial denaturation step. Followed by the amplification, which was in total 40 cycles divided into three steps: the first step 10 seconds at 98 °C, the second step ranged in temperatures which were specific for each target gene 53–56 °C (S: 55 °C, E: 56 °C, M: 53 °C, N: 54 °C) for 10 seconds and the third step 30 seconds at 72 °C. The final extension, for 1 cycle of 72 °C for 5 minutes (Table 9).

Table 7. Components of the master mix and total volume per reaction for the SuperScript IV One-Step RT-PCR System Master Mix by Thermo Fisher Scientific. The table presents reagents of the reaction as well as the volume for each reagent included in the master mix for the SuperScript IV One-Step RT-PCR System Master Mix by Thermo Fisher Scientific.

Reagents	Volume / Reaction (µl)
2X platinum SuperFi RT-PCR Master Mix	25.0
Nuclease Free Water	12.5
T7-Forward primer (20 µM) or 20 picomoles/ µl	1.0
Reverse primer (20 µM) or 20 picomoles/ µl	1.0
SuperScript IV RT mix	0.5
RNA (10^3 copies/µl)	10.0
Total Volume	**50.0**

Table 8. Reaction conditions for RNA Incubation. The table depicts the temperatures and time in minutes that RNA required in order to unfold and then become stabilised.

Temperature (°C)	Time (min)	Function
70	0:20	RNA unfolding
0 (on ice)	0:30	RNA stabilization

Table 9. Thermocycling conditions for SuperScript IV One-Step RT-PCR System by Thermo Fisher Scientific. The table presents the steps, temperatures, time in minutes and cycle repeats for SuperScript IV One-Step RT-PCR System by Thermo Fisher Scientific.

Step	Temperature (°C)	Time (min)	Cycle Number
Reverse Transcription	50	10:00	1X
RT Inactivation/Initial denaturation	98	2:00	1X
Amplification	98	0:10	40X
	S Gene: 55 E Gene: 56 M Gene: 53 N Gene: 54	0:10	
	72	0:30	
Final Extension	72	5:00	1X
Reaction Stop	4	Indefinitely	Hold

After finishing the RNA transcripts generation, the transcribed RNA products underwent column purification using NucAway™ Spin Columns Mix (Thermo Fisher Scientific, Waltham, MA, USA). Then, the samples in the elution tubes were quantified with the NanoDrop Spectrophotometer "NanoDrop® ND-1000". The measured concentration was re-calculated to copies per µl units and serially diluted. To ensure that there was no DNA contamination in the purified transcripts real-time PCR was performed using the same PCR reagents and thermocycling conditions except the reverse transcription (RT) step. Later, real-time RT-PCR was performed to check that the purified RNA transcripts function as templates for the assay. The RNA transcripts used in the validation step with real-time RT-PCR for the detection of SARS-CoV-2 in clinical samples were diluted to 10^6 copies/µl and 10^3 copies/µl.

2.7 Clinical Samples from Diagnostic Surveillance at UCY

During the diagnostic surveillance testing for SARS-CoV-2 that was conducted at UCY for students and personnel, more than 2000 samples were collected in the period between September 2020 to January 2021. The research performed by the laboratory using the samples was firstly approved by the Cyprus National Bioethics Committee (ΕΕΒΚ ΕΠ 2020.01.192) safeguarding the anonymity of patients through double coded samples. The sampling was completed by the nurses of UCY at the UCY Health Center and sent to the BMV laboratory for analysis within four hours from the collection time. Nasopharyngeal samples were collected with the use of nasopharyngeal swabs (Biocomma, Shenzhen, China), then placed in tubes containing the preservation medium (Biocomma, Shenzhen, China), and stored in the fridge (4 °C) before RNA was extracted. Notably, the method used for sampling was the "pooling method" which requires the adding of swabs from multiple patients into a single tube including the transport medium. For the sampling of the diagnostic surveillance, an average of 5 nasopharyngeal swabs were combined in a single tube. Each tube was then labelled with a number that had no connection with any patient's identity. After the end of the daily sampling process, the tubes containing the samples were placed in a sterilized plastic container and transferred immediately to the Biosafety Level 3 (BL-3) of the BMV laboratory at UCY to be analysed with the in-house molecular beacon-based real-time RT-PCR assay.

2.7.1 Handling of Samples by the BMV laboratory

The moment the samples were transferred to the BL-3 of the BMV laboratory, the preparation process for the RNA extraction begun. The laboratory members were trained and aware of the protective measures to avoid possible infection from the samples. Also, to protect their safety each laboratory member entering the BL-3 was already outfitted with single-use back-fastening lab coat, double gloves, face mask, shoe covers and plastic face shield. The first step of preparation was the external sanitising of the samples with 70% ethanol. For each pooled tube, the sample was vigorously mixed, and 1 ml of sample was transferred with a disposable Pasteur pipette into a clean labelled Eppendorf tube. Eppendorf tubes containing 1 ml of sample were then

centrifuged for 10 minutes at 1500 x g (3758 RPM, Eppendorf centrifuge 5417C). Then, 140 μl of the supernatant was transferred from each sample into a QIAcube tube, while the remaining was relocated into a Cryotube, labelled, and stored in the -80 °C freezer of the laboratory.

2.7.2 RNA Extraction of Clinical Samples

RNA extraction was required in order to isolate the viral genetic material before its detection. The extraction process of the RNA samples was operated in the BL-3 area of the BMV laboratory and particularly in Biological Safety Cabinet Class II (NuAir, USA) hood, in order to avoid infection of laboratory members. For this procedure the QIAmp Viral RNA Mini Kit (Qiagen, Hilden, Germany) and an automated QIAcube Connect machine (Qiagen, Hilden, Germany) were used. Firstly, for the RNA extraction, the lysis step was performed manually in the Biological Safety Cabinet Class II (NuAir, USA) hood. In order to do that, 140 μl of sample was mixed in a 1.5 ml centrifuge tube with 560 μl of AVL (lysis) buffer that contained 5.6 μl RNA carrier and then incubated for 10 minutes before loading to the QIAcube Connect machine. RNA carrier was essential to prevent degradation of the RNA virus and guarantee attachment of the RNA to the QIAamp membrane (QIAamp® Viral RNA Mini Handbook – Qiagen, Germany). The machine was prepped every time for the extraction of RNA and after the loading of the samples, the steps were conducted automatically. Firstly, the machine stopped the lysis by adding 560 μl of absolute ethanol to the mixture. Then, mixing and centrifuging followed from which 630 μl were relocated into a QIAamp mini column. Next, the lysate was centrifuged at 6000 x g (8000 rpm) for 1 minute and by the end of centrifuging the filtrate was discarded. This step was repeated to process the remaining lysate. The filtrate was collected in the reservoir, so no replacement of the collection tube was required. Afterwards, two wash steps followed by adding 500 μl of AW1 wash buffer to the column and then centrifuging at 6000 x g (8000 rpm) for 1 minute. The second wash step with addition of 500 μl of AW2 wash buffer to the column and then centrifuged at 20 000 x g (14 000 rpm) for 3 minutes. Next, for the elution step, the column was transferred into a new 1.5 ml microcentrifuge tube and 60 μl of AVE elution buffer was added to it. The mixture was incubated for 1 minute at room temperature and lastly was centrifuged at 6000 x g (8000 rpm) for

1 minute. Immediately, after the end of the run, the extracted RNA was placed on ice for further processing with the real-time RT-PCR assay and to prevent its degradation.

2.7.3 Real-Time RT-PCR of Clinical Samples

The real-time RT-PCR analysis was performed on a 7900HT Fast Real-Time PCR System (Applied Biosystems, USA), and the reagents volume, total volume of the reaction and thermal cycling conditions were kept the same as in the uniplex reaction for real-time RT-PCR described before. Notably, the samples were tested by one target gene each time and if found positive to SARS-CoV-2 they were confirmed with a second target gene. Also, the positive controls used in every run of the assay were of concentrations 10^3 copies/μl and 10^6 copies/μl. After the end of the run, the fluorescence data was collected, and plotted. It is worth mentioning, that in the case that a "pooled" sample returned positive, it required each participants included in the positive pool to be re-tested individually to determine which of them caused the positive result.

3. RESULTS

The results of the thermal denaturation profiles, uniplex real-time RT-PCR reactions, external quality assessments (EQAs) and RNA transcripts were derived from previous work of the personnel of the BMV laboratory (Chrysostomou et al., 2021); however, it is essential for them to be described in order to present the results of the clinical samples/validation pertinent to this thesis.

3.1 Thermal Denaturation Profiles of Molecular Beacons

The fluorescence data collected from the four MBs of the targeted genes S, E, M and N from the run included both beacon-target hybrids and beacons without the presence of target. The fluorescence data were plotted against the temperature to create the thermal denaturation profiles and to define the optimal temperature of hybridization for the MB with the complementary target sequence.

3.1.1 Thermal Profile of Molecular Beacon for S Gene

In Figure 7, for the S gene, the Tm of the MB alone without the complementary target is nearly 60 °C. In the range of 40-55 °C, the MBs with target hybrid elicited the strongest fluorescence signal compared to the beacon alone. A temperature of 53 °C was selected as the optimal for the real-time RT-PCR reactions, by taking into consideration the peak of the fluorescence signal between the probe alone and the probe-target hybrid but also the Tm of the FW and RV primers designed for the assay. Moreover, the concentration of 15 picomoles per reaction for the MBs was selected as the optimal.

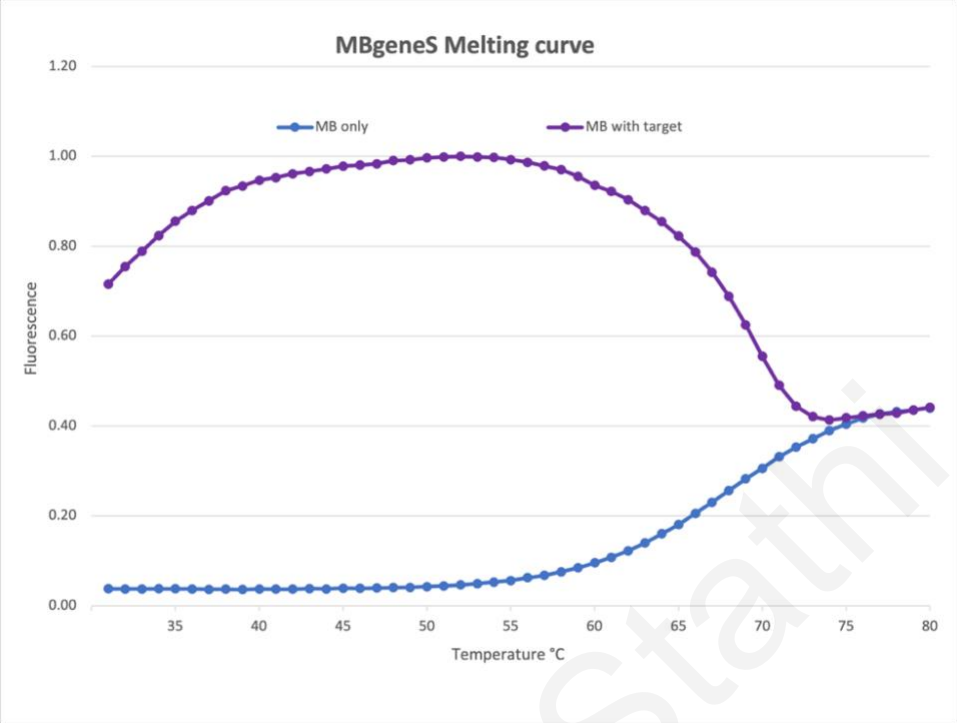

Figure 8. Graphical illustration of the thermal profile of MB for S gene. The fluorescence signal is plotted against temperature. The purple line depicts the molecular beacon-target hybrid, and the blue line depicts the molecular beacon in the absence of target. The data of fluorescence is normalised.

3.1.2 Thermal Profile of Molecular Beacon for E Gene

The fluorescence data plotted against temperature for the targeted gene E is shown in figure 8. As presented in Figure 8, the Tm of the MBs without target is approximately 65 °C. Between the temperatures 35-60 °C it is observed, the strongest fluorescence signal of the hybrid beacon-target, while in the reaction with the beacon alone, no fluorescence signal is detected. The optimal temperature selected for the real-time RT-PCR reaction was 53 °C.

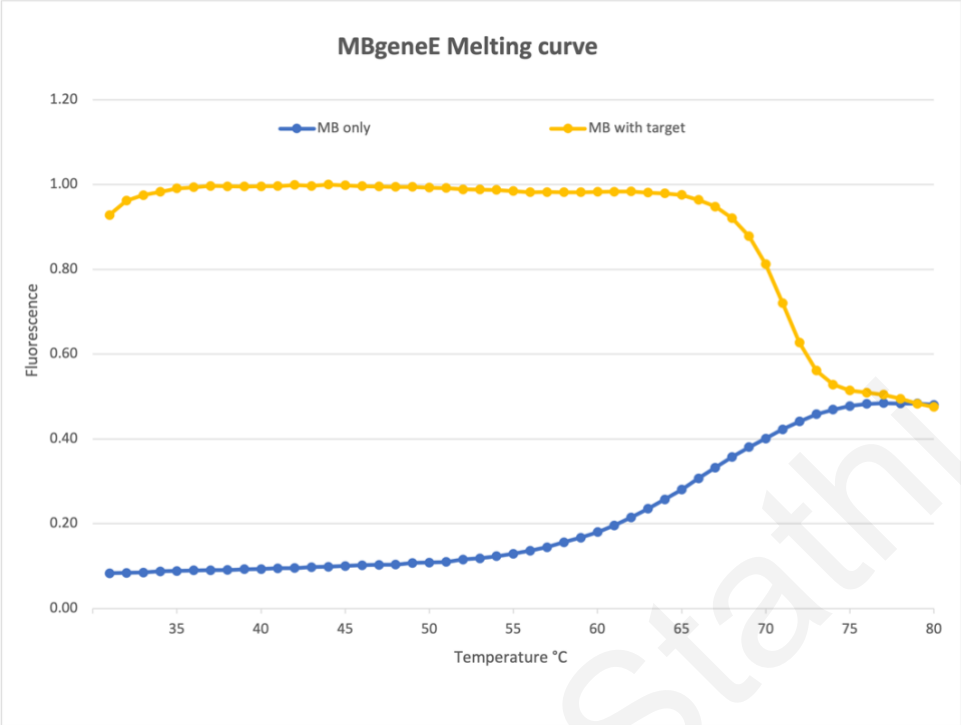

Figure 9. Graphical illustration of the thermal profile of MB for E gene. The fluorescence signal is plotted against temperature. The yellow line depicts the molecular beacon-target hybrid, and the blue line depicts the molecular beacon in the absence of target. The data of fluorescence is normalised.

3.1.3 Thermal Profile of Molecular Beacon for M Gene

The fluorescence data plotted against temperature for the targeted gene M is shown in figure 9. As shown in Figure 9, the Tm of the MBs without target is approximately 60 °C. Between the temperatures 40-55 °C it is observed, the strongest fluorescence signal of the hybrid beacon-target, while in the reaction with the beacon alone, no fluorescence signal is detected. The optimal temperature selected for the real-time RT-PCR reaction was 53 °C.

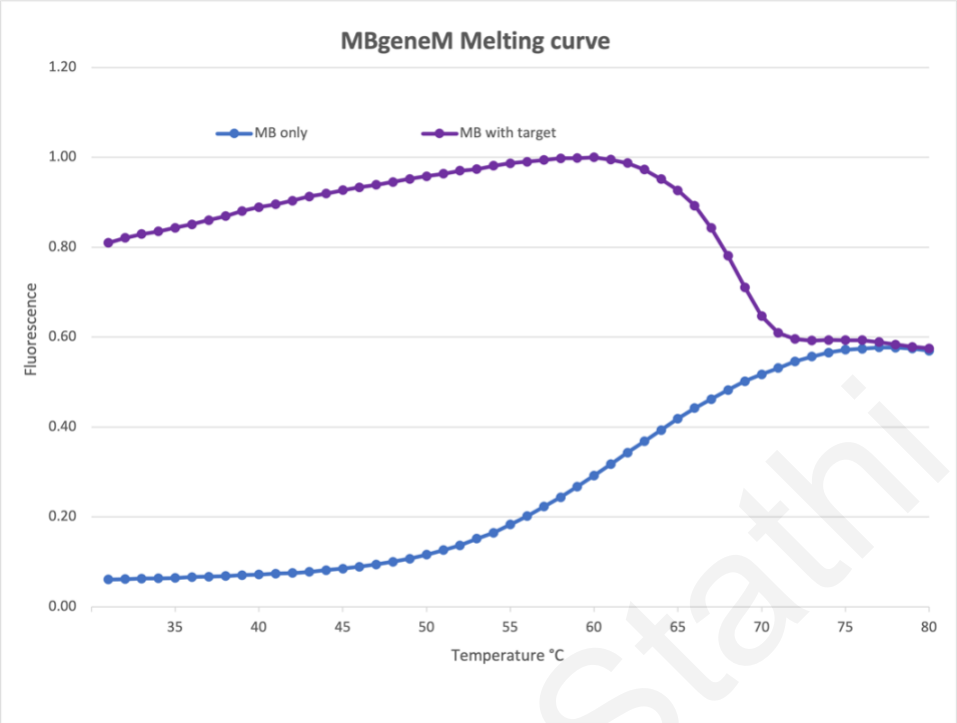

Figure 10. Graphical illustration of the thermal profile of MB for M gene. The fluorescence signal is plotted against temperature. The purple line depicts the molecular beacon-target hybrid, and the blue line depicts the molecular beacon in the absence of target. The data of fluorescence is normalised.

3.1.4 Thermal Profile of Molecular Beacon for N Gene

The fluorescence data plotted against temperature for the targeted gene N is shown in figure 10. As shown in Figure 10, the Tm of the MBs without target is approximately 60 °C. Between the temperatures 40-55 °C it is observed, the strongest fluorescence signal of the hybrid beacon-target, while in the reaction with the beacon alone, no fluorescence signal is detected. The optimal temperature selected for the real-time RT-PCR reaction was 53 °C.

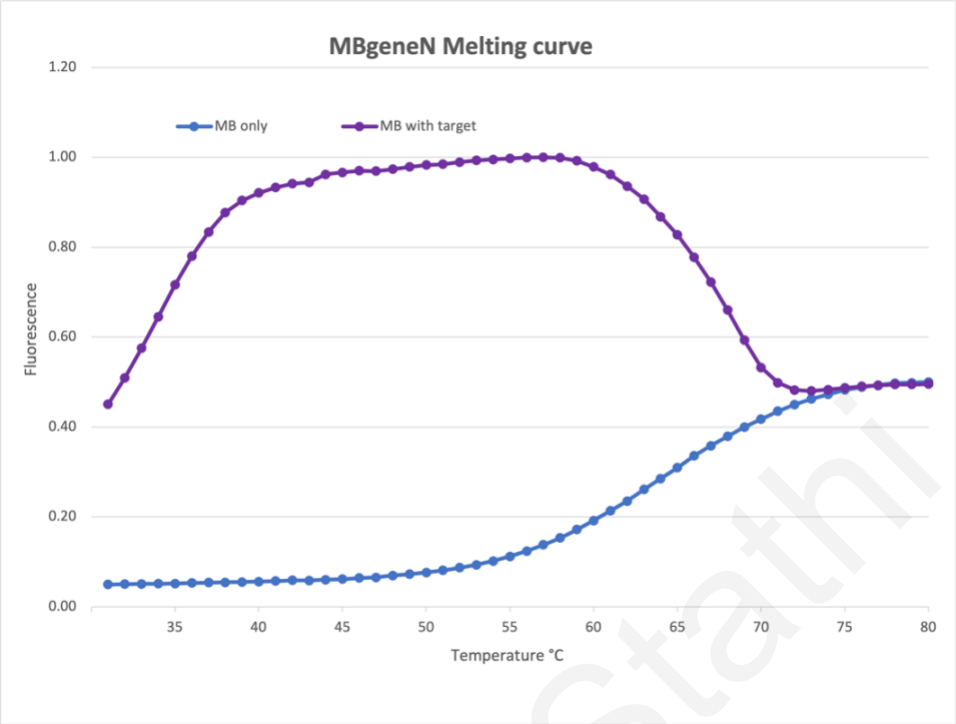

Figure 11. Graphical illustration of the thermal profile of MB for N gene. The fluorescence signal is plotted against temperature. The purple line depicts the molecular beacon-target hybrid, and the blue line depicts the molecular beacon in the absence of target. The data of fluorescence is normalised.

3.2 Real-Time RT-PCR Uniplex Reaction of SARS-CoV-2 Genes

3.2.1 Uniplex real-time RT-PCR Reaction of S gene

The assay was initially tested on purified SARS-CoV-2 RNA from Coronavirus strain grown in cell culture (BetaCoV/Germany/BavPat1/2020 p.1" grown in cell culture (Charité, Berlin, European Virus Archive goes Global, EVAg)). As it is noticeable from Figure 11, the amplification of the target region of gene S was successful, and the designed MB was able to bind to its correct target and emit fluorescence. However, when no target was present neither amplification nor fluorescence was observed. The signal for the S gene sample (10^3/µl) surpassed the threshold line between the cycles 30^{th} to 35^{th}.

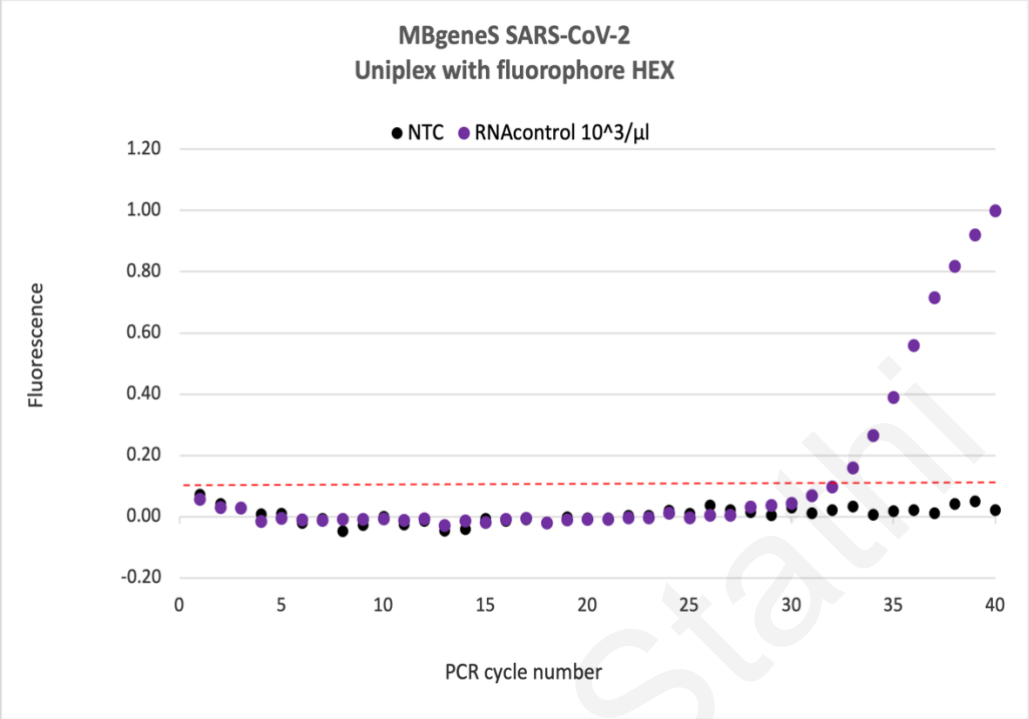

Figure 12. Graphical representation of the uniplex real-time RT-PCR reaction for the S gene of SARS-CoV-2. The fluorescence signal is plotted against the PCR cycles. The figure shows the fluorescence signal of the molecular beacon and its target in purple. The NTC is shown in black. The red line depicts the threshold of the reaction. The data of fluorescence is normalised.

3.2.2 Uniplex real-time RT-PCR Reaction of E gene

In Figure 12, it is noticeable that the amplification of the target region of the E gene was successfully achieved. Consequently, the designed MB was able to hybridize to its correct target and fluoresce. In the absence of target, no amplification nor fluorescence was detected. The E gene sample (10^3/µl) signal surpassed the threshold line at approximately the 30^{th} cycle.

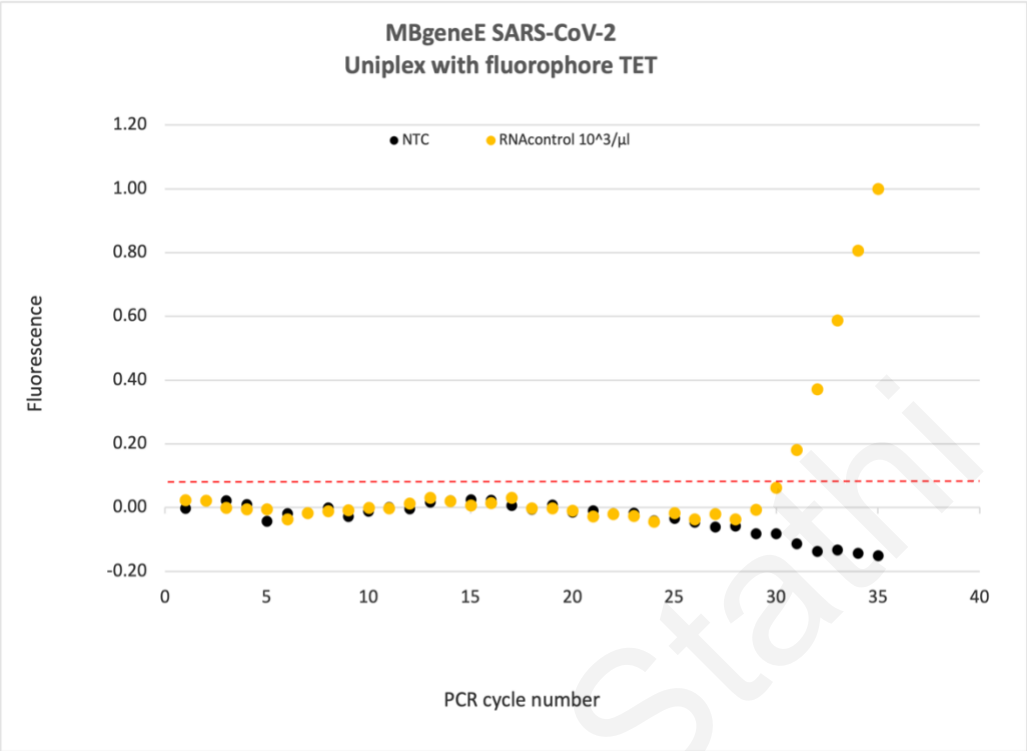

Figure 13. Graphical representation of the uniplex real-time RT-PCR reaction for the E gene of SARS-CoV-2. The fluorescence signal is plotted against the PCR cycles. The figure shows the fluorescence signal of the molecular beacon and its target in yellow. The NTC is shown in black. The red line depicts the threshold of the reaction. The data of fluorescence is normalised.

3.2.3 Uniplex real-time RT-PCR Reaction of M gene

In Figure 13, it is noticeable that the amplification of the target region of the M gene was successfully achieved. Consequently, the designed MB was able to hybridize to its correct target and fluoresce. In the absence of target, no amplification nor fluorescence was detected. The M gene sample (10^3/µl) signal surpassed the threshold line at approximately the 30^{th} to 35^{th} cycle.

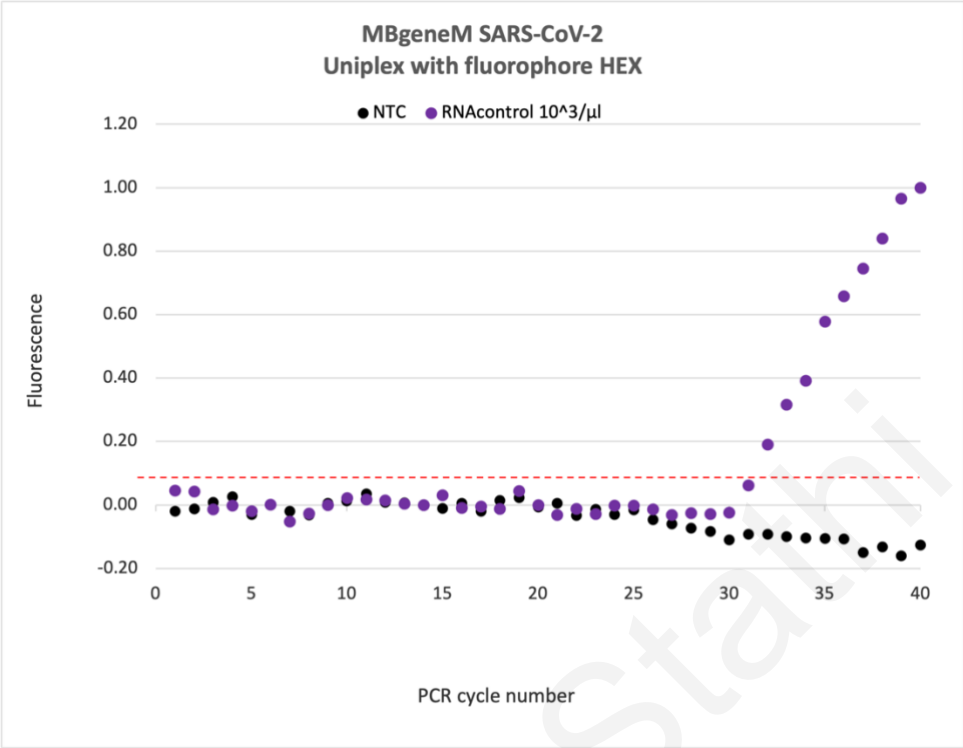

Figure 14. Graphical representation of the uniplex real-time RT-PCR reaction for the M gene of SARS-CoV-2. The fluorescence signal is plotted against the PCR cycles. The figure shows the fluorescence signal of the molecular beacon and its target in purple. The NTC is shown in black. The red line depicts the threshold of the reaction. The data of fluorescence is normalised.

3.2.4 Uniplex real-time RT-PCR Reaction of N gene

In Figure 14, it is noticeable that the amplification of the target region of the N gene was successfully achieved. Consequently, the designed MB was able to hybridize to its correct target and fluoresce. In the absence of target, no amplification nor fluorescence was detected. The N gene sample (10^3/µl) signal surpassed the threshold line at approximately the 25^{th} to 30^{th} cycle.

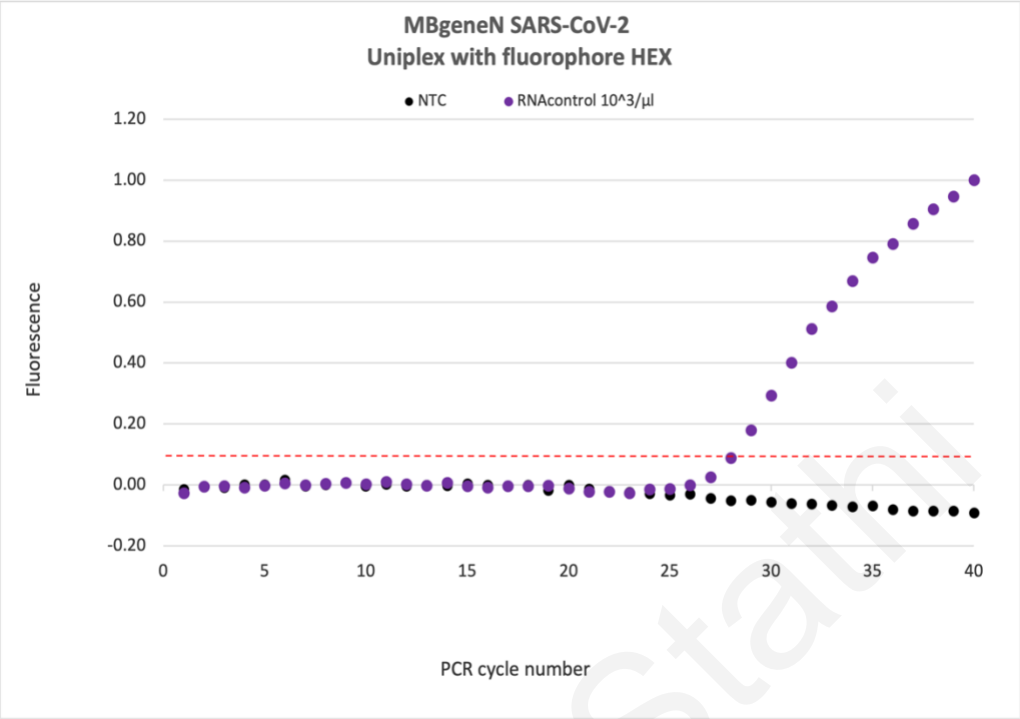

Figure 15. Graphical representation of the uniplex real-time RT-PCR reaction for the N gene of SARS-CoV-2. The fluorescence signal is plotted against the PCR cycles. The figure shows the fluorescence signal of the molecular beacon and its target in purple. The NTC is shown in black. The red line depicts the threshold of the reaction. The data of fluorescence is normalised.

3.3 Assay Validation with External Quality Assessments

The in-house molecular beacon-based real-time RT-PCR assay designed for detection of SARS-CoV-2 by the BMV UCY laboratory was validated by two EQAs, the one from WHO (WHO SARS-CoV-2 EQAP (2020)) and the other one from QCMD (QCMD 2020 Coronavirus Outbreak Preparedness EQA Pilot Study). The developed assay was 100% successful in both EQA panels. Specifically, the blinded panel sent from WHO consisted of lyophilised extracted samples, out of which three samples were SARS-CoV-2 RNA in different concentrations and one human Coronavirus (hCoV) OC43 RNA. The fifth sample was a negative sample. The in-house developed

assay correctly identified all of the blinded samples of SARS-CoV-2 of different concentrations (7.11×10^4, 7.42×10^5 and 1.14×10^6 copies/ml) and the positive control included in WHO panel. Also, the assay did not identify as SARS-CoV-2 the sample containing the human coronavirus (hCoV) OC43 RNA and the negative sample.

Similarly, the assay successfully recognised the blinded samples sent from QCMD which included five samples positive to SARS-CoV-2, two samples with RNA of different Coronaviruses and one negative sample. All five samples with SARS-CoV-2 RNA of different concentration (from ~2×10^2 copies/ml up to ~2×10^5 copies/ml) were recognized from the developed assay. The negative control and the two samples with RNA of different Coronaviruses (hCoV NL63, hCoV OC43) were not identified as SARS-CoV-2 positive by the assay.

Importantly, the purified SARS-CoV-2 RNA from Coronavirus strain grown in cell culture (BetaCoV/Germany/BavPat1/2020 p.1" grown in cell culture (Charité, Berlin, European Virus Archive goes Global, EVAg)) which was added as a positive control and NTC as negative control, were both analysed correctly by the assay. Table 10 presents the results of both EQAs.

Table 10. Real-time RT-PCR results of EQAs from WHO and QCMD. The table depicts the positive control used in the developed assay of purified SARS-CoV-2 RNA from EVAg. Additionally, it shows the ID of specimen analysed of 15 in total samples sent from WHO and QCMD for validation of the assay. Also, it presents the outcome of RT-PCR reaction for each sample, for each gene used each time for detection. The table was adapted from Chrysostomou et al., 2021a.

Sample	ID of Specimen Analysed	RT-PCR Result			
		S	E	M	N
EVAg					
1	Purified RNA of SARS-CoV-2 from Coronavirus strain grown in cell culture	✓	✓	✓	✓
WHO					
1	SARS-CoV-2	✓	✓	✓	✓
2	SARS-CoV-2	✓	✓	✓	✓
3	NEGATIVE	-	-	-	-
4	OC43	-	-	-	-
5	SARS-CoV-2	✓	✓	✓	✓
6	Positive Control - SARS-CoV-2	✓	✓	✓	✓
QCMD					
1	SARS-CoV-2	✓	✓	✓	✓
2	NL63	-	-	-	-
3	SARS-CoV-2	✓	✓	✓	✓
4	OC43	-	-	-	-
5	NEGATIVE	-	-	-	-
6	SARS-CoV-2	✓	✓	✓	✓
7	SARS-CoV-2	✓	✓	✓	✓
8	SARS-CoV-2	✓	✓	✓	✓

3.4 Generation of RNA Transcripts for S, E, M and N genes

The initial step of the RNA transcript generation for the S, E, M and N genes, was the creation of dsDNA with incorporated T7, which is a promoter recognition sequence attached to the 5' end of the FW primer designed for the assay, this was achieved with the RT-PCR method. The correct length of the PCR product was verified on 3% agarose gel on which the incorporated T7 sequence was observed. The S, E, M and N gene transcripts were successfully amplified and there was a visible PCR product at the correct length (S:166bp, E:114bp, M: 136bp, N:140bp). Then, the S, E, M and N gene transcripts were validated for their quantity and quality through the NanoDrop Spectrophotometer "NanoDrop® ND-1000" and the outcomes were re-calculated into number of copies per µl unit. The real-time PCR was performed next, and its results revealed no signal or exponential curve in the purified S, E, M and N gene transcripts which ensures that there was no DNA contamination. Lastly, the RNA transcripts were evaluated with real-time RT-PCR as a confirmation of their amplification and their ability to be detected through the in-house molecular beacon-based real-time RT-PCR assay. As it is presented in Figure 15, 16, 17 and 18 the produced RNA transcripts were successfully amplified and detected during real-time RT-PCR.

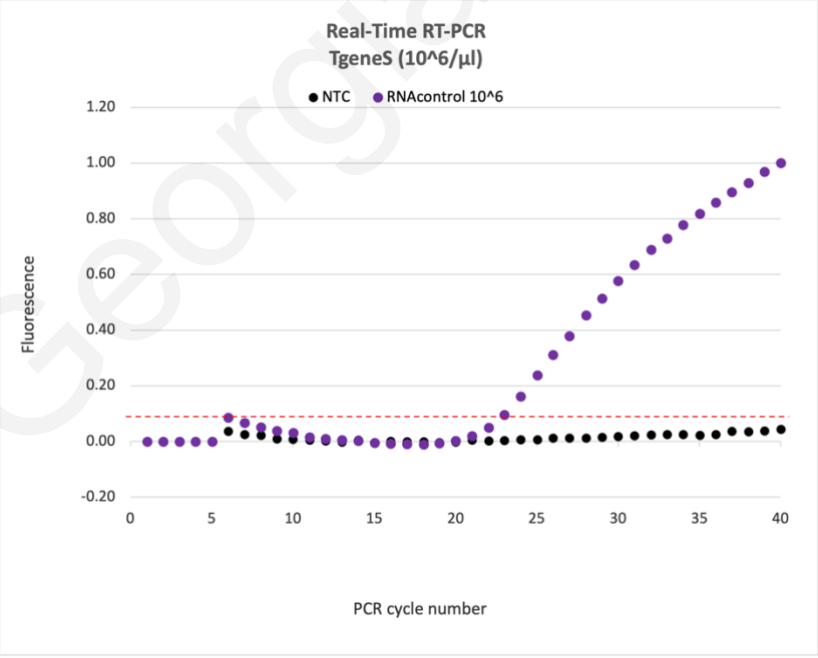

Figure 16. Graphical representation of the real-time RT-PCR reaction of the S gene Transcript. The fluorescence signal is plotted against the PCR cycles. The concentration of the S gene transcript is 10^6 copies/µl. The figure shows the fluorescence signal of the transcript in purple. The NTC is shown in black. The red line depicts the threshold of the reaction. The S gene Transcript surpasses the threshold line between the cycles 20^{th} - 25^{th}. The data of fluorescence is normalised.

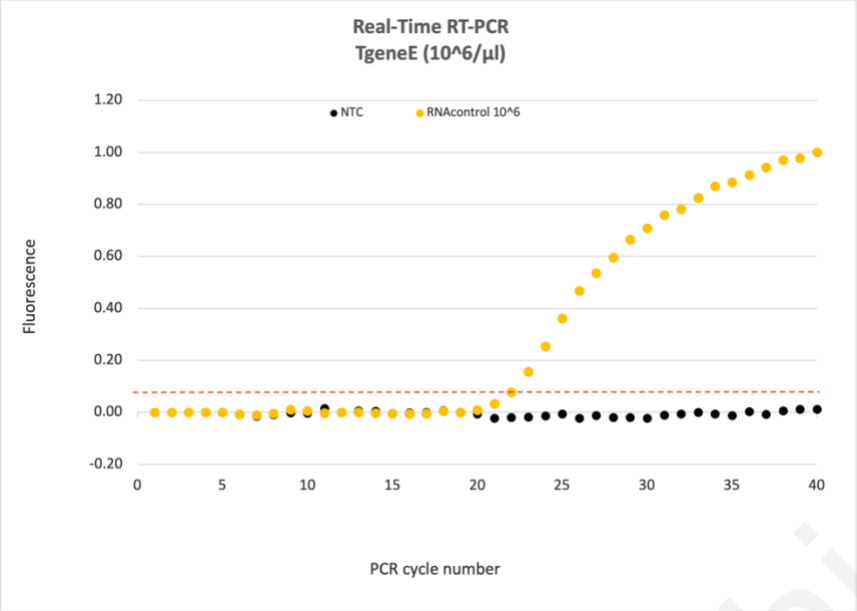

Figure 17. Graphical representation of the real-time RT-PCR reaction of the E gene Transcript. The fluorescence signal is plotted against the PCR cycles. The concentration of the E gene transcript is 10^6 copies/µl. The figure shows the fluorescence signal of the transcript in yellow. The NTC is shown in black. The red line depicts the threshold of the reaction. The E gene Transcript surpasses the threshold line between the cycles 20^{th} - 25^{th}. The data of fluorescence is normalised.

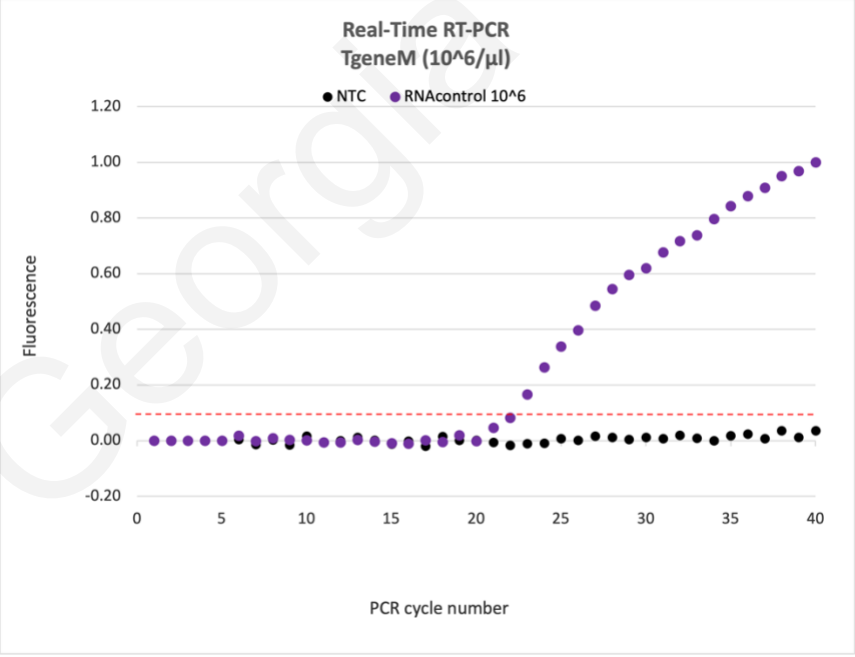

Figure 18. Graphical representation of the real-time RT-PCR reaction of the M gene Transcript. The fluorescence signal is plotted against the PCR cycles. The concentration of the M gene transcript is 10^6 copies/µl. The figure shows the fluorescence signal of the transcript in purple. The NTC is shown in black. The red line depicts the threshold of the reaction. The M gene Transcript surpasses the threshold line between the cycles 20^{th} - 25^{th}. The data of fluorescence is normalised.

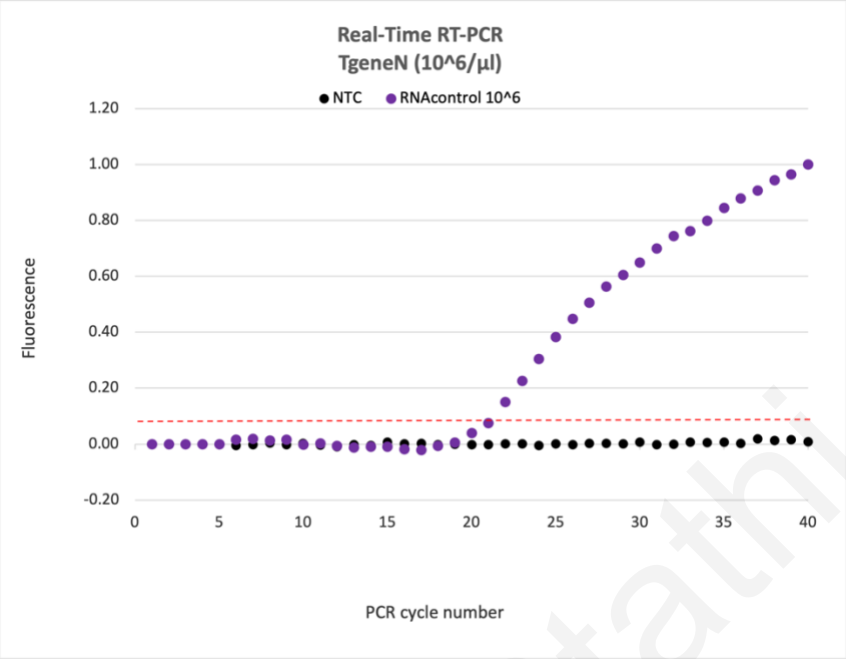

Figure 19. Graphical representation of the real-time RT-PCR reaction of the N gene Transcript. The fluorescence signal is plotted against the PCR cycles. The concentration of the N gene transcript is 10^6 copies/µl. The figure shows the fluorescence signal of the transcript in purple. The N gene Transcript surpasses the threshold line between the cycles 20^{th} - 25^{th}. The NTC is shown in black. The red line depicts the threshold of the reaction. The data of fluorescence is normalised.

3.5 Real-time RT-PCR Testing of Clinical Samples

Throughout the diagnostic surveillance for detection of SARS-CoV-2 that was conducted by the UCY for its students and personnel as part of the Surveillance program, 2231 individuals were tested between the period of September 2020 to January 2021. The samples were examined with the in-house developed mismatch-tolerant molecular beacon-based real-time RT-PCR assay by the "pooling" method. In total, 534 reactions were completed with more than 400 pooled samples and approximately 5 swabs per pool were examined, from which 22 pooled samples were found positive and were re-examined individually (Table 11). From the second individual testing, 15 samples came out positive through real-time RT-PCR and one sample was found positive from antigen rapid test.

The sample testing was conducted with a maximum of twelve pooled samples each time, which were examined on a specific gene produced in the assay (S, E, M or N). Moreover, in each reaction, two positive controls were used, corresponding to the correct target gene that the samples were examined for (Figure 19). In the beginning of the testing of clinical samples, the low positive control used in the real-time RT-PCR was the purified SARS-CoV-2 RNA from Coronavirus strain grown in cell culture (BetaCoV/Germany/BavPat1/2020 p.1" grown in cell culture (Charité, Berlin, European Virus Archive goes Global, EVAg)) in the concentration of 10^3 copies/µl which represents 10^4 RNA copies in reaction. As high positive control, it was used the suitable RNA transcript produced by the BMV laboratory in a 10^6 copies/µl concentration which represents 10^7 RNA copies in reaction (Table 12,13). The average threshold cycle calculated for the positive controls was: 31.7 Ct ± 1.7 for the low positive control and 21.6 Ct ± 1.1 for the high positive control (Tables 12-13).

However, when a sample was detected by the in-house molecular beacon-based real-time RT-PCR assay as positive, the participants were invited for individual re-examination on the following day (Figure 20). In each re-testing, the individual samples were analysed again by the assay and if were found again positive, then a second target was used as a confirmation tool. A sample was considered positive if it exceeded the threshold line before cycle 40^{th}, nonetheless, the samples surpassing the threshold line between the cycles 35^{th} – 40^{th} were considered borderline positive. The threshold cycle (Ct) represents the cycle number at which the fluorescence signal surpasses the threshold and is detectable over and above the background signal. The average Ct for the clinical samples was 31.5 Ct ± 6.8 (Tables 11).

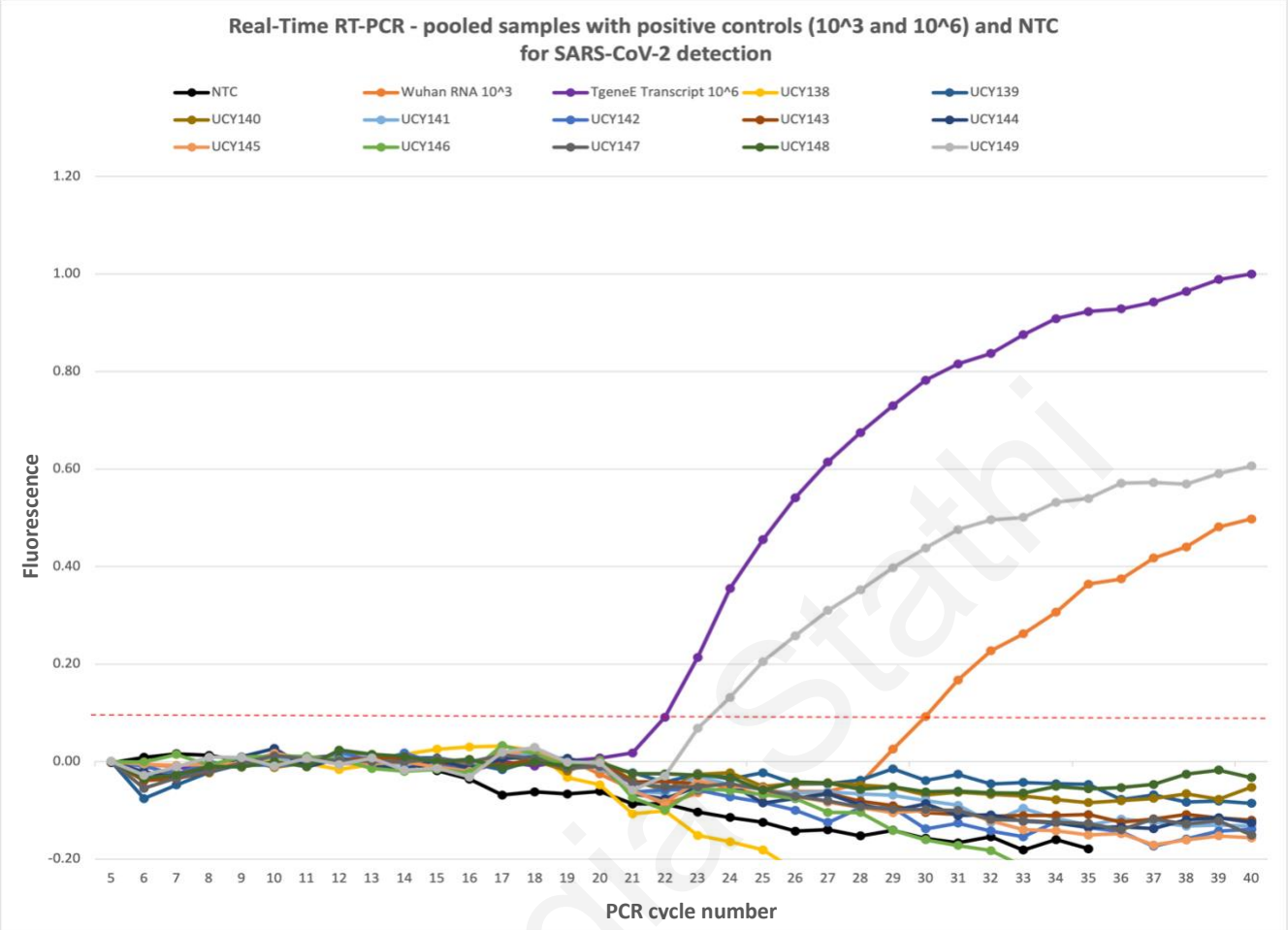

Figure 20. Graphical representation of an example of the real-time RT-PCR reaction of pooled samples for detection of SARS-CoV-2. The MBgeneE was used for this reaction. The fluorescence signal is plotted against the PCR cycles. The low positive control (10^3 copies/µl) in orange colour and high positive control (10^6 copies/µl) in purple colour are shown (TgeneE). The figure shows the fluorescence signal of the pooled samples in the different colours. An NTC is included in the reaction and is shown in black colour. The red line depicts the threshold of the reaction. The data of fluorescence are normalised.

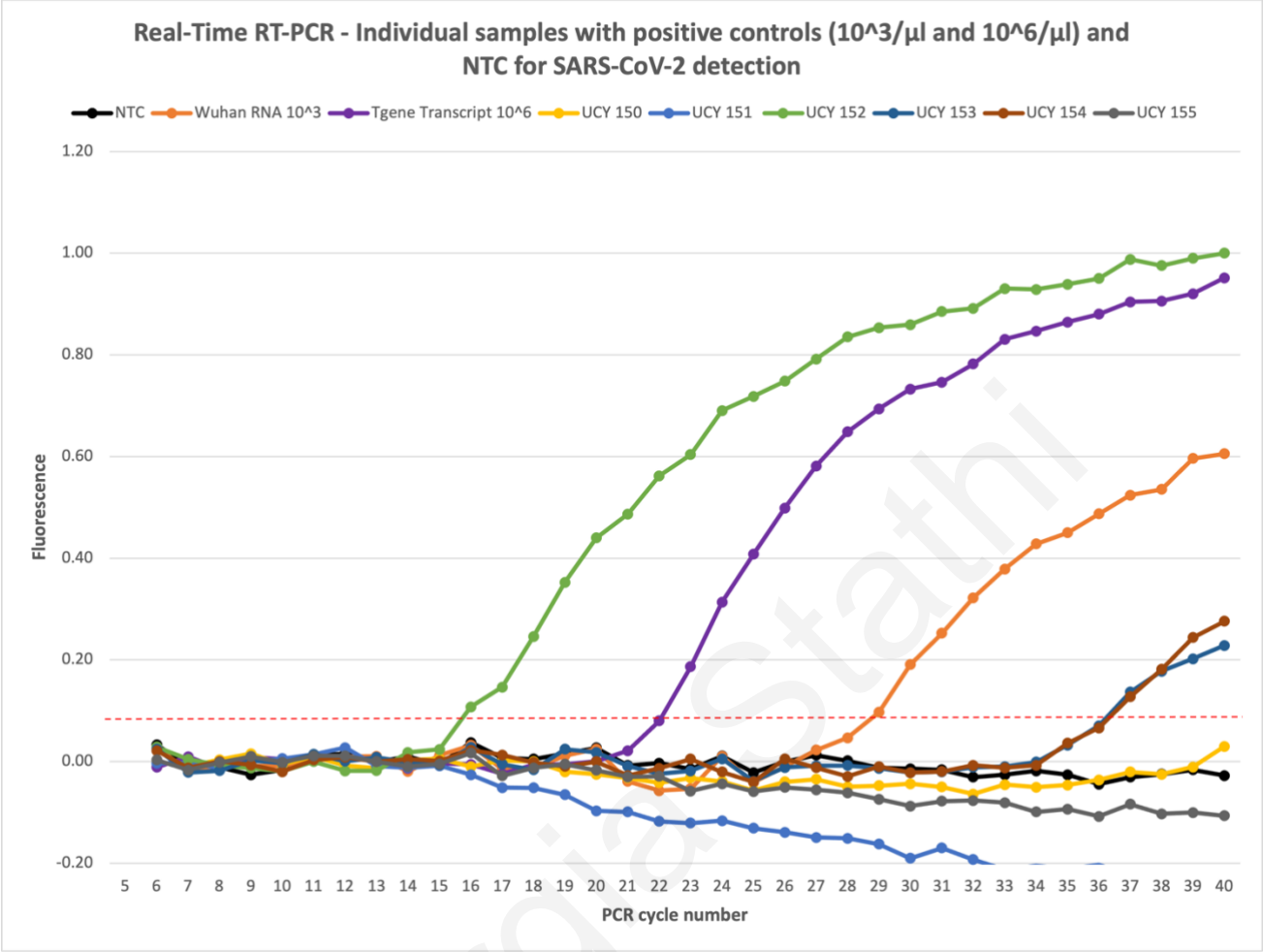

Figure 21. Graphical representation of an example of the real-time RT-PCR reaction of individual samples for detection of SARS-CoV-2. The MBgeneE was used for this reaction. The fluorescence signal is plotted against the PCR cycles. The low positive control (10^3 copies/µl) in orange colour and high positive control (10^6 copies/µl) purple colour are shown (TgeneE). The figure shows the fluorescence signal of the individual samples in the different colours. An NTC is included in the reaction and is shown in black colour. The red line depicts the threshold of the reaction. The data of fluorescence is normalised.

Table 11. Real-time RT-PCR results of clinical samples from the diagnostic surveillance at the UCY. The first column of the table depicts the lab ID of both pooled samples and individual samples after being double coded. The second column shows the number of samples pooled in each tube. Moreover, it presents the date of sampling at the UCY Health center. Additionally, further columns indicate the target gene used in each reaction along with the Ct values and the result of the analysis. The red colour represents the negative result, the yellow colour shows the positivity of the positive controls used and the green colour the positive result of the sample.

LAB ID	N. OF SAMPLES	DATE OF SAMPLING	E GENE		S GENE		M GENE		N GENE	
			Ct VALUES	RESULT	Ct VALUES	RESULT	Ct VALUES	RESULT	Ct VALUES	RESULT
UCY1	5	18/09/2020	>40	Negative	N/A	N/A	N/A	N/A	N/A	N/A
UCY2	5	18/09/2020	>40	Negative	N/A	N/A	N/A	N/A	N/A	N/A
UCY3	5	18/09/2020	>40	Negative	N/A	N/A	N/A	N/A	N/A	N/A
UCY4	5	18/09/2020	>40	Negative	N/A	N/A	N/A	N/A	N/A	N/A
UCY5	5	18/09/2020	>40	Negative	N/A	N/A	N/A	N/A	N/A	N/A
UCY6	5	18/09/2020	>40	Negative	N/A	N/A	N/A	N/A	N/A	N/A
UCY7	5	18/09/2020	>40	Negative	N/A	N/A	N/A	N/A	N/A	N/A
UCY8	5	18/09/2020	>40	Negative	N/A	N/A	N/A	N/A	N/A	N/A
UCY9	2	18/09/2020	>40	Negative	N/A	N/A	N/A	N/A	N/A	N/A
+ Control (10^3)			30.73	Positive	N/A	N/A	N/A	N/A	N/A	N/A
+ Control (10^6)			22.29	Positive	N/A	N/A	N/A	N/A	N/A	N/A
UCY10	5	22/09/2020	>40	Negative	N/A	N/A	N/A	N/A	N/A	N/A
UCY11	5	22/09/2020	>40	Negative	N/A	N/A	N/A	N/A	N/A	N/A
UCY12	5	22/09/2020	>40	Negative	N/A	N/A	N/A	N/A	N/A	N/A
UCY13	5	22/09/2020	>40	Negative	N/A	N/A	N/A	N/A	N/A	N/A
UCY14	5	22/09/2020	>40	Negative	N/A	N/A	N/A	N/A	N/A	N/A
UCY15	4	22/09/2020	>40	Negative	N/A	N/A	N/A	N/A	N/A	N/A
UCY16	2	22/09/2020	>40	Negative	N/A	N/A	N/A	N/A	N/A	N/A
UCY17	5	22/09/2020	>40	Negative	N/A	N/A	N/A	N/A	N/A	N/A
UCY18	5	22/09/2020	>40	Negative	N/A	N/A	N/A	N/A	N/A	N/A

UCY19	4	22/09/2020	>40	Negative	N/A	N/A	N/A	N/A	N/A	N/A
UCY20	5	22/09/2020	>40	Negative	N/A	N/A	N/A	N/A	N/A	N/A
UCY21	4	22/09/2020	>40	Negative	N/A	N/A	N/A	N/A	N/A	N/A
UCY22	1	22/09/2020	>40	Negative	N/A	N/A	N/A	N/A	N/A	N/A
+ Control (10^3)			31.97	Positive	N/A	N/A	N/A	N/A	N/A	N/A
+ Control (10^6)			32.21	Positive	N/A	N/A	N/A	N/A	N/A	N/A
UCY23	5	23/09/2020	>40	Negative	N/A	N/A	N/A	N/A	N/A	N/A
UCY24	5	23/09/2020	>40	Negative	N/A	N/A	N/A	N/A	N/A	N/A
UCY25	5	23/09/2020	>40	Negative	N/A	N/A	N/A	N/A	N/A	N/A
UCY26	5	23/09/2020	>40	Negative	N/A	N/A	N/A	N/A	N/A	N/A
UCY27	5	23/09/2020	>40	Negative	N/A	N/A	N/A	N/A	N/A	N/A
UCY28	5	23/09/2020	>40	Negative	N/A	N/A	N/A	N/A	N/A	N/A
UCY29	5	23/09/2020	>40	Negative	N/A	N/A	N/A	N/A	N/A	N/A
UCY30	5	23/09/2020	>40	Negative	N/A	N/A	N/A	N/A	N/A	N/A
UCY31	5	23/09/2020	>40	Negative	N/A	N/A	N/A	N/A	N/A	N/A
UCY32	4	23/09/2020	>40	Negative	N/A	N/A	N/A	N/A	N/A	N/A
UCY33	2	23/09/2020	>40	Negative	N/A	N/A	N/A	N/A	N/A	N/A
+ Control (10^3)			31.32	Positive	N/A	N/A	N/A	N/A	N/A	N/A
+ Control (10^6)			31.65	Positive	N/A	N/A	N/A	N/A	N/A	N/A
UCY34	3	24/09/2020	>40	Negative	N/A	N/A	N/A	N/A	N/A	N/A
UCY35	5	24/09/2020	>40	Negative	N/A	N/A	N/A	N/A	N/A	N/A
UCY36	3	24/09/2020	>40	Negative	N/A	N/A	N/A	N/A	N/A	N/A
UCY37	5	24/09/2020	>40	Negative	N/A	N/A	N/A	N/A	N/A	N/A
UCY38	4	24/09/2020	>40	Negative	N/A	N/A	N/A	N/A	N/A	N/A
UCY39	2	24/09/2020	>40	Negative	N/A	N/A	N/A	N/A	N/A	N/A
UCY40	5	24/09/2020	>40	Negative	N/A	N/A	N/A	N/A	N/A	N/A
UCY41	4	24/09/2020	>40	Negative	N/A	N/A	N/A	N/A	N/A	N/A
UCY42	4	24/09/2020	>40	Negative	N/A	N/A	N/A	N/A	N/A	N/A
UCY43	4	24/09/2020	>40	Negative	N/A	N/A	N/A	N/A	N/A	N/A
UCY44	4	24/09/2020	>40	Negative	N/A	N/A	N/A	N/A	N/A	N/A

UCY45	5	24/09/2020	39.20	Positive (borderline)	N/A	N/A	N/A	N/A	N/A	N/A
UCY46	2	24/09/2020	>40	Negative	N/A	N/A	N/A	N/A	N/A	N/A
UCY47	1	24/09/2020	>40	Negative	N/A	N/A	N/A	N/A	N/A	N/A
+ Control (10^3)			31.08	Positive	N/A	N/A	N/A	N/A	N/A	N/A
UCY48	1	25/09/2020	>40	Negative	>40	Negative	N/A	N/A	N/A	N/A
UCY49	1	25/09/2020	>40	Negative	>40	Negative	N/A	N/A	N/A	N/A
UCY50	1	25/09/2020	>40	Negative	>40	Negative	N/A	N/A	N/A	N/A
UCY51	1	25/09/2020	>40	Negative	>40	Negative	N/A	N/A	N/A	N/A
UCY52	1	25/09/2020	>40	Negative	>40	Negative	N/A	N/A	N/A	N/A
+ Control (10^3)			32.05	Positive		N/A	N/A	N/A	N/A	N/A
+ Control (10^6)			21.58	Positive	22.76	Positive	N/A	N/A	N/A	N/A
UCY53	4	25/09/2020	>40	Negative	N/A	N/A	N/A	N/A	N/A	N/A
UCY54	5	25/09/2020	>40	Negative	N/A	N/A	N/A	N/A	N/A	N/A
UCY55	3	25/09/2020	>40	Negative	N/A	N/A	N/A	N/A	N/A	N/A
UCY56	4	25/09/2020	>40	Negative	N/A	N/A	N/A	N/A	N/A	N/A
UCY57	4	25/09/2020	>40	Negative	N/A	N/A	N/A	N/A	N/A	N/A
UCY58	5	25/09/2020	>40	Negative	N/A	N/A	N/A	N/A	N/A	N/A
UCY59	5	25/09/2020	>40	Negative	N/A	N/A	N/A	N/A	N/A	N/A
UCY60	5	25/09/2020	>40	Negative	N/A	N/A	N/A	N/A	N/A	N/A
UCY61	4	25/09/2020	>40	Negative	N/A	N/A	N/A	N/A	N/A	N/A
UCY62	5	25/09/2020	>40	Negative	N/A	N/A	N/A	N/A	N/A	N/A
UCY63	3	25/09/2020	>40	Negative	N/A	N/A	N/A	N/A	N/A	N/A
UCY64	2	25/09/2020	>40	Negative	N/A	N/A	N/A	N/A	N/A	N/A
+ Control (10^3)			31.44	Positive	N/A	N/A	N/A	N/A	N/A	N/A
+ Control (10^6)			22.00	Positive	N/A	N/A	N/A	N/A	N/A	N/A
UCY65	5	29/09/2020	>40	Negative	N/A	N/A	N/A	N/A	N/A	N/A
UCY66	5	29/09/2020	>40	Negative	N/A	N/A	N/A	N/A	N/A	N/A
UCY67	5	29/09/2020	>40	Negative	N/A	N/A	N/A	N/A	N/A	N/A
UCY68	5	29/09/2020	>40	Negative	N/A	N/A	N/A	N/A	N/A	N/A
UCY69	5	29/09/2020	>40	Negative	N/A	N/A	N/A	N/A	N/A	N/A

UCY70	5	29/09/2020	>40	Negative	N/A	N/A	N/A	N/A	N/A	N/A
UCY71	4	29/09/2020	>40	Negative	N/A	N/A	N/A	N/A	N/A	N/A
UCY72	3	29/09/2020	>40	Negative	N/A	N/A	N/A	N/A	N/A	N/A
UCY73	5	29/09/2020	>40	Negative	N/A	N/A	N/A	N/A	N/A	N/A
UCY74	5	29/09/2020	>40	Negative	N/A	N/A	N/A	N/A	N/A	N/A
UCY75	5	29/09/2020	>40	Negative	N/A	N/A	N/A	N/A	N/A	N/A
UCY76	4	29/09/2020	>40	Negative	N/A	N/A	N/A	N/A	N/A	N/A
UCY77	1	29/09/2020	>40	Negative	N/A	N/A	N/A	N/A	N/A	N/A
+ Control (10^3)			31.08	Positive	N/A	N/A	N/A	N/A	N/A	N/A
+ Control (10^6)			20.25	Positive	N/A	N/A	N/A	N/A	N/A	N/A
UCY78	6	02/10/2020	>40	Negative	N/A	N/A	N/A	N/A	N/A	N/A
UCY79	5	02/10/2020	>40	Negative	N/A	N/A	N/A	N/A	N/A	N/A
UCY80	3	02/10/2020	>40	Negative	N/A	N/A	N/A	N/A	N/A	N/A
UCY81	4	02/10/2020	>40	Negative	N/A	N/A	N/A	N/A	N/A	N/A
UCY82	4	02/10/2020	>40	Negative	N/A	N/A	N/A	N/A	N/A	N/A
UCY83	4	02/10/2020	>40	Negative	N/A	N/A	N/A	N/A	N/A	N/A
UCY84	3	02/10/2020	>40	Negative	N/A	N/A	N/A	N/A	N/A	N/A
UCY85	6	02/10/2020	>40	Negative	N/A	N/A	N/A	N/A	N/A	N/A
UCY86	5	02/10/2020	>40	Negative	N/A	N/A	N/A	N/A	N/A	N/A
UCY87	6	02/10/2020	>40	Negative	N/A	N/A	N/A	N/A	N/A	N/A
UCY88	1	02/10/2020	>40	Negative	N/A	N/A	N/A	N/A	N/A	N/A
UCY89	1	02/10/2020	>40	Negative	N/A	N/A	N/A	N/A	N/A	N/A
+ Control (10^3)			31.47	Positive	N/A	N/A	N/A	N/A	N/A	N/A
+ Control (10^6)			20.60	Positive	N/A	N/A	N/A	N/A	N/A	N/A
UCY90	3	06/10/2020	>40	Negative	N/A	N/A	N/A	N/A	N/A	N/A
UCY91	2	06/10/2020	>40	Negative	N/A	N/A	N/A	N/A	N/A	N/A
UCY92	5	06/10/2020	>40	Negative	N/A	N/A	N/A	N/A	N/A	N/A
UCY93	3	06/10/2020	>40	Negative	N/A	N/A	N/A	N/A	N/A	N/A
UCY94	1	06/10/2020	>40	Negative	N/A	N/A	N/A	N/A	N/A	N/A
UCY95	5	06/10/2020	>40	Negative	N/A	N/A	N/A	N/A	N/A	N/A
UCY96	5	06/10/2020	>40	Negative	N/A	N/A	N/A	N/A	N/A	N/A

UCY97	2	06/10/2020	>40	Negative	N/A	N/A	N/A	N/A	N/A	N/A
UCY98	5	06/10/2020	>40	Negative	N/A	N/A	N/A	N/A	N/A	N/A
UCY99	5	06/10/2020	>40	Negative	N/A	N/A	N/A	N/A	N/A	N/A
UCY100	5	06/10/2020	>40	Negative	N/A	N/A	N/A	N/A	N/A	N/A
UCY101	4	06/10/2020	>40	Negative	N/A	N/A	N/A	N/A	N/A	N/A
+ Control (10^3)			31.28	Positive	N/A	N/A	N/A	N/A	N/A	N/A
+ Control (10^6)			21.09	Positive	N/A	N/A	N/A	N/A	N/A	N/A
UCY102	3	09/10/2020	>40	Negative	N/A	N/A	>40	Negative	N/A	N/A
UCY103	5	09/10/2020	>40	Negative	N/A	N/A	>40	Negative	N/A	N/A
UCY104	4	09/10/2020	>40	Negative	N/A	N/A	>40	Negative	N/A	N/A
UCY105	4	09/10/2020	>40	Negative	N/A	N/A	>40	Negative	N/A	N/A
UCY106	4	09/10/2020	>40	Negative	N/A	N/A	>40	Negative	N/A	N/A
UCY107	3	09/10/2020	>40	Negative	N/A	N/A	>40	Negative	N/A	N/A
UCY108	3	09/10/2020	>40	Negative	N/A	N/A	>40	Negative	N/A	N/A
UCY109	4	09/10/2020	>40	Negative	N/A	N/A	>40	Negative	N/A	N/A
UCY110	5	09/10/2020	>40	Negative	N/A	N/A	>40	Negative	N/A	N/A
UCY111	6	09/10/2020	>40	Negative	N/A	N/A	>40	Negative	N/A	N/A
UCY112	5	09/10/2020	>40	Negative	N/A	N/A	>40	Negative	N/A	N/A
UCY113	6	09/10/2020	>40	Negative	N/A	N/A	>40	Negative	N/A	N/A
+ Control (10^3)			28.83	Positive	N/A	N/A	30.26	Positive	N/A	N/A
+ Control (10^6)			21.83	Positive	N/A	N/A	20.61	Positive	N/A	N/A
UCY114	6	13/10/2020	>40	Negative	N/A	N/A	>40	Negative	N/A	N/A
UCY115	6	13/10/2020	>40	Negative	N/A	N/A	>40	Negative	N/A	N/A
UCY116	5	13/10/2020	>40	Negative	N/A	N/A	>40	Negative	N/A	N/A
UCY117	4	13/10/2020	>40	Negative	N/A	N/A	>40	Negative	N/A	N/A
UCY118	4	13/10/2020	>40	Negative	N/A	N/A	>40	Negative	N/A	N/A
UCY119	5	13/10/2020	>40	Negative	N/A	N/A	>40	Negative	N/A	N/A
UCY120	5	13/10/2020	>40	Negative	N/A	N/A	>40	Negative	N/A	N/A
UCY121	4	13/10/2020	>40	Negative	N/A	N/A	>40	Negative	N/A	N/A
UCY122	5	13/10/2020	>40	Negative	N/A	N/A	>40	Negative	N/A	N/A
UCY123	5	13/10/2020	>40	Negative	N/A	N/A	>40	Negative	N/A	N/A

UCY124	5	13/10/2020	>40	Negative	N/A	N/A	>40	Negative	N/A	N/A
UCY125	6	13/10/2020	>40	Negative	N/A	N/A	>40	Negative	N/A	N/A
+ Control (10^3)			29.23	Positive	N/A	N/A	32.95	Positive	N/A	N/A
+ Control (10^6)			20.78	Positive	N/A	N/A	20.91	Positive	N/A	N/A
UCY126	6	16/10/2020	>40	Negative	N/A	N/A	N/A	N/A	N/A	N/A
UCY127	5	16/10/2020	>40	Negative	N/A	N/A	N/A	N/A	N/A	N/A
UCY128	3	16/10/2020	>40	Negative	N/A	N/A	N/A	N/A	N/A	N/A
UCY129	5	16/10/2020	>40	Negative	N/A	N/A	N/A	N/A	N/A	N/A
UCY130	5	16/10/2020	>40	Negative	N/A	N/A	N/A	N/A	N/A	N/A
UCY131	6	16/10/2020	>40	Negative	N/A	N/A	N/A	N/A	N/A	N/A
UCY132	5	16/10/2020	>40	Negative	N/A	N/A	N/A	N/A	N/A	N/A
UCY133	4	16/10/2020	>40	Negative	N/A	N/A	N/A	N/A	N/A	N/A
UCY134	6	16/10/2020	>40	Negative	N/A	N/A	N/A	N/A	N/A	N/A
UCY135	6	16/10/2020	>40	Negative	N/A	N/A	N/A	N/A	N/A	N/A
UCY136	6	16/10/2020	>40	Negative	N/A	N/A	N/A	N/A	N/A	N/A
UCY137	6	16/10/2020	>40	Negative	N/A	N/A	N/A	N/A	N/A	N/A
+ Control (10^3)			28.14	Positive	N/A	N/A	N/A	N/A	N/A	N/A
+ Control (10^6)			21.10	Positive	N/A	N/A	N/A	N/A	N/A	N/A
UCY138	5	20/10/2020	>40	Negative	N/A	N/A	N/A	N/A	N/A	N/A
UCY139	6	20/10/2020	>40	Negative	N/A	N/A	N/A	N/A	N/A	N/A
UCY140	5	20/10/2020	>40	Negative	N/A	N/A	N/A	N/A	N/A	N/A
UCY141	5	20/10/2020	>40	Negative	N/A	N/A	N/A	N/A	N/A	N/A
UCY142	3	20/10/2020	>40	Negative	N/A	N/A	N/A	N/A	N/A	N/A
UCY143	5	20/10/2020	>40	Negative	N/A	N/A	N/A	N/A	N/A	N/A
UCY144	4	20/10/2020	>40	Negative	N/A	N/A	N/A	N/A	N/A	N/A
UCY145	4	20/10/2020	>40	Negative	N/A	N/A	N/A	N/A	N/A	N/A
UCY146	6	20/10/2020	>40	Negative	N/A	N/A	N/A	N/A	N/A	N/A
UCY147	6	20/10/2020	>40	Negative	N/A	N/A	N/A	N/A	N/A	N/A
UCY148	5	20/10/2020	>40	Negative	N/A	N/A	N/A	N/A	N/A	N/A
UCY149	6	20/10/2020	23.18	Positive	N/A	N/A	N/A	N/A	N/A	N/A
+ Control (10^3)			29.58	Positive	N/A	N/A	N/A	N/A	N/A	N/A

+ Control (10^6)			21.58	Positive	N/A	N/A	N/A	N/A	N/A	N/A
UCY150	1	21/10/2020	>40	Negative	>40	Negative	N/A	N/A	N/A	N/A
UCY151	1	21/10/2020	>40	Negative	>40	Negative	N/A	N/A	N/A	N/A
UCY152	1	21/10/2020	15.65	Positive	20.04	Positive	N/A	N/A	N/A	N/A
UCY153	1	21/10/2020	35.84	Positive	>40	Negative	N/A	N/A	N/A	N/A
UCY154	1	21/10/2020	35.98	Positive	>40	Negative	N/A	N/A	N/A	N/A
UCY155	1	21/10/2020	>40	Negative	>40	Negative	N/A	N/A	N/A	N/A
+ Control (10^3)			28.32	Positive	32.53	Positive	N/A	N/A	N/A	N/A
+ Control (10^6)			21.81	Positive	21.91	Positive	N/A	N/A	N/A	N/A
UCY156	1	22/10/2020	>40	Negative	>40	Negative	N/A	N/A	N/A	N/A
UCY157	1	22/10/2020	>40	Negative	>40	Negative	N/A	N/A	N/A	N/A
+ Control (10^3)			28.34	Positive	N/A	N/A	N/A	N/A	N/A	N/A
+ Control (10^6)			21.71	Positive	27.21	Positive	N/A	N/A	N/A	N/A
UCY158	5	23/10/2020	>40	Negative	N/A	N/A	N/A	N/A	39.43	Negative
UCY159	6	23/10/2020	>40	Negative	N/A	N/A	N/A	N/A	>40	Negative
UCY160	4	23/10/2020	>40	Negative	N/A	N/A	N/A	N/A	>40	Negative
UCY161	6	23/10/2020	>40	Negative	N/A	N/A	N/A	N/A	>40	Negative
UCY162	6	23/10/2020	>40	Negative	N/A	N/A	N/A	N/A	>40	Negative
UCY163	6	23/10/2020	>40	Negative	N/A	N/A	N/A	N/A	>40	Negative
UCY164	5	23/10/2020	>40	Negative	N/A	N/A	N/A	N/A	N/A	Negative
UCY165	6	23/10/2020	>40	Negative	N/A	N/A	N/A	N/A	>40	Negative
UCY166	6	23/10/2020	>40	Negative	N/A	N/A	N/A	N/A	39.81	Negative
UCY167	6	23/10/2020	>40	Negative	N/A	N/A	N/A	N/A	>40	Negative
UCY168	6	23/10/2020	>40	Negative	N/A	N/A	N/A	N/A	>40	Negative
UCY169	6	23/10/2020	>40	Negative	N/A	N/A	N/A	N/A	>40	Negative
+ Control (10^3)			28.54	Positive	N/A	N/A	N/A	N/A	31.71	Positive
+ Control (10^6)			22.16	Positive	N/A	N/A	N/A	N/A	18.88	Positive
UCY170	5	27/10/2020	>40	Negative	N/A	N/A	N/A	N/A	N/A	N/A
UCY171	6	27/10/2020	>40	Negative	N/A	N/A	N/A	N/A	N/A	N/A
UCY172	6	27/10/2020	>40	Negative	N/A	N/A	N/A	N/A	N/A	N/A
UCY173	6	27/10/2020	>40	Negative	N/A	N/A	N/A	N/A	N/A	N/A

UCY174	5	27/10/2020	>40	Negative	N/A	N/A	N/A	N/A	N/A	N/A
UCY175	5	27/10/2020	>40	Negative	N/A	N/A	N/A	N/A	N/A	N/A
UCY176	4	27/10/2020	>40	Negative	N/A	N/A	N/A	N/A	N/A	N/A
UCY177	6	27/10/2020	>40	Negative	N/A	N/A	N/A	N/A	N/A	N/A
UCY178	5	27/10/2020	>40	Negative	N/A	N/A	N/A	N/A	N/A	N/A
UCY179	4	27/10/2020	>40	Negative	N/A	N/A	N/A	N/A	N/A	N/A
UCY180	6	27/10/2020	>40	Negative	N/A	N/A	N/A	N/A	N/A	N/A
UCY181	5	27/10/2020	>40	Negative	N/A	N/A	N/A	N/A	N/A	N/A
+Control (10^3)			28.72	Positive	N/A	N/A	N/A	N/A	N/A	N/A
+ Control (10^6)			20.49	Positive	N/A	N/A	N/A	N/A	N/A	N/A
UCY182	6	30/10/2020	39.29	Negative	N/A	N/A	N/A	N/A	N/A	N/A
UCY183	6	30/10/2020	34.00	Negative	N/A	N/A	N/A	N/A	N/A	N/A
UCY184	6	30/10/2020	31.06	Negative	N/A	N/A	N/A	N/A	N/A	N/A
UCY185	6	30/10/2020	37.35	Negative	N/A	N/A	N/A	N/A	N/A	N/A
UCY186	6	30/10/2020	38.59	Negative	N/A	N/A	N/A	N/A	N/A	N/A
UCY187	5	30/10/2020	34.35	Negative	N/A	N/A	N/A	N/A	N/A	N/A
UCY188	6	30/10/2020	29.87	Negative	N/A	N/A	N/A	N/A	N/A	N/A
UCY189	6	30/10/2020	34.00	Negative	N/A	N/A	N/A	N/A	N/A	N/A
UCY190	6	30/10/2020	22.03	Positive	N/A	N/A	N/A	N/A	N/A	N/A
UCY191	6	30/10/2020	33.18	Negative	N/A	N/A	N/A	N/A	N/A	N/A
UCY192	5	30/10/2020	30.00	Negative	N/A	N/A	N/A	N/A	N/A	N/A
UCY193	6	30/10/2020	30.44	Positive	N/A	N/A	N/A	N/A	N/A	N/A
+ Control (10^3)			27.75	Positive	N/A	N/A	N/A	N/A	N/A	N/A
+ Control (10^6)			20.60	Positive	N/A	N/A	N/A	N/A	N/A	N/A
UCY194	1	02/11/2020	35.34	Negative	N/A	N/A	N/A	N/A	>40	Negative
UCY195	1	02/11/2020	31.63	Negative	N/A	N/A	N/A	N/A	>40	Negative
UCY196	1	02/11/2020	29.72	Negative	N/A	N/A	N/A	N/A	>40	Negative
UCY197	1	02/11/2020	38.79	Negative	N/A	N/A	N/A	N/A	>40	Negative
UCY198	1	02/11/2020	34.00	Negative	N/A	N/A	N/A	N/A	>40	Negative
UCY199	1	02/11/2020	30.51	Negative	N/A	N/A	N/A	N/A	>40	Negative
UCY200	1	02/11/2020	28.00	Negative	N/A	N/A	N/A	N/A	39.51	Negative

UCY201	1	02/11/2020	34.21	Negative	N/A	N/A	N/A	N/A	35.15	Positive
UCY202	1	02/11/2020	35.50	Negative	N/A	N/A	N/A	N/A	>40	Negative
UCY203	1	02/11/2020	33.98	Negative	N/A	N/A	N/A	N/A	>40	Negative
UCY204	1	02/11/2020	26.37	Positive	N/A	N/A	N/A	N/A	26.68	Positive
UCY205	1	02/11/2020	>40	Negative	N/A	N/A	N/A	N/A	>40	Negative
+ Control (10^3)			27.50	Positive	N/A	N/A	N/A	N/A	29.27	Positive
+ Control (10^6)			20.95	Positive	N/A	N/A	N/A	N/A	18.97	Positive
UCY206	4	03/11/2020	N/A	N/A	N/A	N/A	N/A	N/A	38.88	Negative
UCY207	5	03/11/2020	N/A	N/A	N/A	N/A	N/A	N/A	>40	Negative
UCY208	6	03/11/2020	N/A	N/A	N/A	N/A	N/A	N/A	36.87	Negative
UCY209	5	03/11/2020	N/A	N/A	N/A	N/A	N/A	N/A	38.90	Negative
UCY210	6	03/11/2020	N/A	N/A	N/A	N/A	N/A	N/A	>40	Negative
UCY211	5	03/11/2020	N/A	N/A	N/A	N/A	N/A	N/A	38.11	Negative
UCY212	5	03/11/2020	N/A	N/A	N/A	N/A	N/A	N/A	32.76	Positive
UCY213	6	03/11/2020	N/A	N/A	N/A	N/A	N/A	N/A	>40	Negative
UCY214	6	03/11/2020	N/A	N/A	N/A	N/A	N/A	N/A	38.40	Negative
UCY215	6	03/11/2020	N/A	N/A	N/A	N/A	N/A	N/A	38.50	Negative
UCY216	6	03/11/2020	N/A	N/A	N/A	N/A	N/A	N/A	38.05	Negative
UCY217	6	03/11/2020	N/A	N/A	N/A	N/A	N/A	N/A	39.67	Negative
+ Control (10^3)			N/A	N/A	N/A	N/A	N/A	N/A	28.73	Positive
+ Control (10^6)			N/A	N/A	N/A	N/A	N/A	N/A	19.20	Positive
UCY218	1	04/11/2020	38.43	Negative	N/A	N/A	N/A	N/A	>40	Negative
UCY219	1	04/11/2020	36.49	Negative	N/A	N/A	N/A	N/A	39.18	Negative
UCY220	1	04/11/2020	34.99	Negative	N/A	N/A	N/A	N/A	39.35	Negative
UCY221	1	04/11/2020	>40	Negative	N/A	N/A	N/A	N/A	>40	Negative
UCY222	1	04/11/2020	36.93	Negative	N/A	N/A	N/A	N/A	>40	Negative
UCY223	1	04/11/2020	>40	Negative	N/A	N/A	N/A	N/A	>40	Negative
+ Control (10^3)			27.07	Positive	N/A	N/A	N/A	N/A	30.27	Positive
+ Control (10^6)			20.46	Positive	N/A	N/A	N/A	N/A	18.92	Positive
UCY224	6	06/11/2020	N/A	N/A	N/A	N/A	N/A	N/A	>40	Negative
UCY225	6	06/11/2020	N/A	N/A	N/A	N/A	N/A	N/A	>40	Negative

UCY226	5	06/11/2020	N/A	N/A	N/A	N/A	N/A	N/A	>40	Negative
UCY227	6	06/11/2020	N/A	N/A	N/A	N/A	N/A	N/A	>40	Negative
UCY228	6	06/11/2020	N/A	N/A	N/A	N/A	N/A	N/A	>40	Negative
UCY229	5	06/11/2020	N/A	N/A	N/A	N/A	N/A	N/A	>40	Negative
UCY230	5	06/11/2020	N/A	N/A	N/A	N/A	N/A	N/A	>40	Negative
UCY231	6	06/11/2020	N/A	N/A	N/A	N/A	N/A	N/A	>40	Negative
UCY232	6	06/11/2020	N/A	N/A	N/A	N/A	N/A	N/A	>40	Negative
UCY233	6	06/11/2020	N/A	N/A	N/A	N/A	N/A	N/A	>40	Negative
UCY234	6	06/11/2020	N/A	N/A	N/A	N/A	N/A	N/A	>40	Negative
UCY235	6	06/11/2020	N/A	N/A	N/A	N/A	N/A	N/A	>40	Negative
+ Control (10^3)			N/A	N/A	N/A	N/A	N/A	N/A	32.55	Positive
+ Control (10^6)			N/A	N/A	N/A	N/A	N/A	N/A	18.90	Positive
UCY236	6	10/11/2020	N/A	N/A	N/A	N/A	N/A	N/A	>40	Negative
UCY237	6	10/11/2020	N/A	N/A	N/A	N/A	N/A	N/A	>40	Negative
UCY238	6	10/11/2020	N/A	N/A	N/A	N/A	N/A	N/A	>40	Negative
UCY239	6	10/11/2020	N/A	N/A	N/A	N/A	N/A	N/A	>40	Negative
UCY240	6	10/11/2020	N/A	N/A	N/A	N/A	N/A	N/A	>40	Negative
UCY241	6	10/11/2020	N/A	N/A	N/A	N/A	N/A	N/A	>40	Negative
UCY242	6	10/11/2020	N/A	N/A	N/A	N/A	N/A	N/A	>40	Negative
UCY243	6	10/11/2020	N/A	N/A	N/A	N/A	N/A	N/A	39.38	Negative
UCY244	6	10/11/2020	N/A	N/A	N/A	N/A	N/A	N/A	>40	Negative
UCY245	6	10/11/2020	N/A	N/A	N/A	N/A	N/A	N/A	>40	Negative
UCY246	6	10/11/2020	N/A	N/A	N/A	N/A	N/A	N/A	>40	Negative
UCY247	6	10/11/2020	N/A	N/A	N/A	N/A	N/A	N/A	>40	Negative
UCY248	6	10/11/2020	N/A	N/A	N/A	N/A	N/A	N/A	>40	Negative
UCY249	6	10/11/2020	N/A	N/A	N/A	N/A	N/A	N/A	21.89	Positive
UCY250	6	10/11/2020	N/A	N/A	N/A	N/A	N/A	N/A	>40	Negative
UCY251	6	10/11/2020	N/A	N/A	N/A	N/A	N/A	N/A	>40	Negative
UCY252	6	10/11/2020	N/A	N/A	N/A	N/A	N/A	N/A	>40	Negative
+ Control (10^3)			N/A	N/A	N/A	N/A	N/A	N/A	31.26	Positive
+ Control (10^6)			N/A	N/A	N/A	N/A	N/A	N/A	20.08	Positive

UCY253	1	11/11/2020	>40	Negative	N/A	N/A	N/A	N/A	>40	Negative
UCY254	1	11/11/2020	>40	Negative	N/A	N/A	N/A	N/A	>40	Negative
UCY255	1	11/11/2020	>40	Negative	N/A	N/A	N/A	N/A	>40	Negative
UCY256	1	11/11/2020	>40	Negative	N/A	N/A	N/A	N/A	>40	Negative
UCY257	1	11/11/2020	>40	Negative	N/A	N/A	N/A	N/A	>40	Negative
UCY258	1	11/11/2020	19.04	Positive	N/A	N/A	N/A	N/A	18.29	Positive
+ Control (10^3)			29.59	Positive	N/A	N/A	N/A	N/A	33.93	Positive
+ Control (10^6)			20.07	Positive	N/A	N/A	N/A	N/A	20.37	Positive
UCY259	6	13/11/2020	N/A	N/A	N/A	N/A	N/A	N/A	>40	Negative
UCY260	6	13/11/2020	N/A	N/A	N/A	N/A	N/A	N/A	>40	Negative
UCY261	6	13/11/2020	N/A	N/A	N/A	N/A	N/A	N/A	>40	Negative
UCY262	6	13/11/2020	N/A	N/A	N/A	N/A	N/A	N/A	>40	Negative
UCY263	5	13/11/2020	N/A	N/A	N/A	N/A	N/A	N/A	>40	Negative
UCY264	5	13/11/2020	N/A	N/A	N/A	N/A	N/A	N/A	>40	Negative
UCY265	6	13/11/2020	N/A	N/A	N/A	N/A	N/A	N/A	38.52	Positive
UCY266	6	13/11/2020	N/A	N/A	N/A	N/A	N/A	N/A	>40	Negative
UCY267	6	13/11/2020	N/A	N/A	N/A	N/A	N/A	N/A	>40	Negative
UCY268	6	13/11/2020	N/A	N/A	N/A	N/A	N/A	N/A	>40	Negative
UCY269	6	13/11/2020	N/A	N/A	N/A	N/A	N/A	N/A	>40	Negative
UCY270	6	13/11/2020	N/A	N/A	N/A	N/A	N/A	N/A	>40	Negative
+ Control (10^3)			N/A	N/A	N/A	N/A	N/A	N/A	33.38	Positive
+ Control (10^6)			N/A	N/A	N/A	N/A	N/A	N/A	19.91	Positive
UCY271	6	16/11/2020	>40	Negative	N/A	N/A	N/A	N/A	>40	Negative
UCY272	6	16/11/2020	>40	Negative	N/A	N/A	N/A	N/A	>40	Negative
UCY273	1	16/11/2020	>40	Negative	N/A	N/A	N/A	N/A	>40	Negative
UCY274	1	16/11/2020	>40	Negative	N/A	N/A	N/A	N/A	>40	Negative
UCY275	1	16/11/2020	>40	Negative	N/A	N/A	N/A	N/A	>40	Negative
UCY276	1	16/11/2020	>40	Negative	N/A	N/A	N/A	N/A	>40	Negative
UCY277	1	16/11/2020	>40	Negative	N/A	N/A	N/A	N/A	>40	Negative
UCY278	1	16/11/2020	>40	Negative	N/A	N/A	N/A	N/A	>40	Negative
+ Control (10^3)			31.29	Positive	N/A	N/A	N/A	N/A	32.16	Positive

+ Control (10^6)			20.46	Positive	N/A	N/A	N/A	N/A	20.17	Positive
UCY279	6	17/11/2020	N/A	N/A	N/A	N/A	N/A	N/A	>40	Negative
UCY280	6	17/11/2020	N/A	N/A	N/A	N/A	N/A	N/A	>40	Negative
UCY281	6	17/11/2020	N/A	N/A	N/A	N/A	N/A	N/A	>40	Negative
UCY282	6	17/11/2020	N/A	N/A	N/A	N/A	N/A	N/A	>40	Negative
UCY283	6	17/11/2020	N/A	N/A	N/A	N/A	N/A	N/A	36.03	Positive
UCY284	6	17/11/2020	N/A	N/A	N/A	N/A	N/A	N/A	>40	Negative
UCY285	6	17/11/2020	N/A	N/A	N/A	N/A	N/A	N/A	>40	Negative
UCY286	6	17/11/2020	N/A	N/A	N/A	N/A	N/A	N/A	>40	Negative
UCY287	6	17/11/2020	N/A	N/A	N/A	N/A	N/A	N/A	>40	Negative
UCY288	6	17/11/2020	N/A	N/A	N/A	N/A	N/A	N/A	>40	Negative
UCY289	5	17/11/2020	N/A	N/A	N/A	N/A	N/A	N/A	>40	Negative
UCY290	6	17/11/2020	N/A	N/A	N/A	N/A	N/A	N/A	>40	Negative
+ Control (10^3)			N/A	N/A	N/A	N/A	N/A	N/A	33.34	Positive
+ Control (10^6)			N/A	N/A	N/A	N/A	N/A	N/A	20.213403	Positive
UCY291	1	18/11/2020	>40	Negative	N/A	N/A	N/A	N/A	>40	Negative
UCY292	1	18/11/2020	>40	Negative	N/A	N/A	N/A	N/A	>40	Negative
UCY293	1	18/11/2020	>40	Negative	N/A	N/A	N/A	N/A	37.98	Positive
UCY294	1	18/11/2020	>40	Negative	N/A	N/A	N/A	N/A	>40	Negative
UCY295	1	18/11/2020	>40	Negative	N/A	N/A	N/A	N/A	>40	Negative
UCY296	1	18/11/2020	>40	Negative	N/A	N/A	N/A	N/A	36.37	Positive
+ Control (10^3)			29.83	Positive	N/A	N/A	N/A	N/A	33.28	Positive
+ Control (10^6)			21.06	Positive	N/A	N/A	N/A	N/A	20.42	Positive
UCY297	7	20/11/2020	N/A	N/A	N/A	N/A	N/A	N/A	>40	Negative
UCY298	6	20/11/2020	N/A	N/A	N/A	N/A	N/A	N/A	>40	Negative
UCY299	6	20/11/2020	N/A	N/A	N/A	N/A	N/A	N/A	>40	Negative
UCY300	6	20/11/2020	N/A	N/A	N/A	N/A	N/A	N/A	>40	Negative
UCY301	6	20/11/2020	N/A	N/A	N/A	N/A	N/A	N/A	>40	Negative
UCY302	6	20/11/2020	N/A	N/A	N/A	N/A	N/A	N/A	32.98	Positive
UCY303	6	20/11/2020	N/A	N/A	N/A	N/A	N/A	N/A	38.15	Positive
UCY304	6	20/11/2020	N/A	N/A	N/A	N/A	N/A	N/A	38.74	Positive

UCY305	6	20/11/2020	N/A	N/A	N/A	N/A	N/A	N/A	>40	Negative
UCY306	6	20/11/2020	N/A	N/A	N/A	N/A	N/A	N/A	>40	Negative
UCY307	6	20/11/2020	N/A	N/A	N/A	N/A	N/A	N/A	>40	Negative
UCY308	6	20/11/2020	N/A	N/A	N/A	N/A	N/A	N/A	>40	Negative
+ Control (10^3)			N/A	N/A	N/A	N/A	N/A	N/A	36.09	Positive
+ Control (10^6)			N/A	N/A	N/A	N/A	N/A	N/A	21.47	Positive
UCY309	4	23/11/2020	>40	Negative	N/A	N/A	N/A	N/A	>40	Negative
UCY310	1	23/11/2020	>40	Negative	N/A	N/A	N/A	N/A	>40	Negative
UCY311	1	23/11/2020	>40	Negative	N/A	N/A	N/A	N/A	>40	Negative
UCY312	1	23/11/2020	>40	Negative	N/A	N/A	N/A	N/A	>40	Negative
UCY313	1	23/11/2020	>40	Negative	N/A	N/A	N/A	N/A	>40	Negative
UCY314	1	23/11/2020	>40	Negative	N/A	N/A	N/A	N/A	>40	Negative
UCY315	1	23/11/2020	>40	Negative	N/A	N/A	N/A	N/A	38.76	Positive
UCY316	1	23/11/2020	>40	Negative	N/A	N/A	N/A	N/A	>40	Negative
UCY317	1	23/11/2020	>40	Negative	N/A	N/A	N/A	N/A	>40	Negative
UCY318	1	23/11/2020	>40	Negative	N/A	N/A	N/A	N/A	>40	Negative
UCY319	1	23/11/2020	>40	Negative	N/A	N/A	N/A	N/A	>40	Negative
UCY320	1	23/11/2020	>40	Negative	N/A	N/A	N/A	N/A	>40	Negative
UCY321	1	23/11/2020	>40	Negative	N/A	N/A	N/A	N/A	>40	Negative
UCY322	1	23/11/2020	>40	Negative	N/A	N/A	N/A	N/A	>40	Negative
UCY323	1	23/11/2020	>40	Negative	N/A	N/A	N/A	N/A	>40	Negative
+ Control (10^3)			32.06	Positive	N/A	N/A	N/A	N/A	33.51	Positive
+ Control (10^6)			21.07	Positive	N/A	N/A	N/A	N/A	22.03	Positive
UCY324	6	24/11/2020	N/A	N/A	N/A	N/A	N/A	N/A	>40	Negative
UCY325	6	24/11/2020	N/A	N/A	N/A	N/A	N/A	N/A	>40	Negative
UCY326	6	24/11/2020	N/A	N/A	N/A	N/A	N/A	N/A	23.87	Positive
UCY327	6	24/11/2020	N/A	N/A	N/A	N/A	N/A	N/A	>40	Negative
UCY328	6	24/11/2020	N/A	N/A	N/A	N/A	N/A	N/A	>40	Negative
UCY329	6	24/11/2020	N/A	N/A	N/A	N/A	N/A	N/A	>40	Negative
UCY330	6	24/11/2020	N/A	N/A	N/A	N/A	N/A	N/A	>40	Negative
UCY331	5	24/11/2020	N/A	N/A	N/A	N/A	N/A	N/A	>40	Negative

UCY332	6	24/11/2020	N/A	N/A	N/A	N/A	N/A	N/A	>40	Negative
UCY333	6	24/11/2020	N/A	N/A	N/A	N/A	N/A	N/A	>40	Negative
UCY334	6	24/11/2020	N/A	N/A	N/A	N/A	N/A	N/A	35.39	Positive
UCY335	6	24/11/2020	N/A	N/A	N/A	N/A	N/A	N/A	39.93	Negative
+ Control (10^3)			N/A	N/A	N/A	N/A	N/A	N/A	34.73	Positive
+ Control (10^6)			N/A	N/A	N/A	N/A	N/A	N/A	22.17	Positive
UCY336	1	25/11/2020	>40	Negative	N/A	N/A	N/A	N/A	>40	Negative
UCY337	1	25/11/2020	>40	Negative	N/A	N/A	N/A	N/A	>40	Negative
UCY338	1	25/11/2020	>40	Negative	N/A	N/A	N/A	N/A	>40	Negative
UCY339	1	25/11/2020	>40	Negative	N/A	N/A	N/A	N/A	>40	Negative
UCY340	1	25/11/2020	>40	Negative	N/A	N/A	N/A	N/A	>40	Negative
UCY341	1	25/11/2020	>40	Negative	N/A	N/A	N/A	N/A	>40	Negative
UCY342	1	25/11/2020	32.60	Positive	N/A	N/A	N/A	N/A	33.40	Positive
UCY343	1	25/11/2020	>40	Negative	N/A	N/A	N/A	N/A	>40	Negative
UCY344	1	25/11/2020	>40	Negative	N/A	N/A	N/A	N/A	>40	Negative
UCY345	1	25/11/2020	>40	Negative	N/A	N/A	N/A	N/A	>40	Negative
UCY346	1	25/11/2020	>40	Negative	N/A	N/A	N/A	N/A	>40	Negative
UCY347	1	25/11/2020	>40	Negative	N/A	N/A	N/A	N/A	>40	Negative
+ Control (10^3)			30.10	Positive	N/A	N/A	N/A	N/A	34.40	Positive
+ Control (10^6)			21.48	Positive	N/A	N/A	N/A	N/A	20.04	Positive
UCY348	6	27/11/2020	18.89	Positive	N/A	N/A	N/A	N/A	N/A	N/A
UCY349	6	27/11/2020	>40	Negative	N/A	N/A	N/A	N/A	N/A	N/A
UCY350	6	27/11/2020	>40	Negative	N/A	N/A	N/A	N/A	N/A	N/A
UCY351	6	27/11/2020	>40	Negative	N/A	N/A	N/A	N/A	N/A	N/A
UCY352	6	27/11/2020	>40	Negative	N/A	N/A	N/A	N/A	N/A	N/A
UCY353	6	27/11/2020	>40	Negative	N/A	N/A	N/A	N/A	N/A	N/A
UCY354	6	27/11/2020	>40	Negative	N/A	N/A	N/A	N/A	N/A	N/A
UCY355	6	27/11/2020	>40	Negative	N/A	N/A	N/A	N/A	N/A	N/A
UCY356	6	27/11/2020	>40	Negative	N/A	N/A	N/A	N/A	N/A	N/A
UCY357	6	27/11/2020	36.50	Positive	N/A	N/A	N/A	N/A	N/A	N/A
UCY358	6	27/11/2020	>40	Negative	N/A	N/A	N/A	N/A	N/A	N/A

UCY359	6	27/11/2020	>40	Negative	N/A	N/A	N/A	N/A	N/A	N/A
+ Control (10^3)			29.73	Positive	N/A	N/A	N/A	N/A	N/A	N/A
+ Control (10^6)			21.05	Positive	N/A	N/A	N/A	N/A	N/A	N/A
UCY360	1	01/12/2020	>40	Negative	N/A	N/A	N/A	N/A	N/A	N/A
UCY361	1	01/12/2020	>40	Negative	N/A	N/A	N/A	N/A	N/A	N/A
UCY362	1	01/12/2020	>40	Negative	N/A	N/A	N/A	N/A	N/A	N/A
UCY363	1	01/12/2020	>40	Negative	N/A	N/A	N/A	N/A	N/A	N/A
UCY364	1	01/12/2020	>40	Negative	N/A	N/A	N/A	N/A	N/A	N/A
+ Control (10^3)			31.88	Positive	N/A	N/A	N/A	N/A	N/A	N/A
+ Control (10^6)			21.71	Positive	N/A	N/A	N/A	N/A	N/A	N/A
UCY365	6	02/12/2020	>40	Negative	N/A	N/A	N/A	N/A	N/A	N/A
UCY366	6	02/12/2020	>40	Negative	N/A	N/A	N/A	N/A	N/A	N/A
UCY367	6	02/12/2020	>40	Negative	N/A	N/A	N/A	N/A	N/A	N/A
UCY368	6	02/12/2020	>40	Negative	N/A	N/A	N/A	N/A	N/A	N/A
UCY369	6	02/12/2020	>40	Negative	N/A	N/A	N/A	N/A	N/A	N/A
UCY370	6	02/12/2020	>40	Negative	N/A	N/A	N/A	N/A	N/A	N/A
UCY371	6	02/12/2020	>40	Negative	N/A	N/A	N/A	N/A	N/A	N/A
UCY372	6	02/12/2020	>40	Negative	N/A	N/A	N/A	N/A	N/A	N/A
UCY373	6	02/12/2020	>40	Negative	N/A	N/A	N/A	N/A	N/A	N/A
UCY374	6	02/12/2020	>40	Negative	N/A	N/A	N/A	N/A	N/A	N/A
UCY375	6	02/12/2020	>40	Negative	N/A	N/A	N/A	N/A	N/A	N/A
UCY376	6	02/12/2020	34.51	Positive	N/A	N/A	N/A	N/A	N/A	N/A
+ Control (10^3)			33.23	Positive	N/A	N/A	N/A	N/A	N/A	N/A
+ Control (10^6)			20.32	Positive	N/A	N/A	N/A	N/A	N/A	N/A
UCY377	1	03/12/2020	>40	Negative	N/A	N/A	>40	Negative	N/A	N/A
UCY378	1	03/12/2020	>40	Negative	N/A	N/A	>40	Negative	N/A	N/A
UCY379	1	03/12/2020	39.70	Negative	N/A	N/A	>40	Negative	N/A	N/A
UCY380	1	03/12/2020	>40	Negative	N/A	N/A	>40	Negative	N/A	N/A
UCY381	1	03/12/2020	34.29	Positive	N/A	N/A	37.046295	Positive	N/A	N/A
UCY382	1	03/12/2020	>40	Negative	N/A	N/A	>40	Negative	N/A	N/A
+ Control (10^3)			32.82	Positive	N/A	N/A	32.796972	Positive	N/A	N/A

+ Control (10^6)			20.53	Positive	N/A	N/A	N/A	N/A	N/A	N/A
UCY383	7	04/12/2020	>40	Negative	N/A	N/A	N/A	N/A	N/A	N/A
UCY384	5	04/12/2020	>40	Negative	N/A	N/A	N/A	N/A	N/A	N/A
UCY385	8	04/12/2020	>40	Negative	N/A	N/A	N/A	N/A	N/A	N/A
UCY386	7	04/12/2020	>40	Negative	N/A	N/A	N/A	N/A	N/A	N/A
UCY387	8	04/12/2020	>40	Negative	N/A	N/A	N/A	N/A	N/A	N/A
UCY388	5	04/12/2020	>40	Negative	N/A	N/A	N/A	N/A	N/A	N/A
UCY389	6	04/12/2020	>40	Negative	N/A	N/A	N/A	N/A	N/A	N/A
UCY390	8	04/12/2020	>40	Negative	N/A	N/A	N/A	N/A	N/A	N/A
UCY391	8	04/12/2020	22.37	Negative	N/A	N/A	N/A	N/A	N/A	N/A
UCY392	1	04/12/2020	>40	Negative	N/A	N/A	N/A	N/A	N/A	N/A
UCY393	1	04/12/2020	>40	Negative	N/A	N/A	N/A	N/A	N/A	N/A
UCY394	1	04/12/2020	>40	Negative	N/A	N/A	N/A	N/A	N/A	N/A
UCY395	6	04/12/2020	>40	Negative	N/A	N/A	N/A	N/A	N/A	N/A
UCY396	6	04/12/2020	>40	Negative	N/A	N/A	N/A	N/A	N/A	N/A
UCY397	6	04/12/2020	>40	Negative	N/A	N/A	N/A	N/A	N/A	N/A
+ Control (10^3)			27.12	Positive	N/A	N/A	N/A	N/A	N/A	N/A
+ Control (10^6)			21.16	Positive	N/A	N/A	N/A	N/A	N/A	N/A
UCY398	5	08/12/2020	>40	Negative	N/A	N/A	N/A	N/A	N/A	N/A
UCY399	5	08/12/2020	>40	Negative	N/A	N/A	N/A	N/A	N/A	N/A
UCY400	6	08/12/2020	>40	Negative	N/A	N/A	N/A	N/A	N/A	N/A
UCY401	5	08/12/2020	>40	Negative	N/A	N/A	N/A	N/A	N/A	N/A
UCY402	6	08/12/2020	>40	Negative	N/A	N/A	N/A	N/A	N/A	N/A
UCY403	7	08/12/2020	>40	Negative	N/A	N/A	N/A	N/A	N/A	N/A
UCY404	7	08/12/2020	32.22	Positive	N/A	N/A	N/A	N/A	N/A	N/A
UCY405	6	08/12/2020	>40	Negative	N/A	N/A	N/A	N/A	N/A	N/A
UCY406	6	08/12/2020	>40	Negative	N/A	N/A	N/A	N/A	N/A	N/A
UCY407	6	08/12/2020	>40	Negative	N/A	N/A	N/A	N/A	N/A	N/A
UCY408	5	08/12/2020	>40	Negative	N/A	N/A	N/A	N/A	N/A	N/A
UCY409	4	08/12/2020	>40	Negative	N/A	N/A	N/A	N/A	N/A	N/A
+ Control (10^3)			32.29	Positive	N/A	N/A	N/A	N/A	N/A	N/A

+ Control (10^6)			21.72	Positive	N/A	N/A	N/A	N/A	N/A	N/A
UCY410	1	09/12/2020		Negative	Verified by rapid test					
UCY411	1	09/12/2020		Negative	Verified by rapid test					
UCY412	1	09/12/2020		Negative	Verified by rapid test					
UCY413	1	09/12/2020		Negative	Verified by rapid test					
UCY414	1	09/12/2020		Negative	Verified by rapid test					
UCY415	1	09/12/2020		Negative	Verified by rapid test					
UCY416	1	09/12/2020		Positive	Verified by rapid test					
UCY417	6	11/12/2020	N/A	N/A	N/A	N/A	N/A	N/A	37.89	Negative
UCY418	6	11/12/2020	N/A	N/A	N/A	N/A	N/A	N/A	36.96	Negative
UCY419	5	11/12/2020	N/A	N/A	N/A	N/A	N/A	N/A	38.79	Negative
UCY420	5	11/12/2020	N/A	N/A	N/A	N/A	N/A	N/A	38.07	Negative
UCY421	4	11/12/2020	N/A	N/A	N/A	N/A	N/A	N/A	37.64	Negative
UCY422	4	11/12/2020	N/A	N/A	N/A	N/A	N/A	N/A	30.09	Positive
UCY423	6	11/12/2020	N/A	N/A	N/A	N/A	N/A	N/A	36.62	Negative
UCY424	6	11/12/2020	N/A	N/A	N/A	N/A	N/A	N/A	37.36	Negative
UCY425	1	11/12/2020	N/A	N/A	N/A	N/A	N/A	N/A	37.44	Negative
UCY426	5	11/12/2020	N/A	N/A	N/A	N/A	N/A	N/A	37.54	Negative
UCY427	6	11/12/2020	N/A	N/A	N/A	N/A	N/A	N/A	37.39	Negative
UCY428	7	11/12/2020	N/A	N/A	N/A	N/A	N/A	N/A	37.55	Negative
+ Control (10^3)			N/A	N/A	N/A	N/A	N/A	N/A	35.25	Positive
+ Control (10^6)			N/A	N/A	N/A	N/A	N/A	N/A	19.97	Positive
UCY429	6	14/12/2020	N/A	N/A	N/A	N/A	N/A	N/A	>40	Negative
UCY430	5	14/12/2020	N/A	N/A	N/A	N/A	N/A	N/A	>40	Negative
UCY431	6	14/12/2020	N/A	N/A	N/A	N/A	N/A	N/A	>40	Negative
UCY432	4	14/12/2020	N/A	N/A	N/A	N/A	N/A	N/A	>40	Negative
UCY433	3	14/12/2020	N/A	N/A	N/A	N/A	N/A	N/A	>40	Negative
UCY434	6	14/12/2020	N/A	N/A	N/A	N/A	N/A	N/A	>40	Negative
UCY435	3	14/12/2020	N/A	N/A	N/A	N/A	N/A	N/A	>40	Negative
UCY436	4	14/12/2020	N/A	N/A	N/A	N/A	N/A	N/A	>40	Negative
UCY437	4	14/12/2020	N/A	N/A	N/A	N/A	N/A	N/A	>40	Negative

UCY438	4	14/12/2020	N/A	N/A	N/A	N/A	N/A	N/A	>40	Negative
UCY439	5	14/12/2020	N/A	N/A	N/A	N/A	N/A	N/A	29.00	Negative
UCY440	6	14/12/2020	N/A	N/A	N/A	N/A	N/A	N/A	>40	Negative
UCY441	5	14/12/2020	N/A	N/A	N/A	N/A	N/A	N/A	33.45	Positive
UCY442	6	14/12/2020	N/A	N/A	N/A	N/A	N/A	N/A	>40	Negative
UCY443	4	14/12/2020	N/A	N/A	N/A	N/A	N/A	N/A	>40	Negative
UCY444	6	14/12/2020	N/A	N/A	N/A	N/A	N/A	N/A	>40	Negative
UCY445	1	14/12/2020	>40	Negative	N/A	N/A	N/A	N/A	>40	Negative
UCY446	1	14/12/2020	>40	Negative	N/A	N/A	N/A	N/A	>40	Negative
UCY447	1	14/12/2020	>40	Negative	N/A	N/A	N/A	N/A	>40	Negative
UCY448	1	14/12/2020	>40	Negative	N/A	N/A	N/A	N/A	>40	Negative
+ Control (10^3)			30.78	Positive	N/A	N/A	N/A	N/A	N/A	N/A
+ Control (10^6)			22.08	Positive	N/A	N/A	N/A	N/A	19.72	Positive
UCY449	5	15/12/2020	N/A	N/A	N/A	N/A	N/A	N/A	>40	Negative
UCY450	2	15/12/2020	N/A	N/A	N/A	N/A	N/A	N/A	>40	Negative
UCY451	4	15/12/2020	N/A	N/A	N/A	N/A	N/A	N/A	>40	Negative
UCY452	4	15/12/2020	N/A	N/A	N/A	N/A	N/A	N/A	>40	Negative
UCY453	3	15/12/2020	N/A	N/A	N/A	N/A	N/A	N/A	>40	Negative
UCY454	3	15/12/2020	N/A	N/A	N/A	N/A	N/A	N/A	>40	Negative
UCY455	5	15/12/2020	N/A	N/A	N/A	N/A	N/A	N/A	>40	Negative
UCY456	4	15/12/2020	N/A	N/A	N/A	N/A	N/A	N/A	39.10	Negative
UCY457	5	15/12/2020	N/A	N/A	N/A	N/A	N/A	N/A	>40	Negative
UCY458	6	15/12/2020	N/A	N/A	N/A	N/A	N/A	N/A	>40	Negative
UCY459	5	15/12/2020	N/A	N/A	N/A	N/A	N/A	N/A	>40	Negative
UCY460	5	15/12/2020	N/A	N/A	N/A	N/A	N/A	N/A	>40	Negative
UCY461	1	15/12/2020	>40	Negative	N/A	N/A	N/A	N/A	37.27	Positive
UCY462	1	15/12/2020	>40	Negative	N/A	N/A	N/A	N/A	>40	Negative
UCY463	1	15/12/2020	>40	Negative	N/A	N/A	N/A	N/A	>40	Negative
UCY464	1	15/12/2020	>40	Negative	N/A	N/A	N/A	N/A	>40	Negative
UCY465	1	15/12/2020	>40	Negative	N/A	N/A	N/A	N/A	>40	Negative
+ Control (10^3)			31.14	Positive	N/A	N/A	N/A	N/A	N/A	N/A

+ Control (10^6)			20.89	Positive	N/A	N/A	N/A	N/A	20.68	Positive
UCY466	6	17/12/2020	N/A	N/A	N/A	N/A	N/A	N/A	>40	Negative
UCY467	6	17/12/2020	N/A	N/A	N/A	N/A	N/A	N/A	>40	Negative
UCY468	6	17/12/2020	N/A	N/A	N/A	N/A	N/A	N/A	>40	Negative
UCY469	6	17/12/2020	N/A	N/A	N/A	N/A	N/A	N/A	>40	Negative
UCY470	6	17/12/2020	N/A	N/A	N/A	N/A	N/A	N/A	>40	Negative
UCY471	6	17/12/2020	N/A	N/A	N/A	N/A	N/A	N/A	39.40	Negative
UCY472	6	17/12/2020	N/A	N/A	N/A	N/A	N/A	N/A	>40	Negative
UCY473	6	17/12/2020	N/A	N/A	N/A	N/A	N/A	N/A	37.80	Positive
UCY474	6	17/12/2020	N/A	N/A	N/A	N/A	N/A	N/A	33.92	Positive
UCY475	6	17/12/2020	N/A	N/A	N/A	N/A	N/A	N/A	>40	Negative
UCY476	6	17/12/2020	N/A	N/A	N/A	N/A	N/A	N/A	>40	Negative
UCY477	4	17/12/2020	N/A	N/A	N/A	N/A	N/A	N/A	>40	Negative
+ Control (10^3)			N/A	N/A	N/A	N/A	N/A	N/A	31.77	Positive
+ Control (10^6)			N/A	N/A	N/A	N/A	N/A	N/A	20.68	Positive
UCY488	1	18/12/2020	>40	Negative	N/A	N/A	N/A	N/A	>40	Negative
UCY489	1	18/12/2020	>40	Negative	N/A	N/A	N/A	N/A	>40	Negative
UCY490	1	18/12/2020	>40	Negative	N/A	N/A	N/A	N/A	>40	Negative
UCY491	1	18/12/2020	>40	Negative	N/A	N/A	N/A	N/A	38.05	Positive
UCY492	1	18/12/2020	>40	Negative	N/A	N/A	N/A	N/A	>40	Negative
UCY493	1	18/12/2020	>40	Negative	N/A	N/A	N/A	N/A	36.70	Positive
UCY494	1	18/12/2020	>40	Negative	N/A	N/A	N/A	N/A	>40	Negative
UCY495	1	18/12/2020	>40	Negative	N/A	N/A	N/A	N/A	>40	Negative
UCY496	1	18/12/2020	>40	Negative	N/A	N/A	N/A	N/A	>40	Negative
+ Control (10^3)			29.56174	Positive	N/A	N/A	N/A	N/A	32.54	Positive
+ Control (10^6)			21.18161	Positive	N/A	N/A	N/A	N/A	20.94	Positive
UCY497	5	07/01/2021	N/A	N/A	N/A	N/A	N/A	N/A	>40	Negative
UCY498	6	07/01/2021	N/A	N/A	N/A	N/A	N/A	N/A	>40	Negative
UCY499	1	07/01/2021	N/A	N/A	N/A	N/A	N/A	N/A	>40	Negative
UCY500	1	07/01/2021	N/A	N/A	N/A	N/A	N/A	N/A	>40	Negative
UCY501	1	07/01/2021	N/A	N/A	N/A	N/A	N/A	N/A	28.29	Positive

+ Control (10^3)			N/A	N/A	N/A	N/A	N/A	N/A	33.28	Positive
+ Control (10^6)			N/A	N/A	N/A	N/A	N/A	N/A	21.49	Positive
UCY502	10	08/01/2021	N/A	N/A	N/A	N/A	N/A	N/A	>40	Negative
UCY503	10	08/01/2021	N/A	N/A	N/A	N/A	N/A	N/A	39.16	Negative
UCY504	9	08/01/2021	N/A	N/A	N/A	N/A	N/A	N/A	>40	Negative
UCY505	8	08/01/2021	N/A	N/A	N/A	N/A	N/A	N/A	>40	Negative
UCY506	9	08/01/2021	N/A	N/A	N/A	N/A	N/A	N/A	>40	Negative
UCY507	8	08/01/2021	N/A	N/A	N/A	N/A	N/A	N/A	>40	Negative
UCY508	8	08/01/2021	N/A	N/A	N/A	N/A	N/A	N/A	>40	Negative
UCY509	7	08/01/2021	N/A	N/A	N/A	N/A	N/A	N/A	28.16	Positive
UCY510	12	08/01/2021	N/A	N/A	N/A	N/A	N/A	N/A	>40	Negative
UCY511	7	08/01/2021	N/A	N/A	N/A	N/A	N/A	N/A	>40	Negative
UCY512	10	08/01/2021	N/A	N/A	N/A	N/A	N/A	N/A	>40	Negative
UCY513	10	08/01/2021	N/A	N/A	N/A	N/A	N/A	N/A	>40	Negative
+ Control (10^3)			N/A	N/A	N/A	N/A	N/A	N/A	35.15	Positive
+ Control (10^6)			N/A	N/A	N/A	N/A	N/A	N/A	20.02	Positive
UCY514	3	12/01/2021	N/A	N/A	N/A	N/A	N/A	N/A	>40	Negative
UCY515	2	12/01/2021	N/A	N/A	N/A	N/A	N/A	N/A	>40	Negative
UCY516	1	12/01/2021	N/A	N/A	N/A	N/A	N/A	N/A	>40	Negative
UCY517	1	12/01/2021	N/A	N/A	N/A	N/A	N/A	N/A	>40	Negative
UCY518	5	12/01/2021	N/A	N/A	N/A	N/A	N/A	N/A	>40	Negative
UCY519	4	12/01/2021	N/A	N/A	N/A	N/A	N/A	N/A	>40	Negative
UCY520	4	12/01/2021	N/A	N/A	N/A	N/A	N/A	N/A	>40	Negative
UCY521	4	12/01/2021	N/A	N/A	N/A	N/A	N/A	N/A	>40	Negative
UCY522	5	12/01/2021	N/A	N/A	N/A	N/A	N/A	N/A	>40	Negative
UCY523	5	12/01/2021	N/A	N/A	N/A	N/A	N/A	N/A	>40	Negative
UCY524	1	12/01/2021	N/A	N/A	N/A	N/A	N/A	N/A	39.65	Negative
+ Control (10^3)			N/A	N/A	N/A	N/A	N/A	N/A	33.93	Positive
+ Control (10^6)			N/A	N/A	N/A	N/A	N/A	N/A	20.16	Positive
UCY525	5	14/01/2021	N/A	N/A	N/A	N/A	N/A	N/A	>40	Negative
UCY526	6	14/01/2021	N/A	N/A	N/A	N/A	N/A	N/A	>40	Negative

UCY527	4	14/01/2021	N/A	N/A	N/A	N/A	N/A	N/A	>40	Negative
UCY528	3	14/01/2021	N/A	N/A	N/A	N/A	N/A	N/A	>40	Negative
UCY529	5	14/01/2021	N/A	N/A	N/A	N/A	N/A	N/A	>40	Negative
UCY530	2	14/01/2021	N/A	N/A	N/A	N/A	N/A	N/A	>40	Negative
UCY531	4	14/01/2021	N/A	N/A	N/A	N/A	N/A	N/A	38.09	Negative
UCY532	5	14/01/2021	N/A	N/A	N/A	N/A	N/A	N/A	>40	Negative
UCY533	3	14/01/2021	N/A	N/A	N/A	N/A	N/A	N/A	>40	Negative
+ Control (10^3)			N/A	N/A	N/A	N/A	N/A	N/A	31.99	Positive
+ Control (10^6)			N/A	N/A	N/A	N/A	N/A	N/A	20.44	Positive

Table 12. List of low concentration positive controls used in each real-time RT-PCR run for detection of SARS-CoV-2 in clinical samples. The table depicts the positive control ID of each low positive control (10^3/µl) used in each real-time RT-PCR reaction for the detection of SARS-CoV-2 in clinical samples obtained from the diagnostic surveillance at UCY. Also, it presents the date that each low positive control was used in real-time RT-PCR. Additionally, it indicates the corresponding target gene of the positive control, as well as the CT value that it controls exceeded the threshold line. The yellow colour shows the positivity of the positive control.

POSITIVE CONTROL ID	DATE	E GENE		S GENE		M GENE		N GENE	
		Ct VALUES	RESULT	Ct VALUES	RESULT	Ct VALUES	RESULT	Ct VALUES	RESULT
WuHan RNA 10^3	18/09/2020	30.73	Positive	N/A	N/A	N/A	N/A	N/A	N/A
WuHan RNA 10^3	22/09/2020	31.97	Positive	N/A	N/A	N/A	N/A	N/A	N/A
WuHan RNA 10^3	23/09/2020	31.32	Positive	N/A	N/A	N/A	N/A	N/A	N/A
WuHan RNA 10^3	24/09/2020	31.08	Positive	N/A	N/A	N/A	N/A	N/A	N/A
WuHan RNA 10^3	25/09/2020	32.05	Positive	N/A	N/A	N/A	N/A	N/A	N/A
WuHan RNA 10^3	25/09/2020	31.44	Positive	N/A	N/A	N/A	N/A	N/A	N/A
WuHan RNA 10^3	29/09/2020	31.08	Positive	N/A	N/A	N/A	N/A	N/A	N/A
WuHan RNA 10^3	02/10/2020	31.47	Positive	N/A	N/A	N/A	N/A	N/A	N/A
WuHan RNA 10^3	06/10/2020	31.28	Positive	N/A	N/A	N/A	N/A	N/A	N/A
WuHan RNA 10^3	09/10/2020	28.83	Positive	N/A	N/A	30.26	Positive	N/A	N/A
WuHan RNA 10^3	13/10/2020	29.23	Positive	N/A	N/A	32.95	Positive	N/A	N/A
WuHan RNA 10^3	16/10/2020	28.14	Positive	N/A	N/A	N/A	N/A	N/A	N/A
WuHan RNA 10^3	20/10/2020	29.58	Positive	N/A	N/A	N/A	N/A	N/A	N/A
WuHan RNA 10^3	21/10/2020	28.32	Positive	32.53	Positive	N/A	N/A	N/A	N/A
WuHan RNA 10^3	22/10/2020	28.34	Positive	N/A	N/A	N/A	N/A	N/A	N/A
WuHan RNA 10^3	23/10/2020	28.54	Positive	N/A	N/A	N/A	N/A	31.71	Positive
WuHan RNA 10^3	27/10/2020	28.72	Positive	N/A	N/A	N/A	N/A	N/A	N/A
WuHan RNA 10^3	30/10/2020	27.75	Positive	N/A	N/A	N/A	N/A	N/A	N/A
Tgene RNA 10^3	02/11/2020	27.50	Positive	N/A	N/A	N/A	N/A	29.27	Positive

Tgene RNA 10^3	03/11/2020	N/A	N/A	N/A	N/A	N/A	N/A	28.73	Positive
Tgene RNA Transcript 10^3	04/11/2020	27.07	Positive	N/A	N/A	N/A	N/A	30.27	Positive
Tgene RNA Transcript 10^3	06/11/2020	N/A	N/A	N/A	N/A	N/A	N/A	32.55	Positive
Tgene RNA Transcript 10^3	10/11/2020	N/A	N/A	N/A	N/A	N/A	N/A	31.26	Positive
Tgene RNA Transcript 10^3	11/11/2020	29.585087	Positive	N/A	N/A	N/A	N/A	33.93	Positive
Tgene RNA Transcript 10^3	13/11/2020	N/A	N/A	N/A	N/A	N/A	N/A	33.38	Positive
Tgene RNA Transcript 10^3	16/11/2020	31.29	Positive	N/A	N/A	N/A	N/A	32.16	Positive
Tgene RNA Transcript 10^3	17/11/2020	N/A	N/A	N/A	N/A	N/A	N/A	33.34	Positive
Tgene RNA Transcript 10^3	18/11/2020	29.83	Positive	N/A	N/A	N/A	N/A	33.28	Positive
Tgene RNA Transcript 10^3	20/11/2020	N/A	N/A	N/A	N/A	N/A	N/A	36.09	Positive
Tgene RNA Transcript 10^3	23/11/2020	32.06	Positive	N/A	N/A	N/A	N/A	33.51	Positive
Tgene RNA Transcript 10^3	24/11/2020	N/A	N/A	N/A	N/A	N/A	N/A	34.73	Positive
Tgene RNA Transcript 10^3	25/11/2020	30.10	Positive	N/A	N/A	N/A	N/A	34.40	Positive
Tgene RNA Transcript 10^3	27/11/2020	29.73	Positive	N/A	N/A	N/A	N/A	N/A	N/A
Tgene RNA Transcript 10^3	01/12/2020	31.88	Positive	N/A	N/A	N/A	N/A	N/A	N/A
Tgene RNA Transcript 10^3	02/12/2020	33.23	Positive	N/A	N/A	N/A	N/A	N/A	N/A
Tgene RNA Transcript 10^3	03/12/2020	32.82	Positive	N/A	N/A	32.79697	Positive	N/A	N/A
Tgene RNA Transcript 10^3	04/12/2020	27.12	Positive	N/A	N/A	N/A	N/A	N/A	N/A
Tgene RNA Transcript 10^3	08/12/2020	32.29	Positive	N/A	N/A	N/A	N/A	N/A	N/A
Tgene RNA Transcript 10^3	11/12/2020	N/A	N/A	N/A	N/A	N/A	N/A	35.25	Positive
Tgene RNA Transcript 10^3	14/12/2020	30.78	Positive	N/A	N/A	N/A	N/A	N/A	N/A
Tgene RNA Transcript 10^3	15/12/2020	31.14	Positive	N/A	N/A	N/A	N/A	N/A	N/A
Tgene RNA Transcript 10^3	17/12/2020	N/A	N/A	N/A	N/A	N/A	N/A	31.77	Positive
Tgene RNA Transcript 10^3	18/12/2020	29.56	Positive	N/A	N/A	N/A	N/A	32.54	Positive
Tgene RNA Transcript 10^3	07/01/2020	N/A	N/A	N/A	N/A	N/A	N/A	33.28	Positive
Tgene RNA Transcript 10^3	08/01/2020	N/A	N/A	N/A	N/A	N/A	N/A	35.15	Positive
Tgene RNA Transcript 10^3	12/01/2020	N/A	N/A	N/A	N/A	N/A	N/A	33.93	Positive
Tgene RNA Transcript 10^3	14/01/2020	N/A	N/A	N/A	N/A	N/A	N/A	31.99	Positive

Table 13. List of high concentration positive controls used in real-time RT-PCR run for detection of SARS-CoV-2 in clinical samples. The table depicts the positive control ID of each high positive control (10^6 /μl) used in each real-time RT-PCR reaction for the detection of SARS-CoV-2 in clinical samples obtained from the diagnostic surveillance at UCY. Also, it presents the date that each high positive control was used in real-time RT-PCR. Additionally, it indicates the corresponding target gene of the positive control, as well as the CT value that it controls exceeded the threshold line. The yellow colour shows the positivity of the positive control.

POSITIVE CONTROL ID	DATE	E GENE		S GENE		M GENE		N GENE	
		Ct VALUES	RESULT	Ct VALUES	RESULT	Ct VALUES	RESULT	Ct VALUES	RESULT
Tgene RNA Transcript 10^6	18/09/2020	22.29	Positive	N/A	N/A	N/A	N/A	N/A	N/A
Tgene RNA Transcript 10^6	25/09/2020	21.58	Positive	22.76	Positive	N/A	N/A	N/A	N/A
Tgene RNA Transcript 10^6	25/09/2020	22.00	Positive	N/A	N/A	N/A	N/A	N/A	N/A
Tgene RNA Transcript 10^6	29/09/2020	20.25	Positive	N/A	N/A	N/A	N/A	N/A	N/A
Tgene RNA Transcript 10^6	02/10/2020	20.60	Positive	N/A	N/A	N/A	N/A	N/A	N/A
Tgene RNA Transcript 10^6	06/10/2020	21.09	Positive	N/A	N/A	N/A	N/A	N/A	N/A
Tgene RNA Transcript 10^6	09/10/2020	21.83	Positive	N/A	N/A	20.61	Positive	N/A	N/A
Tgene RNA Transcript 10^6	13/10/2020	20.78	Positive	N/A	N/A	20.91	Positive	N/A	N/A
Tgene RNA Transcript 10^6	16/10/2020	21.10	Positive	N/A	N/A	N/A	N/A	N/A	N/A
Tgene RNA Transcript 10^6	20/10/2020	21.58	Positive	N/A	N/A	N/A	N/A	N/A	N/A
Tgene RNA Transcript 10^6	21/10/2020	21.81	Positive	21.91	Positive	N/A	N/A	N/A	N/A
Tgene RNA Transcript 10^6	22/10/2020	21.71	Positive	27.21	Positive	N/A	N/A	N/A	N/A
Tgene RNA Transcript 10^6	23/10/2020	22.16	Positive	N/A	N/A	N/A	N/A	18.88	Positive
Tgene RNA Transcript 10^6	27/10/2020	20.49	Positive	N/A	N/A	N/A	N/A	N/A	N/A
Tgene RNA Transcript 10^6	30/10/2020	20.60	Positive	N/A	N/A	N/A	N/A	N/A	N/A
Tgene RNA Transcript 10^6	02/11/2020	20.95	Positive	N/A	N/A	N/A	N/A	18.97	Positive
Tgene RNA Transcript 10^6	06/11/2020	N/A	N/A	N/A	N/A	N/A	N/A	19.20	Positive
Tgene RNA Transcript 10^6	10/11/2020	N/A	N/A	N/A	N/A	N/A	N/A	18.90	Positive

Tgene RNA Transcript 10^6	11/11/2020	N/A	N/A	N/A	N/A	N/A	N/A	20.08	Positive
Tgene RNA Transcript 10^6	11/11/2020	20.07	Positive	N/A	N/A	N/A	N/A	20.37	Positive
Tgene RNA Transcript 10^6	13/11/2020	N/A	N/A	N/A	N/A	N/A	N/A	19.91	Positive
Tgene RNA Transcript 10^6	16/11/2020	20.46	Positive	N/A	N/A	N/A	N/A	20.17	Positive
Tgene RNA Transcript 10^6	17/11/2020	N/A	N/A	N/A	N/A	N/A	N/A	20.21	Positive
Tgene RNA Transcript 10^6	18/11/2020	21.06	Positive	N/A	N/A	N/A	N/A	20.42	Positive
Tgene RNA Transcript 10^6	20/11/2020	N/A	N/A	N/A	N/A	N/A	N/A	21.47	Positive
Tgene RNA Transcript 10^6	23/11/2020	21.07	Positive	N/A	N/A	N/A	N/A	22.03	Positive
Tgene RNA Transcript 10^6	24/11/2020	N/A	N/A	N/A	N/A	N/A	N/A	22.17	Positive
Tgene RNA Transcript 10^6	25/11/2020	21.48	Positive	N/A	N/A	N/A	N/A	20.04	Positive
Tgene RNA Transcript 10^6	27/11/2020	21.05	Positive	N/A	N/A	N/A	N/A	N/A	N/A
Tgene RNA Transcript 10^6	01/12/2020	21.71	Positive	N/A	N/A	N/A	N/A	N/A	N/A
Tgene RNA Transcript 10^6	02/12/2020	20.32	Positive	N/A	N/A	N/A	N/A	N/A	N/A
Tgene RNA Transcript 10^6	03/12/2020	20.53	Positive	N/A	N/A	N/A	N/A	N/A	N/A
Tgene RNA Transcript 10^6	04/12/2020	21.16	Positive	N/A	N/A	N/A	N/A	N/A	N/A
Tgene RNA Transcript 10^6	08/12/2020	21.72	Positive	N/A	N/A	N/A	N/A	N/A	N/A
Tgene RNA Transcript 10^6	11/12/2020	N/A	N/A	N/A	N/A	N/A	N/A	19.97	Positive
Tgene RNA Transcript 10^6	14/12/2020	22.08	Positive	N/A	N/A	N/A	N/A	19.72	Positive
Tgene RNA Transcript 10^6	15/12/2020	20.89	Positive	N/A	N/A	N/A	N/A	20.68	Positive
Tgene RNA Transcript 10^6	17/12/2020	N/A	N/A	N/A	N/A	N/A	N/A	20.68	Positive
Tgene RNA Transcript 10^6	18/12/2020	21.18	Positive	N/A	N/A	N/A	N/A	20.94	Positive
Tgene RNA Transcript 10^6	07/01/2020	N/A	N/A	N/A	N/A	N/A	N/A	21.49	Positive
Tgene RNA Transcript 10^6	08/01/2020	N/A	N/A	N/A	N/A	N/A	N/A	20.02	Positive
Tgene RNA Transcript 10^6	12/01/2020	N/A	N/A	N/A	N/A	N/A	N/A	20.16	Positive
Tgene RNA Transcript 10^6	14/01/2020	N/A	N/A	N/A	N/A	N/A	N/A	20.44	Positive

4. DISCUSSION

A previous epidemic caused by SARS-CoV insinuated a probable emergence or re-emergence of novel infectious coronaviruses in the future (Chrysostomou et al., 2021a). Such possibility caused the scientific community to be prepared and weary regarding these types of viruses and instigated global efforts for studying and developing methods to screen and identify upcoming threats (Hadjinicolaou et al., 2011). Indeed, SARS-CoV-2 has emerged since then and it is the causative agent of the on-going COVID-19 pandemic that has caused an international public health emergency (Wozniak et al., 2020). Therefore, the development of a fast and accurate detection assay for the identification of SARS-CoV-2 is essential for the protection of public health (Hadjinicolaou et al., 2011). However, it is equally as important to validate this assay for its performance and accuracy. This study presents the design and development of an in-house molecular beacon-based real-time RT-PCR assay for the detection of SARS-CoV-2 genes S, E, M and N, by the BMV laboratory of UCY, for the purposes of the diagnostic surveillance for the students and staff of the UCY. This in-house assay was based on previous knowledge, derived from the patented SARS-associated work produced by Professor Leondios Kostrikis (US Patent No. 7,709,188 B2, issued 4 May 2010) for the detection of SARS-CoV, and was later modified for SARS-CoV-2 (Chrysostomou et al., 2021a, Hadjinicolaou et al., 2011). Moreover, the in-house molecular beacon-based real-time RT-PCR assay for the detection of SARS-CoV-2 was designed with mismatch-tolerant MBs to account for the genetic variability caused by unexpected new mutations that may possibly occur in the genome of SARS-CoV-2 (Chrysostomou et al., 2021a). Additionally, the validity and efficiency of the designed assay was tested initially with EQAs and later with clinical samples from the UCY surveillance. Overall, the development of such accurate and efficient detection method for SARS-CoV-2 can be considered as a crucial weapon to monitor the infection and be able to inform health authorities in order to control the rampart transmission of the virus and protect public health.

For the adaptation of the pre-existing SARS-CoV detection assay from the patented SARS-associated work produced by Professor Leondios Kostrikis (US Patent No. 7,709,188 B2, issued 4 May 2010), for the purposes of the detection of SARS-CoV-2 in the clinical samples from the surveillance at the UCY, it was required to check the similarity between the targeted regions of

the assay. The SARS-CoV assay was designed to specifically detect the S, E, M, and N genes, consequently a multiple sequence alignment was completed for these regions from SARS-CoV (Urbani and Tor2) and SARS-CoV-2 (MN908947.3 and MT066156) and was used for the generation of MBs and primers of the assay. Because the assay was designed to target four distinct regions of the genome; the specificity and sensitivity of the assay was subsequently increased. Also, the MBs of the assay were designed with long loops (24-26 nucleotides) which provided them with the ability of being mismatch-tolerant. Mismatch-tolerant beacons are more flexible to account unexpected polymorphisms that may occur from genetic drift of the virus (Marras et al., 2005).

Thermal denaturation profiles were completed to determine the window of discrimination of the assay, specifically the range of temperature in which perfectly complementary beacon-target hybrids can form and mismatched beacon-target hybrids cannot form (Biosynthesis, 2015). From the plotted data, it was discovered that the melting temperature of all MBs designed for the assay was approximately 60 °C and taking into account Tm of the primers, the optimal temperature selected for the real-time RT-PCR assay was 53 °C (Figure 7-10). This was in compliance with the standard guidelines for optimal beacon design that state that the Tm of beacons should be 7-10 °C above the annealing temperature of the real-time RT-PCR reaction (Biosynthesis, 2015). In regard to the decreased fluorescence signal observed in lower temperatures of the MB-target hybrid, it may have been due to the decrease in temperature of the reaction in which the MBs become less specific for hybridization and consequently, MBs prefer to close instead of hybridizing with an incorrect target (Kostrikis et al., 1998). This decrease in fluorescence does not affect the experiment process, because the optimal temperature selected for the experiment is set at higher temperature at which the specificity of the beacon to the target is maintained. Additionally, different concentrations of MBs were tested during the thermal denaturation profiles, however, the concentration of 15 picomoles per reaction was eventually selected as the most suitable based on the signal beacon-target versus background ratio.

Having explained the design and development part of this assay, it is important to move on to its validation through clinical samples, which was the focal point of this thesis. The validation of every assay is an essential process that estimates its sensitivity and specificity as a diagnostic test (Garrido, 2020). More importantly, validation with clinical samples should be performed to

every assay developed (Garrido, 2020). The reason for this is because, in vivo validation of an assay reassures optimal conditions of the samples, however, clinical blinded samples may not be as perfect as in vitro due to different concentrations (Garrido, 2020). Through clinical samples validation, diagnostic assays must present the necessary sensitivity to identify a high percentage of infected individuals (Garrido, 2020). Additionally, such assays for the detection of diseases through clinical samples must show great specificity, so false-negative results are avoided (Younes et al., 2020). Accordingly, for the validation process of the in-house molecular beacon-based real-time RT-PCR assay presented in this thesis, clinical samples obtained from the surveillance at the UCY for the detection of SARS-CoV-2 were analysed. It is important to note that surveillance testing is primarily used to obtain information about the community as a total, instead of an individual level and help in the monitoring of the disease (FDA, 2020).

From the surveillance at the UCY, more than 2000 individuals were tested from September 2020 to January 2021. The samples were analysed with the use of the in-house molecular beacon-based real-time RT-PCR assay designed for detection of SARS-CoV-2 developed by the BMV UCY laboratory. Before the beginning of the study, bioethical approval was received by the Cyprus National bioethics Committee (ΕΕΒΚ ΕΠ 2020.01.192), and the samples were double coded guaranteeing the anonymity of the study subjects. By the end of the diagnostic surveillance, a total of 534 tubes containing either pooled or individual samples were analysed, from which the 22 pooled samples were found positive. These 22 samples were re-examined after individual sampling and 15 of them were confirmed positive. The pooling method used in the collection of the samples offers several benefits; first, it is a technique with lower expenses than individual testing as it requires smaller amounts of reagents and resources. Also, it demands less amount of time for the diagnosis because the specimens are analysed in groups (CDC, 2021), more specifically in groups of 5 nasopharyngeal samples in average. Generally, the pooling method is most effective when applied to populations with low expectance of positive results, otherwise it can have opposite effect in efficiency (Aspinall and Yamashiro, 2020).

For this surveillance testing at the UCY, upon reception of the samples, the RNA was extracted and uniplex real-time RT-PCR was performed on the clinical samples, since it was important to validate the results that were acquired in the design and development part of the assay with clinical data. Specifically, when the uniplex real-time RT-PCR was performed for the design

and development part of the assay, it was tested on the purified SARS-CoV-2 RNA from Coronavirus strain grown in cell culture (BetaCoV/Germany/BavPat1/2020 p.1" grown in cell culture (Charité, Berlin, European Virus Archive goes Global, EVAg)). It was verified that all four MBs designed for each targeted gene showed amplification and fluoresced exponentially in the presence of the perfectly complementary target. Fluorescence of all MB-targets in the tested sample exceeded the threshold line on average in the 31.4 Ct ± 0.9, thus confirming the uniform amplification and detection abilities among the targeted genes. Similarly, for the clinical validation part of the assay, these results were also confirmed by the clinical samples where the Cts on average were 31.5 ± 6.8 and for the positive controls (used for the clinical samples) the average Ct values were 31.7 ± 1.7 for the positive control with concentration 10^3 copies/μl and 21.6 ± 1.1 for the positive control with concentration 10^6 copies/μl (Table 11-13). The larger standard deviation for the clinical samples, can be explained by the variability in viral load for each sample, which is apparent when observing the Cts for the positive controls where a lower Ct is resulted as the viral concentration increases. Thus, the threshold cycle is inversely proportional to the viral load. It is important to mention that for a sample to be considered as positive a clear exponential growth curve should surpass the threshold line before the 40^{th} cycle (Kapoor et al., 2021). Additionally, the validation process of the assay which was also completed through EQAs conducted with blinded samples of different concentrations of human coronaviruses (from WHO and QCMD) indicated the specificity and sensitivity of the assay. Specifically, the sensitivity of the in-house assay was proven when it successfully detected SARS-CoV-2 in all SARS-CoV-2 positive samples of different concentrations from both panels ranging as low as ~2 x 10^2 copies/ml and as high as ~1 x 10^6 copies/ml. Furthermore, it did not recognize any of the samples that contained other than SARS-CoV-2 virus or negative controls. Thus, these results validate the accuracy, sensitivity, and specificity of the developed assay. The exponential curve of the results indicates the correct amplification of the target and confirms that the design of the MBs and primers of the assay was successful. Moreover, in the absence of target, no amplification was observed, therefore no fluorescence was observed. This again supports the specificity of the assay design and the theory that when in the absence of the correct target, the MBs prefer to stay in a closed conformation instead of emitting false signal (Biosynthesis, 2015).

Nonetheless, it is important to explain the differences in Ct values presented in the results of the clinical samples (higher standard deviation). One explanation can be that when a sample is examined by a different target gene, differences can be observed in the Ct values and this could possibly be due to SARS-CoV-2 "RNA shedding" (Boeckmans et al., 2021). In such cases, the viral RNA can be detected in patients in the form of fragments even after the individuals are not infective (Owusu et al., 2021). Consequently, some fragments of the virus are in larger quantities than others, and this could possibly be the explanation on why different Ct values are presented from different target genes for the same sample. This could also justify the persistent detection of the SARS-CoV-2 virus even after weeks of infection (Owusu et al., 2021). Obviously, this phenomenon cannot be observed in the Ct values measured in the purified SARS-CoV-2 RNA from Coronavirus strain grown in cell culture (BetaCoV/Germany/BavPat1/2020 p.1" grown in cell culture (Charité, Berlin, European Virus Archive goes Global, EVAg)) control and gene RNA transcripts. This is not possible because of the consistent findings in the nature of both controls. The positive control from EVAg was purified and cultured which means that the whole genome of the virus was present and was also diluted to a standard working concentration of 10^3 copies/μl. Accordingly, the gene RNA transcripts were also purified and used at standard concentrations (10^3 copies/μl and 10^6 copies/μl).

In specific cases from the clinical samples examined by the in-house developed assay, pooled samples were marked as borderline positive but when re-examined individually, they were found negative. A possible explanation could be that during the first examination, the study subjects were towards the end of infection; so, the viral concentrations of the samples were low but still detectable from real-time RT-PCR. However, the next day of examination, the participants received a negative result because the virus concentration was undetectable (Mallett et al., 2020). Additionally, differences in the Ct values of the same samples may be caused by the sampling skills of the medical personnel and the different sampling techniques they use; specifically nasopharyngeal, oropharyngeal, or nasal swabs (Boeckmans et al., 2021).

It is imperative to highlight the importance of the RNA transcripts that were designed and produced by the BMV laboratory with the purpose of being used as positive controls during the performance of the in-house molecular beacon-based real-time RT-PCR assay, for detection of SARS-CoV-2 in clinical samples from the diagnostic surveillance at the UCY. The transcripts

generated for S, E, M and N genes enhanced the quality and accuracy of the in-house developed assay because they ensured avoidance of false-negative results. As stated above, during the clinical samples analyses with the assay, the produced RNA transcripts were used in two different concentrations, 10^3 copies/µl which was the same concentration as the initial positive control used in the assay (purified SARS-CoV-2 RNA from Coronavirus, EVAg) and 10^6 copies/µl, which was considered as a high positive control in real-time RT-PCR. These known concentrations of the controls also gave an approximate indication of the viral loads of the samples. The production of RNA transcripts had various advantages for the validation of the assay through clinical samples. Firstly, the transcripts were generated in large quantities, providing a steady supply of positive controls, and eliminating the need for purchasing commercially available positive controls. This enabled the validation process to proceed smoothly and greatly reduced the overall time and costs of the assay since in the RNA transcripts were produced and validated in-house, in contrast to the purchased purified SARS-CoV-2 RNA from Coronavirus strain grown in cell culture (BetaCoV/Germany/BavPat1/2020 p.1" grown in cell culture (Charité, Berlin, European Virus Archive goes Global, EVAg)), which arrived in a limited amount and a specific concentration (10^4 copies/µl). Moreover, the purified RNA transcripts showed high consistency with the low positive control (10^3 copies/µl), when tested on clinical samples from the diagnostic surveillance, consequently they successfully replaced them in the reaction. Overall, the use of RNA transcripts as positive controls was an important and useful part of the validation of the assay through clinical samples.

As it is described above, the in-house molecular beacon-based real-time RT-PCR assay developed from the BMV laboratory of UCY had several strengths, it was successfully validated through EQAs and later applied to clinical samples for the detection of SARS-CoV-2. Nonetheless, taking a deeper look into the period of the design, development, and implementation of the assay, it was shown that there was a variety of lineages of SARS-CoV-2 that were circulating in Cyprus however, the most prevalent were B.1.258, B.1.129 and B.1.177 (Chrysostomou et al., 2021b). This indicates that there was a specific pool of circulating lineages that the assay could be tested on; and even though, the assay was not limited because the mutations of these lineages were not in the targeted regions, it is important to constantly re-examine the assay for its effectiveness and accuracy against the current emergence of novel mutations in the genome of SARS-CoV-2.

Nevertheless, the fact that the designed assay targets four different genes of the virus is considered as a major advantage for the successful detection of SARS-CoV-2 (Chrysostomou et al., 2021a), since the likelihood of false-negative results with variants that contain mutations in the primer or MB binding region of one of the target genes is decreased (Bland et al., 2021). To verify the MBs mismatch tolerance on single nucleotide polymorphisms present in the target recognition site, the developed assay has to be tested with a larger cohort of clinical samples that are classified within the actively circulating lineages (Chrysostomou et al., 2021a). Also, the primers and MBs of the designed assay can be regularly blasted against the SARS-CoV-2 available genomes in databases to ensure that the new mutations do not affect the performance of the assay. However, in case the efficiency of the assay in detecting SARS-CoV-2 would be compromised, the design can be easily modified due to its adaptable character.

SARS-CoV-2 is a virus that receives evolutionary pressures from the constant transmission as well as the immune system of the host and in order to survive and proliferate it has acquired a myriad of mutations and deletions, in a short span since its emergence (Zhou et al., 2021). These mutations/deletions are divided into lineages and sub-lineages of SARS-CoV-2 and some of them were denoted as as "Variants of Concern" (VOCs) by WHO/ECDC (Gomez et al., 2021). Currently, the list of VOCs encompasses the B.1.351 South Africa variant (Beta), P.1 Brazil variant (Gamma), B.1.617.2 Indian Variant (Delta) and B.1.1.529 South Africa and Botswana variant (Omicron) (ECDC, 2021). The VOCs are described as having increased transmissibility, enhanced disease severity and immune evasion (Zella et al., 2021). Consequently, it is urgent to check if the current assays can detect them such as the one presented in this thesis, and/or create efficient and accurate detection methods that will specifically target VOCs, to avoid uncontrollable transmission of the virus (Gomez et al., 2021). The aforementioned methodology described can be used for the development of a novel design based on molecular beacon real-time RT-PCR which will specifically target mutations or deletions of the different VOCs of SARS-CoV-2. To achieve successful discrimination between VOCs, the molecular beacons for this assay will be designed as mismatch sensitive. This will be accomplished with the design of shorter loops which will prohibit nucleotide substitutions and longer stems with high GC content which will help in avoidance of wrong hybridization of the MBs (Tyagi et al., 1997). This highlights the adaptability of this assay

and the possibility of improvement as the virus evolves which can further contribute towards the eradication of SARS-CoV-2 (Sharun et al., 2021).

Additionally, the present assay can be further improved upon by creating standard curves in order to accurately quantify the clinical samples that are analysed through real-time RT-PCR (Wei et al., 2009). To achieve that, samples with known concentrations, specifically from the purified RNA transcripts produced by the BMV laboratory, will be further utilized, to create serial dilutions, and then construct a standard curve to define the limit of detection for each of the tested MBs (Overbergh et al., 2017). The purified gene RNA transcripts will be serially 10-fold diluted in range 10^8 to 10^1 copies/µl and their Ct values will be expected to differ by ~3.3 cycles (Overbergh et al., 2017). After the construction of the standard curve, the Ct value of an unknown concentration clinical sample will be plotted on the standard curve and the viral concentration of the sample can be determined (Overbergh et al., 2017).

Another improvement on the assay could be the performance of multiplex real-time RT-PCR with the use of the in-house developed molecular beacon-based real-time RT-PCR assay, for the detection of SARS-CoV-2 in clinical samples. With multiplex real-time RT-PCR, multiple targets can be amplified in the same reaction by a different set of primers and MBs with distinct fluorophores (IDT, 2013). Therefore, the expression levels of multiple targets of genes can be measured simultaneously (IDT, 2013). An internal positive control (IPC) can be also incorporated in the multiplex real-time RT-PCR reaction and be co-amplified with its complementary target sequence to ensure the validity of the molecular test. An IPC was already designed by the BMV laboratory of UCY, in the form of a mosaic of the four targeted genes S, E, M and N of SARS-CoV-2 and can be easily adapted to the developed in-house molecular beacon-based real-time RT-PCR assay for multiplex real-time RT-PCR. In order to accomplish a successful multiplex real-time RT-PCR reaction, the Tm of the primers and beacons must be consistent because only one annealing temperature will be used (Mahony, 1996). Also, all the primers and MBs included in the reaction should not exhibit any interaction, either homodimers or heterodimers (IDT, 2013). Furthermore, the volumes of reagents and the total volume of reaction should be re-adjusted and re-calculated to serve the purposes of the multiplex real-time RT-PCR (Markoulatos et al., 2002). Overall, the in-house developed molecular beacon-based real-time RT-PCR assay can be definitely modified to fit the needs of multiplex real-time RT-PCR for the detection of SARS-CoV-2 in

clinical samples. Subsequently, this will benefit the diagnosis of clinical samples by saving effort, time, and reagent cost (IDT, 2013).

CONCLUSION

Rapid and accurate diagnostic methods of SARS-CoV-2 are crucial for early detection, reporting, and minimisation of the transmission of the virus. To achieve that, all developed diagnostic assays must be validated for their specificity and sensitivity through clinical samples. In this study, the methodology for the design of a molecular beacon-based real-time RT-PCR assay developed from the BMV laboratory is presented. Moreover, the successful validation of the assay's performance through clinical samples obtained from the diagnostic surveillance executed at the UCY, is described. Through this thesis and the validation performed on clinical samples, the aforementioned assay was proven to be a reliable and efficient method for the diagnosis of SARS-CoV-2 which can be easily modified to adapt to the requirements of future emerging mutations/deletions in the genome of the virus.

ABBREVIATIONS

ABBREVIATION	MEANING
A	Adenine
ACE2	Angiotensin-Converting Enzyme 2
BL-3	Biosafety Level 3
BMV	Biotechnology and Molecular Virology
C	Cytosine
CoV	Coronavirus
COVID-19	Coronavirus Disease 2019
CNS	Central Nervous System
CTD	Carboxy (C)-Terminal Domain
dH2O	Distilled Water
E	Envelope
EQA	External Quality Assessment
FAM	6-carboxyfluorescein
FW	Forward Primer
G	Guanine
HEX	N-HEX-6-aminohexanol
HIV	Human Immunodeficiency Virus
HSSM	Huanan South Seafood Market
IDT	Integrated DNA Technologies
IPC	Internal Positive Control
M	Membrane

MB	Molecular Beacon
N	Nucleocapsid
Nsp	Non-Structural Proteins
NTC	No-Template Control
NTD	Amino (N)-Terminal Domain
ORF	Open Reading Frame
QCMD	Quality Control for Molecular Diagnostics
RBD	Receptor-Binding Domain
RT	Reverse Transcriptase
RT-PCR	Reverse Transcription Polymerase Chain Reaction
RV	Reverse Primer
S	Surface
SARS	Severe Acute Respiratory Syndrome
SARS-CoV-2	Severe Acute Respiratory Syndrome Coronavirus 2
T	Thymine
TET	N-TET-6-aminohexanol
Tm	Melting Temperature
Tmd	Transmembrane Domain
TMPRSS2	Type II Transmembrane Serine Protease
UCY	University of Cyprus
US CDC	United States Centres of Disease Control and Prevention
UTR	Untranslated Region
VLP	Virus-Like Particle
WHO	World Health Organization

REFERENCES

ABDULJALIL, J.M., 2020. Laboratory diagnosis of SARS-CoV-2: available approaches and limitations. *New microbes and new infections,* vol. 36, pp. 100713.

ASPINALL, M. G. and YAMASHIRO, C., 2020. Testing More by Testing Less Pooling test samples: How and when it works. *ASU*. https://chs.asu.edu/diagnostics-commons/blog/pooling-test-samples.

BIOSYNTHESIS. 2015. Design rules of Molecular Beacons. *Technical & Educational Warehouse.* https://www.biosyn.com/tew/Design-rules-for-Molecular-Beacons.aspx.

BLAND, J., KAVANAUGH, A., HONG, L. K., PEREZ, O., and KADKOL, S. S. 2021. A Multiplex One-Step RT-qPCR Protocol to Detect SARS-CoV-2 in NP/OP Swabs and Saliva. *Current protocols*, vol. 1, no. 5, e145.

BOECKMANS, J., CARTUYVELS, R., HILKENS, P., BRUCKERS, L., MAGERMAN, K., WAUMANS, L. and RAYMAEKERS, M., 2021. Follow-up testing of borderline SARS-CoV-2 patients by rRT-PCR allows early diagnosis of COVID-19. *Diagn Microbiol Infect Dis.*, vol. 100, no. 2, 115350

BONNET, G., TYAGI, S., LIBCHABER, A., and KRAMER, F. R. 1999. Thermodynamic basis of the enhanced specificity of structured DNA probes. *Proceedings of the National Academy of Sciences of the United States of America*, vol. *96*, no.11, 6171–6176. https://doi.org/10.1073/pnas.96.11.6171.

CANDEL, F.J., BARREIRO, P., SAN ROMAN, J., ABANADES, J.C., BARBA, R., BARBERAN, J., BIBIANO, C., CANORA, J., CANTON, R., CALVO, C., CARRETERO, M., CAVA, F., DELGADO, R., GARCIA-RODRIGUEZ, J., GONZALEZ DEL CASTILLO, J., GONZALEZ DE VILLAUMBROSIA, C., HERNANDEZ, M., LOSA, J.E., MARTINEZ-PEROMINGO, F.J., MOLERO, J.M., MUNOZ, P., ONECHA, E., ONODA, M., RODRIGUEZ, J., SANCHEZ-CELAYA, M., SERRA, J.A. and ZAPATERO, A., 2020. Recommendations for use of antigenic tests in the diagnosis of acute SARS-CoV-2 infection in the second pandemic wave: attitude in different clinical settings. *Revista espanola de quimioterapia : publicacion oficial de la Sociedad Espanola de Quimioterapia,* vol. 33, no. 6, pp. 466-484.

CDC. 2021. Testing Overview. *COVID-19. https://www.cdc.gov/coronavirus/2019-ncov/hcp/testing-overview.html.*

CHAU, C.H., STROPE, J.D. and FIGG, W.D., 2020. COVID-19 Clinical Diagnostics and Testing Technology. *Pharmacotherapy: The Journal of Human Pharmacology and Drug Therapy*, vol. 40, no. 8, pp. 857-868.

CHAN, K.K., DOROSKY, D., SHARMA, P., ABBASI, S.A., DYE, J.M., KRANZ, D.M., HERBERT, A.S. and PROCKO, E., 2020. Engineering human ACE2 to optimize binding to the spike protein of SARS coronavirus 2. *Science (New York, N.Y.)*, 20200804, vol. 369, no. 6508, pp. 1261-1265 ISSN 1095-9203; 0036-8075. DOI 10.1126/science.abc0870 [doi].

CHRYSOSTOMOU, A.C, RODOSTHENOUS, J.H., TOPCU, C., PAPA, C., ARISTOKLEOUS, A., STATHI, G., CHRISTODOULOU, C., ELEFTHERIOU, C., STYLIANOU, D.C and KOSTRIKIS, L.G. 2021a. A Multiallelic Molecular Beacon-Based Real-Time RT-PCR Assay for the Detection of SARS-CoV-2. *Life*, vol. 11, no. 11, pp. 1146.

CHRYSOSTOMOU, A. C., VRANCKEN, B., KOUMBARIS, G., THEMISTOKLEOUS, G., ARISTOKLEOUS, A., MASIA, C., ELEFTHERIOU, C., IOANNOU, C., STYLIANOU, D. C., IOANNIDES, M., PETROU, P., GEORGIOU, V., HATZIYIANNI, A., LEMEY, P., VANDAMME, A.M., PATSALIS, P.P. and KOSTRIKIS, L.G. 2021b. A Comprehensive Molecular Epidemiological Analysis of SARS-COV-2 Infection in Cyprus from April 2020 to January 2021: Evidence of a Highly Polyphyletic and Evolving Epidemic. *Viruses*, vol. 13, no. 6, 2021, p. 1098.

D'CRUZ, R.J., CURRIER, A.W. and SAMPSON, V.B., 2020. Laboratory testing methods for novel severe acute respiratory syndrome-coronavirus-2 (SARS-CoV-2). *Frontiers in cell and developmental biology*, vol. 8.

DEEKS, J.J., DINNES, J., TAKWOINGI, Y., DAVENPORT, C., SPIJKER, R., TAYLOR-PHILLIPS, S., ADRIANO, A., BEESE, S., DRETZKE, J. and DI RUFFANO, L.F., 2020. Antibody tests for identification of current and past infection with SARS-CoV-2. *Cochrane Database of Systematic Reviews*, no. 6.

DEVAUX, C.A., 2012. Emerging and re-emerging viruses: A global challenge illustrated by Chikungunya virus outbreaks. *World Journal of Virology*, vol. 1, no. 1, pp. 11-22 ISSN 2220-3249; 2220-3249. DOI 10.5501/wjv.v1.i1.11 [doi].

DHAMA, K., KHAN, S., TIWARI, R., SIRCAR, S., BHAT, S., MALIK, Y.S., SINGH, K.P., CHAICUMPA, W., BONILLA-ALDANA, D.K. and RODRIGUEZ-MORALES, A.J., 2020. Coronavirus Disease 2019-COVID-19. *Clinical microbiology reviews*, vol.33, no. 4, pp. 10.1128/CMR.00028-20.

DHAMA, K., PATEL, S. K., SHARUN, K., PATHAK, M., TIWARI, R., YATOO, M. I., MALIK, Y. S., SAH, R., RABAAN, A. A., PANWAR, P. K., SINGH, K. P., MICHALAK, I., CHAICUMPA, W., MARTINEZ-PULGARIN, D. F., BONILLA-ALDANA, D. K., and RODRIGUEZ-MORALES, A. J. 2020. SARS-CoV-2 jumping the species barrier: Zoonotic lessons from SARS, MERS, and recent advances to combat this pandemic virus. *Travel medicine and infectious disease*, vol. *37*, 101830.

DO VALE, B., LOPES, A.P., DA CONCEIÇÃO FONTES, M., SILVESTRE, M., CARDOSO, L. and COELHO, A.C., 2021. Bats, pangolins, minks and other animals-villains or victims of SARS-CoV-2?. *Veterinary Research Communications*, pp. 1-19.

EUROPEAN CENTRE FOR DISEASE PREVENTION AND CONTROL; SARS-CoV-2 variants of concern as of 3 December 2021 Available online: https://www.ecdc.europa.eu/en/covid-19/variants-concern (accessed on December 03, 2021).

ESAKANDARI, H., NABI-AFJADI, M., FAKKARI-AFJADI, J., FARAHMANDIAN, N., MIRESMAEILI, S. and BAHREINI, E., 2020. A comprehensive review of COVID-19 characteristics. *Biological Procedures Online,* 22, pp. 1-10.

FAUCI, A. S. 2001. Infectious Diseases: Considerations for the 21st Century, Clinical Infectious Diseases, vol. 32, no. 5, pp. 675–685.

FAUCI, A.S. AND MORENS, D.M., 2012. The perpetual challenge of infectious diseases. New England Journal of Medicine, vol. 366, no. 5, pp. 454-461.

FDA. 2020. Pooled Sample Testing and Screening Testing for COVID-19. *Coronavirus (COVID-19) and Medical Devices.* https://www.fda.gov/medical-devices/coronavirus-covid-19-and-medical-devices/pooled-sample-testing-and-screening-testing-covid-19.

FERNANDEZ, H. and MELAMED, E., 2020. Virology of SARS-CoV-2. *Melemad Lab.* http://sites.utexas.edu/melamed-lab/virology-of-sars-cov-2/.

FEHR, A.R. and PERLMAN, S., 2015. Coronaviruses: an overview of their replication and pathogenesis. *Coronaviruses,* pp. 1-23.

FRIEND, T. and STEBBING, J., 2021. What is the intermediate host species of SARS-CoV-2?. *Future Virology.* Vol. 16, no. 3.

GALIPEAU, Y., GREIG, M., LIU, G., DRIEDGER, M. and LANGLOIS, M., 2020. Humoral Responses and Serological Assays in SARS-CoV-2 Infections. *Frontiers in immunology*, vol. 11.

GARRIDO, N. 2020. How to Validate and Assess a Diagnostic Test. *IVIRMA Innovation.* https://www.ivi-rmainnovation.com/how-to-validate-assess-diagnostic-test/.

GIACOBBO, A., RODRIGUES, M.A.S., FERREIRA, J.Z., BERNARDES, A.M. and DE PINHO, M.N., 2021. A critical review on SARS-CoV-2 infectivity in water and wastewater. What do we know?. *Science of the Total Environment*, pp. 145721.

GÓMEZ, C.E., PERDIGUERO, B. and ESTEBAN, M. Emerging sars-cov-2 variants and impact in global vaccination programs against sars-cov-2/covid-19. *Vaccines* 2021, *9*, 1–13.

GREMMELS, H., WINKEL, B.M., SCHUURMAN, R., ROSINGH, A., RIGTER, N.A., RODRIGUEZ, O., UBIJAAN, J., WENSING, A.M., BONTEN, M.J. and HOFSTRA, L.M.,

2021. Real-life validation of the PanbioTM COVID-19 antigen rapid test (Abbott) in community-dwelling subjects with symptoms of potential SARS-CoV-2 infection. *EClinicalMedicine,* vol. 31, pp. 100677.

GROBE, N., CHERIF, A., WANG, X., DONG, Z. and KOTANKO, P., 2021. Sample pooling: burden or solution?. *Clinical Microbiology and Infection,* vol. 27, no. 9, pp. 1212-1220.

GUGLIELMI, G., 2020. Fast coronavirus tests: what they can and can't do. *Nature,* vol. 585, no. 7826, pp. 496-498.

HADJINICOLAOU, A. V., FARCAS, G. A., DEMETRIOU, V. L., MAZZULLI, T., POUTANEN, S. M., WILLEY, B. M., LOW, D. E., BUTANY, J., ASA, S. L., KAIN, K. C., & KOSTRIKIS, L. G. 2011. Development of a molecular-beacon-based multi-allelic real-time RT-PCR assay for the detection of human coronavirus causing severe acute respiratory syndrome (SARS-CoV): a general methodology for detecting rapidly mutating viruses. *Archives of virology*, vol. 156, no. 4, pp. 671–680. https://doi.org/10.1007/s00705-010-0906-7

HAN, H., WEN, H., ZHOU, C., CHEN, F., LUO, L., LIU, J. and YU, X., 2015. Bats as reservoirs of severe emerging infectious diseases. *Virus Research,* vol. 205, pp. 1-6.

HAN, S. X., JIA, X., MA, J. L., & ZHU, Q. 2013. Molecular beacons: a novel optical diagnostic tool. *Archivum immunologiae et therapiae experimentalis*, vol. *61*, no. 2, 139–148. https://doi.org/10.1007/s00005-012-0209-7.

HEDMAN, H.D., KRAWCZYK, E., HELMY, Y.A., ZHANG, L. AND VARGA, C., 2021. Host Diversity and Potential Transmission Pathways of SARS-CoV-2 at the Human-Animal Interface. Pathogens, vol. 10, no. 2, pp. 180.

HUANG, Y., YANG, C., XU, X., XU, W. and LIU, S., 2020. Structural and functional properties of SARS-CoV-2 spike protein: potential antivirus drug development for COVID-19. *Acta Pharmacologica Sinica*, vol. 41, no. 9, pp. 1141-1149.

IDT, I.D.T., 2021. *OligoAnalyzerTM Tool.* [viewed December 2021]. Available from: https://www.idtdna.com/calc/analyzer.

IDT, 2013. Multiplex qPCR – how to get started. *IDT*. [viewed December 2021]. Available from: https://www.idtdna.com/pages/education/decoded/article/multiplex-qpcr-how-to-get-started.

JANIK, E., BARTOS, M., NIEMCEWICZ, M., GORNIAK, L. and BIJAK, M., 2021. SARS-CoV-2: outline, prevention, and decontamination. *Pathogens,* vol. 10, no. 2, pp. 114.

JHU. 2021. *COVID-19 Map-Johns Hopkins Coronavirus Resource Center.* 24-October-2021, [viewed October 2021]. Available from: https://coronavirus.jhu.edu/map.html.

KAPOOR, M., KALITA, D. and PANDA, P.K. 2021. Cycle threshold values versus reverse transcription-polymerase chain reaction positivity in COVID-19 de-isolation. *Indian J Med Microbiol.* Vol. 39, no.1, pp. 133-135.

KHALIL, O., KHALIL, S., 2020. SARS-CoV-2: taxonomy, origin and constitution SARS-CoV-2: taxonomia, *origem e constituição*.

KONTOU, P.I., BRALIOU, G.G., DIMOU, N.L., NIKOLOPOULOS, G. and BAGOS, P.G., 2020. Antibody tests in detecting SARS-CoV-2 infection: a meta-analysis. *Diagnostics,* vol. 10, no. 5, pp. 319.

KOSTRIKIS, L.G, TYAGI, S., MHLANGA, M.M., HO, D.D. and KRAMER, F.R., 1998. Spectral Genotyping of Human Alleles. *Science.* Vol. 279, no. 5354.

KUBINA, R. and DZIEDZIC, A., 2020. Molecular and serological tests for COVID-19 a comparative review of SARS-CoV-2 coronavirus laboratory and point-of-care diagnostics. *Diagnostics,* vol. 10, no. 6, pp. 434.

LARSEN, J.R., MARTIN, M.R., MARTIN, J.D., KUHN, P. and HICKS, J.B., 2020. Modeling the Onset of Symptoms of COVID-19. *Frontiers in Public Health*, vol. 8, pp. 473.

LI Y, ZHOU X and YE D.2008. Molecular beacons: an optimal multifunctional biological probe. *Biochem Biophys Res Commun*, vol. 373, no. 4, pp. 457-461.

MAHONY, J.B., 1996. Multiplex polymerase chain reaction for the diagnosis of sexually transmitted diseases. *Clinics in laboratory medicine,* vol. 16, no. 1, pp. 61-71.

MALLETT, S., ALLEN, A.J. and GRAZIADIO, S. et al. 2020. At what times during infection is SARS-CoV-2 detectable and no longer detectable using RT-PCR-based tests? A systematic review of individual participant data. *BMC Med*, vol. 18, no. 346.

MALIK, Y.A., 2020. Properties of coronavirus and SARS-CoV-2. *The Malaysian journal of pathology*, vol. 42, no. 1, pp. 3-11.

MARKOULATOS, P., SIAFAKAS, N. and MONCANY, M., 2002. Multiplex polymerase chain reaction: a practical approach. *Journal of clinical laboratory analysis,* vol. 16, no.1, pp. 47-51.

MARRAS, S.A.E., TYAGI, S. and KRAMER, F.R., 2005. Real-time assays with molecular beacons and other fluorescent nucleic acid hybridization probes. *Clinical Chemica Acta*, vol. 363, no. 2006, pp. 48-60.

MASTERS, P. S. 2019. Coronavirus genomic RNA packaging. *Virology*, vol. 537, pp. 198-207.

MONROY-CONTRERAS, R., and VACA, L. 2011. Molecular beacons: powerful tools for imaging RNA in living cells. *Journal of nucleic acids*, 2011, 741723. https://doi.org/10.4061/2011/741723.

NAQVI, A.A.T., FATIMA, K., MOHAMMAD, T., FATIMA, U., SINGH, I.K., SINGH, A., ATIF, S.M., HARIPRASAD, G., HASAN, G.M. and HASSAN, M.I., 2020. Insights into SARS-CoV-2 genome, structure, evolution, pathogenesis and therapies: Structural genomics approach. *Biochimica et Biophysica Acta (BBA)-Molecular Basis of Disease,* vol. 1866, no. 10, pp. 165878.

OLIVEIRA, B.A., OLIVEIRA, L.C.D., SABINO, E.C. and OKAY, T.S., 2020. SARS-CoV-2 and the COVID-19 disease: a mini review on diagnostic methods. *Revista do Instituto de Medicina Tropical de Sao Paulo,* vol. 62.

OVERBERGH, L., VIG, S., COUN, F. and MATHIEU, C. 2017. Quantitative Polymerase Chain Reaction. *Molecular Diagnostics (Third Edition)*. pp. 41-58.

OWUSU, D., POMEROY, M.A., LEWIS, N.M., WADHWA, A., YOUSAF, A.R., WHITAKER, B., DIETRICH, E., HALL, A.J., CHU, V., THORNBURG, N., CHRISTENSEN, K., KIPHIBANE, T., WILLARDSON, S., WESTERGAARD, R., DASU, T., PRAY, I.W., BHATTACHARYYA, S., DUNN, A., TATE, J.E., KIRKING, H.L. and MATANOCK, A., 2021. Household Transmission Study Team, Persistent SARS-CoV-2 RNA Shedding Without Evidence of Infectiousness: A Cohort Study of Individuals With COVID-19, *The Journal of Infectious Diseases*, vol. 224, no. 8, pp. 1362–1371.

PETROSILLO, N., VICECONTE, G., ERGONUL, O., IPPOLITO, G. and PETERSEN, E., 2020. COVID-19, SARS and MERS: are they closely related? *Clinical Microbiology and Infection,* vol. 26, no. 6, pp. 729-734.

RAI, P., KUMAR, B.K., DEEKSHIT, V.K., KARUNASAGAR, I. and KARUNASAGAR, I., 2021. Detection technologies and recent developments in the diagnosis of COVID-19 infection. *Applied Microbiology and Biotechnology,* vol. 105, no. 2, pp. 1-15.

RAVI, N., CORTADE, D.L., NG, E. and WANG, S.X., 2020. Diagnostics for SARS-CoV-2 detection: A comprehensive review of the FDA-EUA COVID-19 testing landscape. *Biosensors and Bioelectronics,* vol. 165, pp. 112454.

REDONDO, N., ZALDÍVAR-LÓPEZ, S., GARRIDO, J. J. and MONTOYA, M. 2021. SARS-CoV-2 Accessory Proteins in Viral Pathogenesis: Knowns and Unknowns. *Frontiers in Immunology*, vol.12, no. 2698. Mini Review.

PEIRIS, J.S.M., YUEN, K.Y., OSTERHAUS, A.D.M.E. and STÖHR, K. 2003.The Severe Acute Respiratory Syndrome. *N. Engl. J. Med.*, vol. *349*, pp. 2431–2441.

PILLAY, T.S., 2020. Gene of the month: the 2019-nCoV/SARS-CoV-2 novel coronavirus spike protein. *Journal of clinical pathology,* vol. 73, no. 7, pp. 366-369.

SANTOS-SÁNCHEZ, N.F. and SALAS-CORONADO, R., 2020. Origin, structural characteristics, prevention measures, diagnosis, and potential drugs to prevent and COVID-19. *Medwave,* vol. 20, no. 8.

SATARKER, S. and NAMPOOTHIRI, M., 2020. Structural proteins in severe acute respiratory syndrome coronavirus-2. *Archives of Medical Research*, vol. 51, no. 6, pp.482-491.

SCHOEMAN, D. and FIELDING, B.C., 2019. Coronavirus envelope protein: current knowledge. *Virology journal,* vol. 16, no. 1, pp. 1-22.

SCOHY, A., ANANTHARAJAH, A., BODÉUS, M., KABAMBA-MUKADI, B., VERROKEN, A. and RODRIGUEZ-VILLALOBOS, H., 2020. Low performance of rapid antigen detection test as frontline testing for COVID-19 diagnosis. *Journal of Clinical Virology*, vol. 129, pp. 104455.

SHANG, J., WAN, Y., LUO, C., YE, G., GENG, Q., AUERBACH, A. and LI, F., 2020. Cell entry mechanisms of SARS-CoV-2. *Proceedings of the National Academy of Sciences of the United States of America*, 20200506, vol. 117, no. 21, pp. 11727-11734 ISSN 1091-6490; 0027-8424. DOI 10.1073/pnas.2003138117 [doi].

SHARUN, K., TIWARI, R., DHAMA, K., EMRAN, T. B., RABAAN, A. A., and AL MUTAIR, A. 2021. Emerging SARS-CoV-2 variants: impact on vaccine efficacy and neutralizing antibodies. *Human vaccines & immunotherapeutics*, vol. 17, no. 10, pp. 3491–3494.

SHEN, M., ZHOU, Y., YE, J., AL-MASKRI, A.A.A., KANG, Y., ZENG, S. and CAI, S., 2020. Recent advances and perspectives of nucleic acid detection for coronavirus. *Journal of Pharmaceutical Analysis*, vol. 10, no. 2, pp. 97-101.

SHI, Y., WANG, G., CAI, X.P., DENG, J.W., ZHENG, L., ZHU, H.H., ZHENG, M., YANG, B. and CHEN, Z., 2020. An overview of COVID-19. *Journal of Zhejiang University.Science.B,* vol. 21, no. 5, pp. 343-360.

SOFI, M. S., HAMID, A. AND BHAT, S. U. 2020. SARS-CoV-2: A critical review of its history, pathogenesis, transmission, diagnosis and treatment. *Biosafety and Health*, vol. 2, no. 4, pp. 217-225.

SULE, W.F. and OLUWAYELU, D.O., 2020. Real-time RT-PCR for COVID-19 diagnosis: challenges and prospects. *The Pan African Medical Journal,* vol. 35, Suppl 2.

SYANGTAN, G., BISTA, S., DAWADI, P., RAYAMAJHEE, B., SHRESTHA, L.B., TULUDHAR, R. and JOSHI, D.R., 2021. Asymptomatic SARS-CoV-2 Carriers: A Systematic Review and Meta-Analysis. *Insights in Coronavirus Diseaqse (COVID-19)-Surveillance, Prevention and Treatment*, vol. 8, 587374.

TYAGI S., BRATU D. P. and KRAMER R. S. 1998. Multicolor Molecular Beacons for Allele Discrimination. *Nat. Biotech*. 19:49-53.

VELLAS, C., DELOBEL, P., BARRETO, P.D.S. and IZOPET, J., 2020. COVID-19, virology and geroscience: a perspective. *The journal of nutrition, health & aging,* vol. 24, no. 7, pp. 685-691.

VET, J. and MARRAS, S. 2005. Design and optimization of molecular beacon real-time polymerase chain reaction assays. *Methods in molecular biology*. vol. 288, pp. 273-290.

VILLAPOL, S., 2020. Gastrointestinal symptoms associated with COVID-19: impact on the gut microbiome. *Translational Research*.

WANG, H., LI, X., LI, T., ZHANG, S., WANG, L., WU, X. and LIU, J., 2020. The genetic sequence, origin, and diagnosis of SARS-CoV-2. *European Journal of Clinical Microbiology & Infectious Diseases,* vol. 39, no. 9, pp. 1-7.

WEI, C., LIPTON, J.H. and KAMEL-REID, S. 2009. Chapter 14 – Monitoring of Minimal Residual Hematologic Disease. *Cell and Tissue Based Molecular Pathology.* Pp. 135-144.

WHO. 2021. How an outbreak became a pandemic: the defining moments of the COVID-19 pandemic. *The Independent Panel.* https://theindependentpanel.org/wp-content/uploads/2021/05/How-an-outbreak-became-a-pandemic_final.pdf.

WU, D., WU, T., LIU, Q. AND YANG, Z., 2020. The SARS-CoV-2 outbreak: what we know. International Journal of Infectious Diseases, vol. 94, pp. 44-48.

WOZNIAK, A., CERDA, A., IBARRA-HENRÍQUEZ, C., SEBASTIAN, V., ARMIJO, G., LAMIG, L., MIRANDA, C., LAGOS, M., SOLARI, S., GUZMAN, A.M., QUIROGA, T., HITSCFELD, S., RIVERAS, E., FERRES, M., GUTIERREZ, A. and GARCIA, P. 2020. A simple RNA preparation method for SARS-CoV-2 detection by RT-qPCR. *Sci Reports*. No. 10, pp. 16608.

YANG, Y., PENG, F., WANG, R., GUAN, K., JIANG, T., XU, G., SUN, J. and CHANG, C., 2020. The deadly coronaviruses: The 2003 SARS pandemic and the 2020 novel coronavirus epidemic in China. *Journal of Autoimmunity,* vol. 109, pp. 102434.

YANG, Y., XIAO, Z., YE, K., HE, X., SUN, B., QIN, Z., YU, J., YAO, J., WU, Q. and BAO, Z., 2020. SARS-CoV-2: characteristics and current advances in research. *Virology Journal,* vol. 17, no. 1, pp. 1- 17.

YOUNES, N., AL-SADEQ, D.W., AL-JIGHEFEE, H., YOUNES, S., AL-JAMAL, O., DAAS, H.I., YASSINE, H. and NASRALLAH, G.K., 2020. Challenges in laboratory diagnosis of the novel coronavirus SARS-CoV-2. *Viruses,* vol. 12, no. 6, pp. 582.

ZAKI, A.M., VAN BOHEEMEN, S., BESTEBROER, T.M., OSTERHAUS, A.D.M.E. and FOUCHIER, R.A.M. 2012. Isolation of a novel coronavirus from a man with pneumonia in Saudi Arabia. *N. Engl. J. Med.*, vol, *367*, pp. 1814–1820.

ZELLA, D., GIOVANETTI, M., CELLA, E., BORSETTI, A., CIOTTI, M., CECCARELLI, G., D'ETTORRE, G., PEZZUTO, A., TAMBONE, V., and CAMPANOZZi, L., 2021. The importance of genomic analysis in cracking the coronavirus pandemic. *Expert Rev. Mol. Diagn.*, pp. 1–16, doi:10.1080/14737159.2021.1917998.

ZHOU, D., DEJNIRATTISAI, W., SUPASA, P., LIU, C., MENTZER, A.J., GINN, H.M., ZHAO, Y., DUYVESTEYN, H.M.E., TUEKPRAKHON, A. and NUTALAI, R., 2021. Evidence of escape of SARS-CoV-2 variant B.1.351 from natural and vaccine-induced sera. *Cell*, doi:10.1016/j.cell.2021.02.037.

ZHOU, Z., QIU, Y. and GE, X., 2021. The taxonomy, host range and pathogenicity of coronaviruses and other viruses in the Nidovirales order. *Animal Diseases* 1, vol. 5. https://doi.org/10.1186/s44149-021-00005-9.